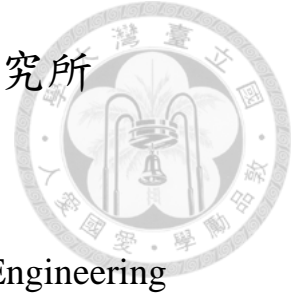


國立臺灣大學工學院環境工程學研究所
碩士論文



Department of Graduate Institute of Environmental Engineering
College of Engineering
National Taiwan University
Master Thesis

以活性碳/黏土薄層覆蓋法整治含汞底泥之縮模研究

Using Activated Carbon/Clay-Based Thin Layer Capping for
Mercury-Contaminated Sediment Remediation: Microcosms
Study

丁昱

Yu Ting

指導教授：席行正 博士

Advisor: Hsing-Cheng Hsi, Ph.D.

中華民國 108 年 7 月

July 2019

國立臺灣大學碩士學位論文

口試委員會審定書

以活性碳/黏土薄層覆蓋法整治含汞底泥之縮模研究

Using Activated Carbon/Clay-Based Thin Layer Capping for Mercury-Contaminated Sediment Remediation: Microcosms Study

本論文係 丁昱 君(學號 R05541212)在國立臺灣大學環境工程學研究所完成之碩士學位論文，於民國 108 年 7 月 5 日承下列考試委員審查通過及口試及格，特此證明

論文審查委員：

林居慶

林居慶 博士
國立中央大學環境工程研究所副教授

范致豪

范致豪 博士
國立台灣大學生物環境系統工程學系教授

席行正

席行正 博士
國立台灣大學環境工程學研究所教授

許正一

許正一 博士
國立台灣大學農業化學系教授

指導教授：

席行正

所長：

林居慶

Acknowledgements



I would like to thank my advisor, Dr. Hsing-Cheng Hsi (席行正), for his guidance, for having confidence in me, and for putting up with my stubbornness. I am also grateful to Dr. Chu-Ching Lin (林居慶), Dr. Chih-Hao Fan (范致豪), and Dr. Zeng-Yei Hseu (許正一) for their precious advises on my master thesis and for their assistance in instrumental analysis.

I would like to thank my team members, Chi Chen(陳祺), Boon-Lek Ch-ng (莊文歷) and Kenya Ou (歐夢圓), for working by my side all along and I really enjoy your company. I would also like to thanks my peers for accompany me during my time in NTU (name in Chinese): 許哲榮、王映琳、徐子琇、施東甫、陳明茵、李孟竺、陳韻心、陳昱廷、陳秉圻、林聰鎮、李昇憲、潘冠璇、陳煜偈、周宥丞、廖華永、蕭燕澤、戴瑋, etc.

I would like address my deepest gratitude to my dad and mom for being so supportive when I faced challenges and so inspiring to me when I was confused.

中文摘要



近年來，現地薄層覆蓋法技術之突破為整治汞污染底泥帶來新的可能性，也提供除疏濬法以外新的整治策略。本研究分為兩部分，利用數種活性碳/黏土基之薄層覆蓋層在微型系統中評估整治汞底泥之可能性。在本研究第一部分中，自製之含硫活性碳(SAC)在等溫吸附實驗中發現對於二價汞及甲基汞之吸附親和性(K_D 值分別為 9.42×10^4 及 7.66×10^5) 比起其原始活性碳(AC)有顯著提升(K_D 值分別為 3.69×10^4 及 2.25×10^5)。但在底泥競爭吸附實驗中，AC 對比 SAC 對於汞底泥(14.2–235.8 mg-Hg/kg)中具有較佳之汞溶出抑制能力，並在 3% 添加量下具有最佳之汞溶出抑制效率(99.88%)。其原理可能為 SAC 在吸附實驗平衡後形成穩定的 $HgS_{(s)}$ 奈米顆粒，使底泥競爭吸附實驗之 AC 抑制汞溶出之能力優於 SAC。另外，研究之各式覆蓋層(SAC+皂白土、SAC+低汞底泥、AC+皂白土)在上流式微型系統中對於總汞及甲基汞均具有良好溶出抑制能力。在本研究第二部分為探討底泥擾動事件對於覆蓋穩定之影響，開發一具有自製震盪系統之橫向流微型系統。三種不同黏土材料之活性碳/黏土基覆蓋層施加於實場汞底泥中(76.0 ± 2.59 mg-Hg/kg)，發現 AC(3%)+皂白土(3%)以及 AC(3%)+高嶺土(3%)在模擬橫向流及表層底泥擾動之條件下，對於實場底泥中總汞及甲基汞皆能達到約 75–95% 及 64–98% 之溶出抑制效果達 75 天之久(實驗全時程)。而 AC(3%)+蒙脫土(3%)的薄層覆蓋層由於蒙脫土在水中沉降性及穩定性較差，使總汞及甲基汞溶出抑制效率不佳。本研究發現穩定性高之薄層覆蓋層有較佳之汞溶出抑制能力，並於間歇性底泥擾動下有較佳之抵抗能力；而穩定性較差之薄層覆蓋層可能造成甲基汞大量溶出。

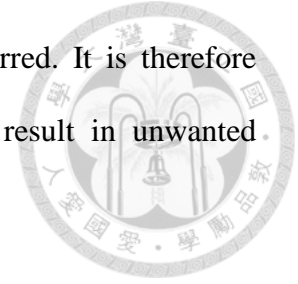
關鍵字：汞、甲基汞、底泥整治、薄層覆蓋法

Abstract



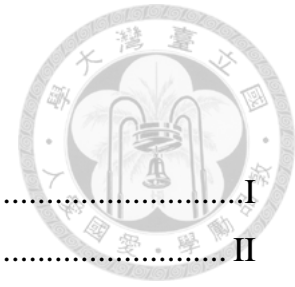
The breakthrough of in-situ thin layer capping technology in recent years has shed light on the remediation of Hg-contaminated sediment and provides a promising alternative besides traditional dredging. In this thesis, the plausibility of several activated carbon (AC)/clay-based thin layer caps were demonstrated in two microcosm studies. In the first study, a lab-synthesized sulfurized activated carbon (SAC) performed greater sorption affinity to both aqueous Hg^{2+} ($K_D=9.42 \times 10^4$) and MeHg ($K_D=7.66 \times 10^5$) compared to those for raw activated carbon ($K_D=3.69 \times 10^4$ and 2.25×10^5 , respectively) in isotherm adsorption tests. However, AC appeared to have greater sequestration ability than SAC in Hg-spiked sediment (14.2–235.8 mg-Hg/kg), with the optimistic dosage of 3wt% AC causing reduction of THg with 99.88%. It may suggest that possibly formed nano-HgS particles could be released thus elevates the porewater Hg when SAC existed. Also, a 83-d trial of up-flow microcosms was demonstrated with various caps (SAC + bentonite, SAC + clean sediment, and AC + bentonite) and all observed significant inhibition of both THg and MeHg. In the second study, a horizontal-flow microcosm with lab-made vibration system was designed to evaluate the capping efficiency during turbation events. AC/clay-based caps with clay combinations were applied to actual Hg-contaminated estuary sediment (76.0 ± 2.59 mg-Hg/kg). The caps with AC + bentonite and AC + kaolin were efficient in reducing both total mercury (THg) and methylmercury (MeHg) concentrations in overlying water by 75–95% and 64–98%, respectively in the later stage of 75-d operation. In contrast, the AC (3%) + montmorillonite (3%) cap did not show a significant reduction on THg and MeHg in overlying water, probably due to the unstable, suspension property of montmorillonite. The stable caps showed higher resistance to Hg breakthrough under occasional turbation events; however, a labile cap

appeared to have dramatic Hg breakthrough when turbation occurred. It is therefore essential to note that with unstable caps, turbation events may result in unwanted secondary resuspension of contaminants.



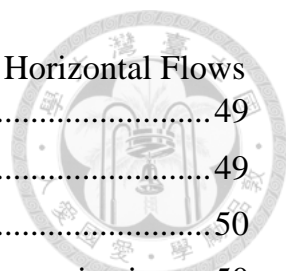
Keywords: mercury, methylmercury, sediment remediation, thin layer capping

Contents



Acknowledgement	I
中文摘要	II
Abstract.....	III
Contents	V
List of Figures.....	VII
List of Tables	XI
Chapter 1 Introduction.....	1
Chapter 2 Hg Management and Thin Layer Capping.....	3
2.1 Mercury Risk and Global Management Efforts	3
2.2 In-situ Approach and Thin Layer Capping.....	5
2.3 Capping Materials.....	7
2.4 Real Site Practice	10
2.5 Estimation of Remediation Cost.....	13
2.6 Challenges and Opportunities.....	15
Chapter 3 Capping of Mercury Sediment with SAC.....	18
3.1 Introduction.....	18
3.2 Materials and Methods	20
3.2.1 Materials.....	20
3.2.2 Physical and Chemical Analysis of Materials	20
3.2.3 Aqueous Adsorption Experiment.....	21
3.2.4 Sediment Competition Adsorption Experiment.....	22
3.2.5 Microcosm Experiment.....	22
3.2.6 Mercury and Methylmercury Analysis	24
3.3 Results and Discussion	25
3.3.2 Aqueous Adsorption Experiment.....	28
3.3.3 Sediment Competition Adsorption Experiment.....	34
3.3.4 Microcosm Experiment.....	38
3.4 Summaries	40
3.5 Supporting Information	42

Chapter 4 AC/clay-based Caps Reduce Mercury Escape under Horizontal Flows and Sediment Turbation	49
4.1 Introduction.....	49
4.2 Materials and Methods	50
4.2.1 Sorbents Preparation, Sediment Collection, and Characterization	50
4.2.2 Artificial Vibration System.....	51
4.2.3 Microcosms Setup and Operation	52
4.2.4 Sample Collection and Analysis	53
4.3 Results and Discussion	54
4.3.2 Sulfide, Sulfate, Chloride, and Total Fe in Overlying Water	56
4.3.3 Reduction of Aqueous THg and MeHg by Thin Layer Cap.....	59
4.3.4 ORP, THg, and MeHg in Sediment	63
4.3.5 The Stability of Thin Layer Caps during Turbation	67
4.4 Summaries	67
4.5 Supporting Information	69
Chapter 5 Conclusions and Suggestions.....	89
References	91



List of Figures

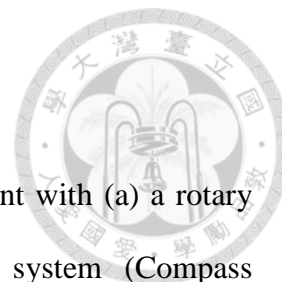


Figure 2-1. Cho et al. [8] performed mechanical mixing amendment with (a) a rotary cultivator (Aquatic Environments, Inc.,) and (b) an injection system (Compass Environmental, Inc., GA).	11
Figure 2-2. Menzie et al. [63] performed a spray thin layer capping using self-made equipment (Vortex TR Aquatic system).	12
Figure 2-3. Cornelissen et al.[87] premixed AC, clay and seawater and preformed a spray thin layer capping by a spraying system on a ship.	13
Figure 2-4. Menzie et al. [63] compared several remedies with a case study in Canal Creek, Maryland.	14
Figure 3-1. (a) photo image; (b) scheme diagram of vertical up-flow microcosms construction. Vertical flows were delivered from the bottom of the columns. The depth of sediment (TY03) is approximately 15 cm. From column A to D: (A) no caps; (B) SAC + bentonite; (C) SAC + additional TY03 sediment; (D) AC + bentonite.	23
Figure 3-2. Micropores size distribution of raw AC and SAC based on QSDFT model. .	27
Figure 3-3. Deconvoluted S2p peak for AC and SAC.	28
Figure 3-4. Hg ²⁺ adsorption by AC and SAC as a function of time. For here [Hg ²⁺] = 1 mg/L, Hg solution = 50 mL, adsorbent dosage = 50 mg, and pH = 7.0±0.1.	30
Figure 3-5. Adsorption isotherm of AC and SAC adsorbing (a) Hg ²⁺ and (b) MeHg. Adsorption time = 24 h. Hg solution = 50 mL, adsorbent dosage = 50 mg, pH = 7.0±0.1.	33
Figure 3-6. Hg concentrations in porewater versus in sediment at (a) 1 wt%; (b) 3 wt%; (c) 6 wt% adsorbent addition based on sediment competition adsorption test. DI water is 50 mL and Hg sediment is 5.0 g.	36
Figure 3-7. Proposed adsorption/desorption mechanisms of Hg adsorption on SAC in the	

sediment environment.37

Figure 3-8. Overlying water (a) THg and (b) MeHg concentrations of vertical up-flow microcosms during operation.....39

Figure S3-1. SEM images of raw AC and AC after sulfurization (i.e., SAC) under x1500 magnification.43

Figure S3-2. Follow-up aqueous adsorption tests of AC and SAC to justify the discussion in Section 3.3. The adsorption condition is as the same as the aqueous adsorption tests described in Section 2.3. [Hg]₀= 1 mg/L, Temperature = 30°C, 125 rpm, n = 3. Adsorption time was extended to 48 h and 72 h. Aqueous samples obtained with different pore-sized filtration are compared. SAC: sulfurized activated carbon; AC: raw activated carbon; “nof”: no filtered treatment after adsorption test; “0.20”: 0.20 μm filtered treatment; “0.45”: 0.45 μm filtered treatment.44

Figure S3-3. pH value variation of four vertical up-flow microcosms (A–D) during the operation of 86 days. From column A to D: (A) no caps; (B) SAC + bentonite; (C) SAC + additional TY03 sediment; (D) AC + bentonite.45

Figure S3-4. ORP variation of four vertical up-flow microcosms (A–D) during the operation of 86 days. From column A to D: (A) no caps; (B) SAC + bentonite; (C) SAC + additional TY03 sediment; (D) AC + bentonite.46

Figure S3-5. Temperature variation of four vertical up-flow microcosms (A–D) during the operation of 86 days. From column A to D: (A) no caps; (B) SAC + bentonite; (C) SAC + additional TY03 sediment; (D) AC + bentonite.47

Figure S3-6. Flow rate variation of four vertical up-flow microcosms (A–D) during the operation of 86 days. From column A to D: (A) no caps; (B) SAC + bentonite; (C) SAC + additional TY03 sediment; (D) AC + bentonite.48

Figure 4-1. (a) Sulfate, (b) chloride, and (c) total Fe concentration in the overlying water

of four cells of the microcosm. The gray bar between day 20 and 30 represents intermittent turbation test; the gray bar at day 54 represents the sediment sampling event.57

Figure 4-2. (a) THg and (b) MeHg concentration in the overlying water of four cells of the microcosm. The gray bar between day 20 and 30 represents intermittent turbation test; the gray bar at day 54 represents the sediment sampling event.61

Figure 4-3. The ORP in sediment of the four cells of the microcosm. The ORP was measured within 1–3 cm depth.64

Figure 4-4. THg and MeHg in the sediment (1–3 cm depth) of the four cells of the microcosm (n = 3).66

Figure S4-1. The texture of ANS sediment.76

Figure S4-2. Photo diagrams for commercial motors (RISUN PVN 1305D 3V) before (left) and after (right) coated with layers of Hg-free epoxy resin and plastic steels.77

Figure S4-3. Photo diagram (left) and circuit diagram (right) of the lab-made current controller.78

Figure S4-4. Photo diagram of the whole microcosm. The yellow stars represent the location of the motors; the blue arrow represents the sampling point for overlying water and the beneath sediment.79

Figure S4-5. Scheme diagram of the microcosm construction.80

Figure S4-6. Photo diagrams for the start-up of the microcosm, including the pressure test (up), sediment incubation (middle; day -98) and rectifier added (down; day -97).81

Figure S4-7. Top view of cell A (control), cell B (AC + bentonite), cell C (AC + kaolin) and cell D (AC + montmorillonite); the photographs were taken at day 70.82

Figure S4-8. (a) Temperature, (b) DO, (c) pH, and (d) EC of the overlying water in the microcosm.83

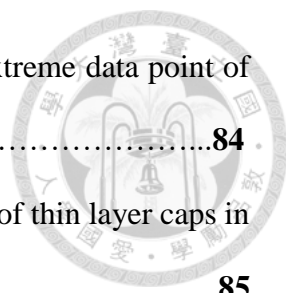


Figure S4-9. Correlation of sulfate to (a) EC and (b) total Fe. An extreme data point of day 60 was removed from the plot.84

Figure S4-10. (a) THg reduction and (b) MeHg reduction efficiency of thin layer caps in comparison to control.85

Figure S4-11. Correlation of THg to (a) sulfate and (b) total Fe. Extreme data points of day 60 were removed.86

Figure S4-12. Correlation of MeHg to (a) sulfate and (b) total Fe. Extreme data points of day 34 and day 60 were removed.87

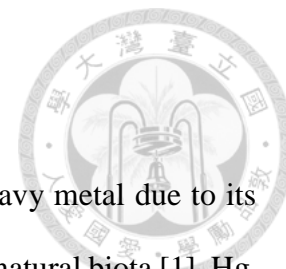
Figure S4-13. Correlation of THg to MeHg. An extreme data point of day 60 was removed.88

List of Tables



Table 2-1. Field application cases for thin layer capping remediation. (Partially adopted from Patmont et al.[57]).	6
Table 2-2. SAC enhances Hg sorption capacity in aqueous adsorption tests.	9
Table 3-1. Physical and chemical properties of precursor AC and resulting SAC.	26
Table 3-2. Fitting parameters of AC and SAC adsorption by pseudo-first and second order reaction models.	30
Table S3-1. Characteristics of sediment TY03 sampled from a river in Northern Taiwan.	42
Table S4-1. Properties for ANS sediment.	69
Table S4-2. Properties for ANS surface water.	70
Table S4-3. Operation record for the microcosm.	71
Table S4-4. Temperature, DO, pH, and EC of the overlying water in the microcosm.	73
Table S4-5. chloride, sulfide, sulfate and total Fe contents of the overlying water in the microcosm.	74
Table S4-6. THg and MeHg of the overlying water in the microcosm.	75

Chapter 1 Introduction



Mercury (Hg) has been recognized as one of the most toxic heavy metal due to its high volatility, persistence, and bioaccumulation to human beings or natural biota [1]. Hg, in general, exists in the form of divalent Hg (i.e., Hg^{2+}) in the aqueous phase and may transform to methylmercury (MeHg), which is one of the most toxic Hg forms via biomethylation under an anoxic sediment environment [2]. Although ex-situ strategies have been proven promising in removing Hg out of sediment [3, 4], problems such as unfeasible cost [5], resuspension of contaminants [6, 7], and production of contaminated sediment residues [6, 7] may discourage their application. Therefore, the development of novel and feasible techniques in remediating Hg-contaminated sediment is highly needed.

The breakthrough of using in-situ thin layer capping, or "in-situ active capping," to remediate contaminated sediment has drawn much attention in the past decade. In particular, using activated carbon-based thin layer capping to sequester persistent organic pollutants (POPs) has received promising effects on some full-scale sites [8-11]. This breakthrough also shed light on the remediation of Hg-contaminated sediment, which is the other major polluted sediment within concern.

There are several knowledge gaps that have to be filled up before thin layer capping be put to application. One of which is the development of sorption materials with better stability and Hg sorption affinity. Sulfur-impregnated activated carbon (SAC) has been verified to enhance Hg adsorption capacity than its raw AC precursor in aqueous adsorption tests [12-14]. However, studies on using SAC as the thin layer capping material for inhibiting the release of Hg and MeHg from sediment environment are scarce.

One of the other major knowledge gaps for the thin layer capping is its capping

stability and the potential risks of Hg escape from caps. The sediment turbations caused by bioturbation or physical erosion have been identified as critical mechanisms in contaminant transport in the natural aquatic environment [15-18]. It is intriguing how sediment turbation may affect the efficiency of the thin layer capping in treating Hg-contaminated sediment, but related studies remain with little information.

In this master thesis, the plausibility of thin layer caps to remediate Hg-contaminated sediment was discussed and the activated carbon/clay-based thin layer caps were demonstrated in two microcosm studies. In chapter 2, a brief review is provided for practical details about Hg management and thin layer capping in real site application. The first study (chapter 3) addressed the Hg sorption behavior of a lab-made coconut-based SAC to mercury-containing sediment remediation by thin layer capping method via batch and microcosm experiments. The second study (chapter 4) evaluated the Hg leaching inhibition performance of thin layer caps under horizontal flows and artificial sediment turbation operated in microcosms.

Chapter 2 Hg Management and Thin Layer Capping

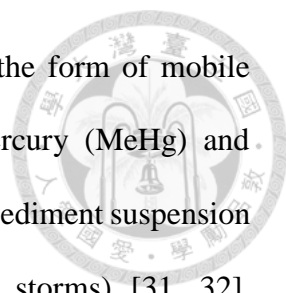


2.1 Mercury Risk and Global Management Efforts

Mercury (Hg) has been recognized as one of the most hazardous heavy metals due to its high volatility, persistence, and bioaccumulation in human beings and natural biota [1]. Long-term, high-dosage exposure of humans to Hg may pose risk to the brain, heart, kidneys, lungs, and the immune system by causing various neurodegenerative diseases, such as Minamata disease, Alzheimer's disease, and Parkinson's disease [1, 19-22]. Hg can be released from both natural or anthropogenic sources. With elevating human industrial activities, much Hg has been mined out of the earth and discharged to the environment as waste. Major anthropogenic Hg sources include gold mining, coal combustion, and metal production [1, 3, 23-25], which have created a huge amount of Hg-containing wastewater to be discharged into wetlands, rivers, and seawater. Amos et al. [26] estimated that around 5500 ± 2700 Mg of aquatic Hg is released into rivers annually across the globe. Excluding natural mobilization of Hg from terrestrial ecosystems, Kocman et al. [27] estimated riverine discharge of Hg with a smaller value of around 800 to 2200 Mg/year.

Global efforts on Hg management have been put together through the Minamata Convention on Mercury, a global treaty to protect human health and the environment from adverse effects of Hg. Updated on August 2018, 128 nations have signed the treaty with requirements including banning of primary Hg mining, reductions in Hg release to the environment (air or water), exposure through products and consumptions, remediation of contaminated regions, monitoring, outreach, and other means.

As Hg is discharged into the aquatic environment (i.e., wetlands, lakes, and coasts),



sediments may serve as the sink for Hg [28], which is mainly in the form of mobile divalent mercury (Hg^{2+}) and may transform to monomethyl mercury (MeHg) and gaseous mercury (Hg^0) through resuspension and diffusion [29, 30]. Sediment suspension can be induced by natural physical processes (e.g., waves and storms) [31, 32], anthropogenic activities (e.g., dredging, trawling, and boating) [33] and biological activities (e.g., bioturbation) [34].

Hg in natural waters occurs in forms including Hg^0 , ionic mercury (e.g., Hg^+ and Hg^{2+}), and methylated mercury (e.g., CH_3Hg^+ , $(\text{CH}_3)_2\text{Hg}$) [35]. While all forms of Hg are toxic, its methylated form, MeHg, is specifically problematic. MeHg has high bioaccumulation and biomagnified ability and poses a threat to biota and human [36]. MeHg usually occurs in minor proportions, at around 0.1–1.5% of total Hg [37-40] in anoxic sediment environments, but can pose a high risk to human health.

Much effort on Hg control has been put in water treatment and sediment remediation. For wastewater treatment of Hg, lime softening, chemical precipitation, coagulation, reverse osmosis, ion exchange, and membrane filtration have been considered [41]. As for sediment and groundwater Hg remediation, many techniques have been employed, such as adsorption, biosorption, ion exchange, chemical precipitation, reduction, and stabilization/fixation. Among these methods, adsorption and stabilization/fixation have been proved to be the most practical techniques [24, 42, 43]. Dredging followed by ex-situ methods have been commonly executed due to its long-term effectiveness and relatively short remediation period [5]. However, dredging can be preventatively costly. Also, dredging may cause remobilization of contaminants during remediation, and may inevitably retain contaminants, posing a long-term threat [44].

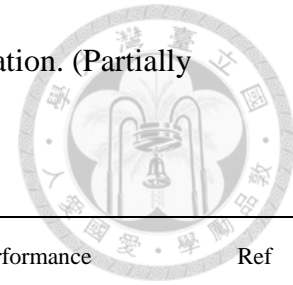
2.2 In-situ Approach and Thin Layer Capping

One of the main advantages of in-situ technologies is that they used toward reducing environmental impacts and avoiding the huge cost of dredging. The main challenges are related to the difficulties in ensuring that the contaminants are effectively reduced by the technologies due to the heterogeneity of sediment and the uncertainty in the distribution of contaminants. In-situ technologies require a treatability test to evaluate their efficiency at the specific site [45].

A relatively new term of “thin layer capping”, which involves the use of chemically reactive materials to sequester contaminants to reduce their mobility, toxicity, and bioavailability in sediment. The remediation cost of thin layer capping is likely to be smaller than for conventional strategies (e.g., dredging or sand capping). Additionally, thin layer capping may further enhance or improve habitat recolonization by benthic organisms [46]. Active materials, such as activated carbon, have been shown to reduce the toxicity of persistent organic pollutants (POPs) such as polychlorinated biphenyls (PCBs), polycyclic aromatic hydrocarbons (PAHs), or pesticides in laboratory or field studies [47-56]. Updated in 2015, more than 25 field studies have been conducted by thin layer capping approaches [57] (Table 2-1).



Table 2-1. Field application cases for thin layer capping remediation. (Partially adopted from Patmont et al.[57])



location	pollutants	Engineering method	Remediation performance	Ref
Hunters Point Shipyard, USA	PCBs	Mixed ~3.7% of AC into 1 ft. deep of sediment.	Bioaccumulation of clam decrease 62% after capping for 7 months.	[58]
South Basin, USA	PCBs	Mixed 2.0~3.2% of AC into 30–40 cm deep of sediment.	Surface water PCBs conc. decrease 90% after capping for 18 months.	[8]
Hunters Point Shipyard, USA	PCBs	Mixed ~3.7% of AC into 1 ft deep of sediment.	PCBs conc. reduce 73% in passive sampler.	[59]
Trondheim Harbor, Norway	PAHs, PCBs	Pre-mixing of AC, clay and sand into slurry, followed by direct capped on the surface of sediment.	AC-clay mixing caps have highest in conc. decrease during 9–12 months sampling, no obvious impact on biodiversity.	[9]
Eidangerfjord and Ormerfjord, Norway	PCBs, furans	Pre-mixing of AC(2%) and clay, followed by direct capped on the surface of sediment.	During 20 months capping, conc. of low-chloride PCBs decrease >90%, while high-chloride PCBs decrease 60–70% in porewater.	[60]
Eidangerfjord and Ormerfjord, Norway	PCBs, furans	Pre-mixing of AC(2%) and clay, followed by direct capped on the surface of sediment.	After 2 yrs of capping, control site decrease pollutant flux 70–90%, while capping sites decrease 50–60%. After 3–5 yrs, capping sites decrease 80–90%, while control sites reduce 20–60%.	[61]
St. Lawrence River, USA	PCBs	Spraying, mixing, and injecting of mixture containing two AC on to sediment	PCB bioaccumulation of benthic organisms decrease 69–93% during 3 yrs of capping. Porewater conc. decrease 93%.	[10]
Lower Canal Creek, USA	PCBs, DDT, Hg	Direct spraying of AC(SediMite®)	During 10 months of capping, PCBs and DDT bioaccumulation have dramatic decrease, MeHg decrease for 50%.	[62]
Grenland fjords, Norway	Dioxins, Hg	Pre-mixing of AC, clay and limestone into slurry, followed by direct capped on the surface of sediment.	Up to 90% biodiversity reduction have been observed in AC capped sites, capping using non-AC material have smaller bio-impact.	[63]

2.3 Capping Materials

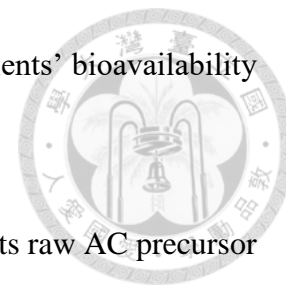
For the application of thin layer capping on Hg-contaminated sites, laboratory studies have been conducted using AC [14, 57, 64-66], biochar [64, 67], or surface-modified black carbon [14] to immobilize Hg. Some studies have shown that the amendment of black carbon may successfully reduce bioavailable Hg and MeHg to benthic organisms [65, 66]. Beside bench-scale studies, several field-scale studies [62, 68] have also been carried out to and observed with moderate success in reducing Hg in porewater or biotas.

Activated carbon (AC) is composed of defective graphene layers, which are formed by gasification of carbon atoms via activation (often by thermal treatment). After activation, AC can be filled with pores that greatly increase surface area (as high as 500–1500 m²/g; [24]) and intensify van der Waals force. With its high specific surface area, AC has proven to be a promising option for remediation of contaminated sites for not only organic pollutants[47-56] but also Hg [64-66, 68, 69]. AC has several kinds of acid functional groups such as carboxyl groups on its surface, and are expected to chemically adsorb Hg [13].

Nevertheless, the sorption capacity of AC toward Hg is still limited due to the nonpolar characteristics of activated carbon, which hinder interactions between charged metal species and the solid surface [43].

The other main concern of applying black carbon to sediment remediation is its possible adverse effects on the benthic organisms itself. One-fifth of previous studies have reported adverse bio-effects using black carbon to sequestrate Hg [70]. Benthic biotas suffered from reduced species richness, biomass loss, reduced feeding rate, organ damage, or reduced growth after carbon amendment. Several studies suggested that the

possible explanations are because the black carbon may reduce nutrients' bioavailability [71], or reduce ingestion rate by harming gut structures [72].



SAC has been verified to enhance Hg adsorption capacity than its raw AC precursor in aqueous adsorption tests (Table 2-2; [12, 13, 41, 73, 74]). Sulfurization of AC enhance Hg sorption capacity in most essays [12, 13, 41, 73, 74] and sometimes over 100% by magnitude [12, 13]. For example, Wang et al. [12] demonstrated that an increase in Hg adsorption capacity of coconut AC from 150 to 820 mg/g by sulfurization with sulfur powder (C/S ratio: 1:2) was shown. Li et al. [13] increased Hg adsorption capacity of coke from 315.8 to 694.9 mg/g by impregnated the coke with sulfuric acid (80°C, 13 h). Also, the stability of Hg sorption to SAC was also known to increase as Hg was found stably sorbed to SAC in a broad pH range [12]. However, SAC has yet been tested to apply on Hg-contaminated sediment.

Biochar is another attractive sorbents as a potential remediation material since it is less costly than AC and may play the role of fertilizer if applied in soil [75]. Similar to AC, biochar is a porous, carbon-rich, black carbon material produced by thermally decomposing biomass under low-oxygen concentrations and temperatures between 300–1000°C. Gomez-Eyles et al. [64] conducted an experiment testing Hg sorption affinity of 13 kinds of biochars and 4 kinds of AC, the results showed that both AC and biochar have efficient Hg sorption affinity with AC superior in Hg²⁺ sorption.

Clay is a general term for a broad range of inorganic mineral with the size within 2 mm. With good thermal stability, cation exchange capacity, and settling clay may be the other potential capping material [76]. Clay minerals could be further modified to organoclays, and was reported to enhance sorption capacity up to 10–30 times to Cr, As,

Pb, Cd, and Zn [77-79].

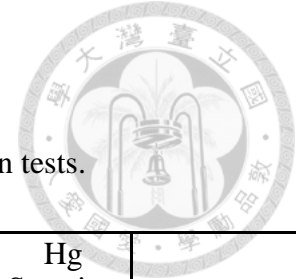
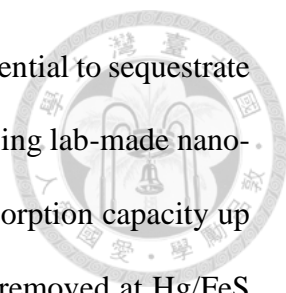


Table 2-2. SAC enhances Hg sorption capacity in aqueous adsorption tests.

Raw materials	Activation method	S_{BET} (m ² /g)	S (%)	Adsorption conditions (solution/temperature/pH)			Hg Sorption capacity (mg/g)	Reference
Sugar cane	SO ₂ and H ₂ S 400°C, 30 min	500.05	8.9	HgCl ₂ solution	30°C	6	188.68	[73]
Coconut	Non-sulfurized	1884	0		25°C	5.5	150	[12]
	Sulfur powder, S:C=1:2 400°C, 2 h	-1000	22				820	
Coke	Non-sulfurized	193.7	1.39		25°C	5	315.8	[13]
	H ₂ SO ₄ , 80°C, 13 h	136.7	3.33				694.9	
Almond seed	Activated by phosphoric acid +C ₂ S sulfurization, S:C=2:1 600°C, 1 h	1637	9.9		25°C	6	-230	[41]
					35°C		-280	
					45°C		-290	
					25°C	3	-190	
Coal	Non-sulfurized	828	1.5		30°C	7	455	[74]
	Dimethyl disulfide 30°C, 48 h	348	9.6	441				
	Sulfur powder, S/C=4:1 145°C, 30 min 600°C, 30 min	596	10.8	529				

Iron sulfide minerals (Fe_xS_y) have been found to have good immobilizing ability to double-valent metals, such as Mn²⁺, Ca²⁺, Mg²⁺, Ni²⁺, Cu²⁺, Cd²⁺, Co²⁺, Zn²⁺, Pb²⁺, and Hg²⁺ [80-85], basically due to their adsorption or precipitation properties. In addition, iron sulfides have also been reported to degrade organic contaminants by reduction mechanisms. The common forms of iron sulfide minerals include mackinawite (FeS), greigite (Fe₃S₄), pyrite (FeS₂), and pyrrhotite (Fe_{1-x}S) [86]. In earlier research,



mackinawite, pyrite, and pyrrhotite have been shown to have high potential to sequester Hg [87, 88]. Some of the more recent studies have been conducted using lab-made nano-mackinawite to sequester Hg. Liu et al. [86] reported FeS with adsorption capacity up to 1700 mg/g (by calculation) at pH = 5.6; more than 99% Hg was removed at Hg/FeS ratio < 1000, with 77% of the removal by precipitation and 23% by adsorption (Hg/FeS = 0.22). Sun et al. [89] found that commercial pyrite had lower Hg sorption capacity (9.9 mg/g) as compared to lab-synthesized mackinawite (769.2 mg/g), probably due to the smooth surface of pyrite. Skyllberg and Drott [90] conducted a slurry batch study, discovering that the dosage of 2% FeS in 5000 µg-Hg/g organic-rich soil may outcompete O/N ligands in sediment for Hg sorption, resulting in 50% Hg sorbed on FeS to form HgS₄ (metacinnabar). As the ratio of FeS increased to up to 20%, a complete outcompete with 100% Hg sorbed on FeS was observed.

To date, a promising active material in remediating Hg-contaminated sites is yet to be proven with good adsorption efficiency, stability, and eco-friendliness. Consequently, further research is needed in several areas, including (1) fabricating novel capping materials with good adsorption affinity for Hg or other heavy metals; (2) establishing competitive adsorption models of amendments in sediment condition to evaluate real adsorption outcomes in nature disturbance; (3) introducing amendments with biological tests to prove the efficiency of reducing Hg bioavailability; (4) developing efficient, low-impact capping delivery systems; (5) assessing long-term stability and ecological recovery of placing active caps; (6) conducting life-cycle analysis for thin layer capping remediation.

2.4 Real Site Practice

In real site application, thin layer capping can be performed in two existing methods:

(1) mechanical mixing amendment; (2) spray thin layer capping. Mechanical mixing amendment involves applying of capping materials and mixing of materials into top layer of sediment. Several advantages of mechanical mixing amendment can be anticipated, such as better transportation of materials, less material lost by water flow, or less possibility of adverse effect to benthic organisms [9, 58]. However, mechanical mixing amendment also tends to mobilize sediment during engineering procedure, and is likely to be costlier due to the mixing of sediment. Cho et al. [8] demonstrated two types of machinery to perform mechanical mixing amendment (Figure 2-1). The first machinery is modified by a rotary cultivator originally used for weeds removal in swamps. The second machinery, the injection system, was originally used for injection of cement to stabilize sediment.



Figure 2-1. Cho et al. [8] performed mechanical mixing amendment with (a) a rotary cultivator (Aquatic Environments, Inc.,) and (b) an injection system (Compass Environmental, Inc., GA).

Spray thin layer capping involves pre-mix of capping materials and directly spraying into the water body without further mixing. As the material sink to the bottom of the water body, a thin layer of cap formed on the surface of the sediment. With the assistant of benthic biotas, capping materials would be able to mix with the top of surface sediment, therefore immobilize pollutants in the porewater [9]. Menzie et al. [62] performed spray

thin layer capping in a shallow wetland with a self-made spreader, consisted of a 250-pound hopper and a diesel sprayer (Figure 2-2). Cornelissen et al. [60] performed a spray thin layer capping in a fjord with 100 m of water depth by using a spraying instrument in a ship (Figure 2-3). The ship was designed with 275 m³ water tank and a dredging pumps. The capping materials were premixed in the tank by a pump (500 hp), latter spraying through an elastic tubing in 10 m deep into the water by the other pump (204 hp). Spray thin layer capping appears to be more flexible in real site practice since it can be applied in both shallow or deep regions. Also, spray thin layer capping is less costly as it doesn't need additional mixing device. In addition, several studies [10, 51] have concluded that contaminants immobilizing efficiency did not differ with or without artificial mixing of sediment.



Figure 2-2. Menzie et al. [62] performed a spray thin layer capping using self-made equipment (Vortex TR Aquatic system).



Figure 2-3. Cornelissen et al.[60] premixed AC, clay and seawater and performed a spray thin layer capping by a spraying system on a ship.

2.5 Estimation of Remediation Cost

Despite all technological difficulties, the cost of remediation may be just as important since sediment remediation can be quite costly and even to a degree of unrealistic. Remediation methods with “in-situ” strategies have huge advantages that they can be operated with reduced environmental impact and without costs associated with dredging [45].

As one of the most promising in-situ remedies, thin layer capping was studied of its remediation cost [5, 62]. The material cost and operational cost are two major portions of its cost. Some other portions of costs may also be needed on other aspects [62], including laboratory studies, construction of types of machinery, materials transportation etc. The cost of thin layer capping was estimated within the following paragraphs, with an exchange rate calculated by USD/NTD = 1:30, and Euro/NTD = 1:40.

Menzie et al. [62] compared several remedies (i.e. thin layer caps, sand caps, and dredging) with a case study in Canal Creek, Maryland. In the estimation, capping material

SediMite[®] costed US\$3,730 per ton (NTD\$111.9 per kg), slightly higher than commercial AC (NTD\$60–100 per kg); amendment dose was 4.53 kg/m²; instruments costed US\$23,000 (NTD\$690,000); deliver operation costed US\$14.085 per m² (NTD\$422.5 per m²); laboratory studies costed US\$23,500 (NTD\$700,000). As the results, to remediate 10 acres of sediment may cost US\$89,000 per acre (NTD\$6,640,000 per HA) by SediMite[®] thin layer caps. If applying dredging technology, the same 10-acre contaminated site may cost US\$800,000 per acre (NTD\$59,300,000 per HA) by dredging with 3 ft. Calculation of some other remedies was included in Menzie et al. [62] and can be shown in Figure 2-4.

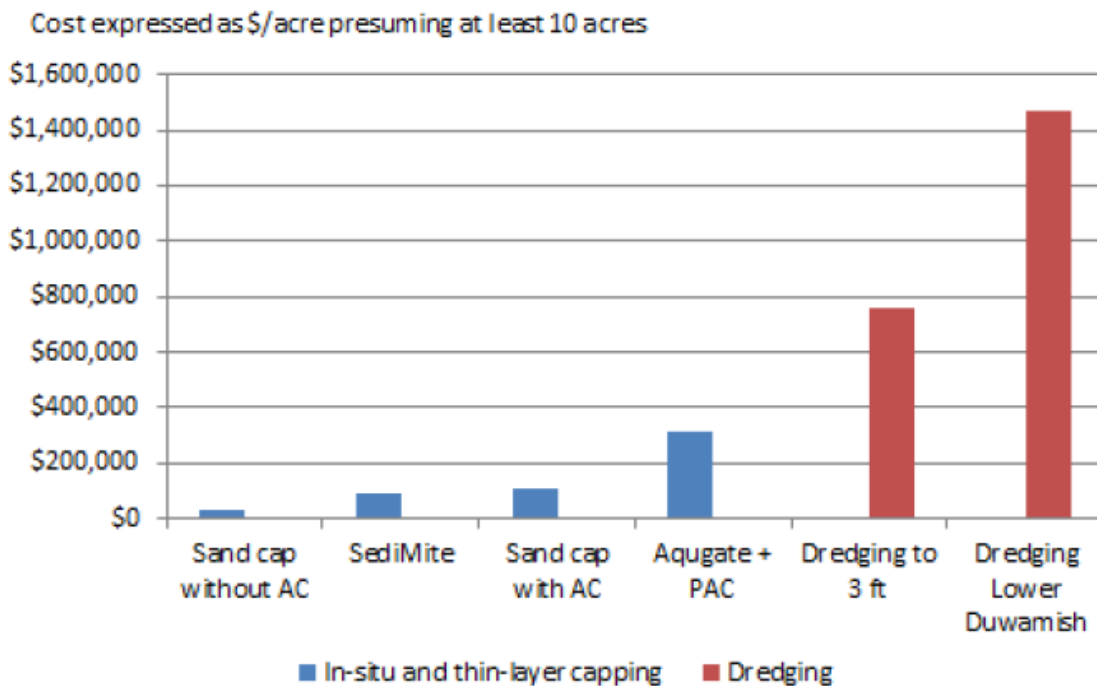
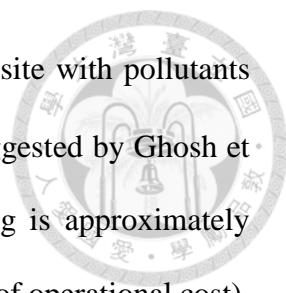


Figure 2-4. Menzie et al. [62] compared several remedies with a case study in Canal Creek, Maryland.

The other estimation based on the parameters from Kupryianchyk et al. [5] was made by the author and matched the results of Menzie et al. [62]. Kupryianchyk et al. [5] provided parameters including the material cost for thin layer capping: 3€/kg; operational cost: 30 €/m³; dredging cost: 1–10 €/m³; the cost of thermal treatment: 60



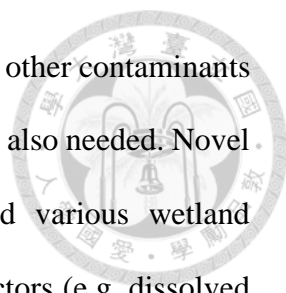
€/m³; the cost of disposal: 10–20 €/m³. Assuming a contaminated site with pollutants within 50 cm deep; providing thin layer caps with 3.5 kg/m² (as suggested by Ghosh et al. [7]). Thus, a brief calculation on the cost of thin layer capping is approximately NTD\$4,800,000 per HA (with 87.5% of the material cost and 12.5% of operational cost). In terms of dredging and thermal treatment, a cost of NTD\$14,200,000–18,000,000 per HA were needed.

Based on the estimation of Kupryianchyk et al. [5] and Menzie et al. [62], a brief cost thin layer capping (about NTD\$5,000,000–6,000,000 per HA) is likely to be much cheaper to ex-situ treatment (various within NTD\$20,000,000–60,000,000 per HA). This estimation of dredging also be matched by NRC [91], which estimated the cost of dredging may be in between US\$145–530 per CY (NTD\$16,620,000–60,770,000 per HA). Although it should be fair to point out that some aspects may not be included, such as that the estimation based on Kupryianchyk et al. [5] only estimated the major portion of the thin layer capping (i.e. material cost and operational cost). Also, some other factors remain complex and can be site-specific, which is also not included in the estimation. As a whole, however, it can be fair to point out that the thin layer capping technology can be less costly compared to ex-situ methods if operated correctly.

2.6 Challenges and Opportunities

As demonstrated in the previous chapters, the thin layer capping technology is a promising alternative for the sediment remediation, but challenges remain in various aspects. Therefore, future studies are needed to fill in knowledge gaps as suggested below:

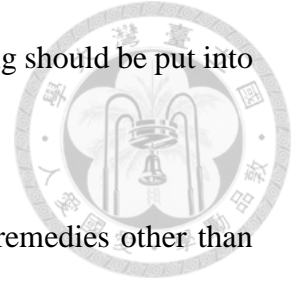
- (1) In the field of material science, the relationship between sediment contaminants and the capping materials should be further studied. Although the sequestration



of POPs by AC has been widely studied, the sequestration of other contaminants (e.g. Hg) that pose high threat to ecology and human health is also needed. Novel sorbents are needed to adopt different contaminants and various wetland conditions [14]. Also, the impact of various geochemical factors (e.g. dissolved organic matter, ions, microbial, or biotas) can have major roles in determining the success of the thin layer capping, and the interaction of which should be further studied.

- (2) In the field of geology, submarine groundwater flow [92], river erosion [17, 18], tidal effects [15, 16], and bioturbation [93] have been identified as critical mechanisms in contaminant transport in the natural aquatic environment. The stability and successfulness of thin layer capping under water can be determined by such geological condition. The research establishing the efficiency of thin layer capping with sediment turbation is scarce. One of the reasons may be due to the difficulty of simultaneously quantifying turbation magnitude [94, 95] and providing a comparable condition to real site capping application.
- (3) In the field of engineering and the real site practice, the anchoring problems for lighter materials (e.g. AC) sometimes results in settling problems or material loss [9]. The strategies such as the granulating materials, adding anchoring materials, or manufacturing materials into geotextile mat [96] may be useful but requires further studies.
- (4) In the field of ecology, some studies reported that the AC amendment did not result in ecological disturbance in field studies [70, 97, 98], while other found benthic biotas suffered from reduced species richness, biomass loss, reduced feeding rate, organ damage, or reduced growth after carbon amendment in labs

[70-72] or field sites [63]. The materials for thin layer capping should be put into tests before real site application.



- (5) In the field of legislation and regulations, the bias against remedies other than removal still exists. There are also perceptions and regulatory precedents to "get it out". This view of sediment remediation may be appropriate but there are numerous occasions where removal is not realistic or ineffective for risk reduction [7].

Chapter 3 Capping of Mercury Sediment with SAC

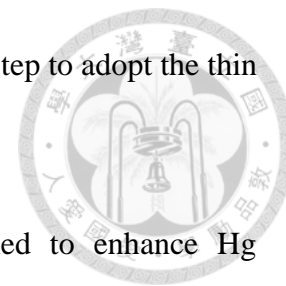


3.1 Introduction

With high neurotoxicity, volatility, and bioaccumulation ability, mercury (Hg) has been considered as one of the most toxic heavy metal in the environment. Hg, in general, exists in the form of divalent Hg (i.e., Hg^{2+}) in the aqueous phase and may transform to methylmercury (MeHg), which is one of the most toxic Hg forms via biomethylation under an anoxic sediment environment [2]. With high affinity in organism tissue [35], MeHg has high tendency to accumulate in biota and biomagnify through food chains, thus causing adverse effects to biota or human. Although ex-situ strategies have been proven promising in removing Hg out of sediment [3, 4], problems such as unfeasible cost [5], resuspension of contaminants [6, 7], and production of contaminated sediment residues [6, 7] may discourage their application. Therefore, development of novel and feasible techniques in remediating Hg-contaminated sediment is highly needed.

In-situ thin layer capping is a newly emerged in-situ remediation concept that can be applied to remediate Hg-contaminated sediment. Thin layer capping involves the use of active materials to sequester contaminants in sediment, therefore achieving the remediation goal of reducing uptake of contaminants by biota and subsequently by the human. It has been shown that thin layer capping using activated carbon (AC) could be a promising treatment in reducing organic contaminant bioavailability in sediment, and has been demonstrated either in full-scale studies [8-10, 59, 61, 62] or long-term prediction models [48, 99]. As for Hg-contaminated sediment, however, fewer studies have been conducted [62, 66, 100], the reason may be because that AC generally has higher affinity to organic pollutants ($\log K_D \approx 7.0-10.0$) than Hg ($\log K_D \approx 3.0-7.0$) [64]. Therefore, seeking

effective active materials with higher affinity to Hg is an important step to adopt the thin layer capping technique to Hg-contaminated sediment.



Sulfur-impregnated activated carbon (SAC) has been verified to enhance Hg adsorption capacity than its raw AC precursor in aqueous adsorption tests [12-14]. The results were reasonable considering its reaction thermodynamics, for which Hg has high affinity to sulfur (i.e., $\log K \approx 52.7-53.3$) [23], as compared to that for Hg to organic matter (i.e., $\log K = 22-28$) [35]. Wang et al. [12] demonstrated that an increase in Hg adsorption capacity of coconut AC from 150 to 820 mg/g by sulfurization with sulfur powder (C/S ratio: 1:2) was shown. Furthermore, Li et al. [13] increased Hg adsorption capacity of coke from 315.8 to 694.9 mg/g by impregnated the coke with sulfuric acid (80°C, 13 h).

Based on the previous research, we expected that SAC may have strong potential as thin layer capping material to remediate Hg-contaminated sediment. However, studies on using SAC as the thin layer capping material for inhibiting the release of Hg and MeHg from sediment environment are not done and presented. In this research, aqueous adsorption tests, sediment competition adsorption tests, and microcosm experiments were carried out to verify the Hg adsorption abilities of SAC and its raw AC counterpart. The feasibility of using SAC as the capping material for inhibiting the release of Hg and MeHg from sediment environment was further evaluated. The results obtained in this study are practically critical because a highly Hg-contaminated site in Southern Taiwan is currently remediated, for which thin layer capping has been considered as one of the feasible approaches for limiting the accessibility of biota to the Hg present in the contaminated seawater ponds.



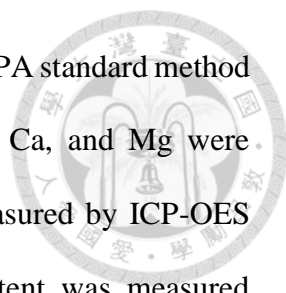
3.2 Materials and Methods

3.2.1 Materials

The actual sediment used in the study, designated as TY03, was sampled from Taoyuan irrigation channel, Taiwan, acquired according to the Taiwan Environmental Protection Administration (TEPA) standard method (NIEA S104.32B). Sediment within 0–15 cm depth was collected using a stainless crab bucket. Sampled sediment was immediately measured for oxidation-reduction potential (ORP) and then sealed in bags and transported back to the laboratory within 4 h. Wet sediment was air-dried in a laboratory hood, picked out branches and benthic biota, then ground and sieved to pass through 20 mesh sieve. Dry sediment was stored in room temperature without sunlight. Commercial AC was obtained as raw AC material (10–18 mesh). Received AC was first rinsed with DI water for several times and dried in 60°C for 24 h, then stored in a drying kettle. SAC was prepared by mixing 20 g of AC and 4 g of sulfur powder in a heating boat, heated to 400°C for 1 h and maintained for 2 h in a tubular furnace (Lindberg/Blue-M model STF55346C); 50 mL/min of nitrogen gas was constantly flowed through the furnace tube to maintain an oxygen-free environment. The prepared SAC was then sieved to 10–18 mesh and stored under the same condition as that for AC.

3.2.2 Physical and Chemical Analysis of Materials

Sediment pH was measured by pH meter (SunTex SP-2300) based on TEPA standard method (NIEA S410.62C); readings of pH value were recorded after adding 20 g of dried sediment and 20 mL DI water in a 50 mL beaker and set for 1 h. The texture of sediment was measured using a bouyoucos hydrometer [101]. The cation exchangeable capacity (CEC) of sediment was measured by available K, Na, Ca, and Mg, which were extracted



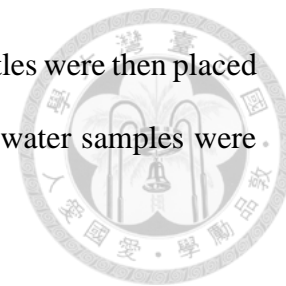
by leaching dry sediment through 1 N NH₄OAc solution, based on TEPA standard method (NIEA S201.61C). Other elements including Fe, Mn, Al, K, Na, Ca, and Mg were extracted by citrate bicarbonate buffer solution [102] and then measured by ICP-OES (Agilent 710 Series, Agilent Technology). Sediment organic content was measured through Walkley-Black wet oxidation [103]. The concentrations of NH₄⁺-N and NO₃⁻-N were measured by steam distillation using MgO and the Devarda's alloy [104].

The specific surface area and pore size distribution of the adsorbents (AC and SAC) were measured using a physisorption analyzer (ASAP 2020M, Micromeritics Inc.). Nitrogen adsorption-desorption isotherm at 77K was obtained using a Micromeritics ASAP 2020; the Brunauer-Emmett-Teller (BET) method was used to determine the specific surface area at relative pressure (P/P_0) within 0.05 to 0.3 based on ASTM D4820-96a. Micropore size distribution was determined by the quenched solid density functional theory (QSDFT) model. The surface morphology of adsorbent was measured by a scanning electron microscope (SEM, JSM-7600F, JOEL). X-ray photoelectron spectra (XPS) were recorded using a ULVAC PHI-5000 VersaProbe spectrometer with monochromatic Al K α radiation. Element analysis was carried out by an elemental analyzer (Flash 2000, Thermo ScientificTM) to measure elements including C, H, O, N, and S in the adsorbents.

3.2.3 Aqueous Adsorption Experiment

The aqueous adsorption experiment was performed resembling Wang et al. [12] In brief, analysis-grade AAS Hg standard (1000 mg/L Hg, J.T.Baker) and MeHg standard (1 mg/L, BrooksRand) were used as Hg stocks and diluted to prepare Hg²⁺ and MeHg solution, respectively. Hg solution was adjusted to pH =7.0 \pm 0.1 using NaOH (0.01–0.1 M) and HCl (0.01–0.1 M) solution. Adsorbent (AC or SAC) of 50 mg and 50 mL Hg

solution were added into clean 100 mL HDPE bottles. The HDPE bottles were then placed in a water bath shaker (30°C, 125 rpm). After the adsorption tests, water samples were collected for analysis of THg and MeHg.



3.2.4 Sediment Competition Adsorption Experiment

Hg-containing sediment in this study was prepared by spiking Hg solution in the sampled sediment. Hg stock solution (5000 mg-Hg/L) was prepared by dissolving HgCl₂ in DI water with 0.2% HCl. The spiking procedure was carried out by adding 200 g of dried sediment into a clean 400 mL glass jar; Hg stock was diluted with DI water and added to the glass jar to an anticipated Hg sediment concentration of 15–250 mg/kg. The glass jar was then filled with DI water, capped with stainless steel caps and sealed with parafilm. Spiked sediment jars were incubated for 117 d. After incubation, overlying water was removed, and sediment was freeze-dried and stored in a 4°C refrigerator.

Sediment competition adsorption experiments were carried out by adding 5 g of dried Hg sediment, 50 mg of adsorbent, and 50 mL of DI water in a HDPE bottle. The HDPE bottles were placed in the water bath shaker (30°C, 125 rpm) for 96 h. After the adsorption tests, water samples were collected, filtered through 0.45 µm mixed cellulose ester filter (DISMIC-25AS, Toyo Roshi Kaisha, Ltd), added 0.1% BrCl₂ solution and stored in glass bottles. Sediment samples and adsorbents were separated, freeze-dried, and sieved (20 mesh). Microwave digestion was then carried out using aqua regia to treat the sediment and adsorbent samples to obtain the aqueous aliquots for subsequent Hg measurement.

3.2.5 Microcosm Experiment

Vertical upflow microcosms were constructed in this study to measure the Hg release from sediment to its overlying water (Figure 3-1). Vertical microcosms were designed to

have a total height of 30 cm with an internal height of 15 cm and an internal diameter of 6 cm and with glass fiber filter at the bottom. Tap water was initially filtered with MF filter and stored in a 20 L equalizer. Filtered water was then pumped into the columns as inflow fluid by a peristaltic pump with a flow rate of 1.0 mL/min.

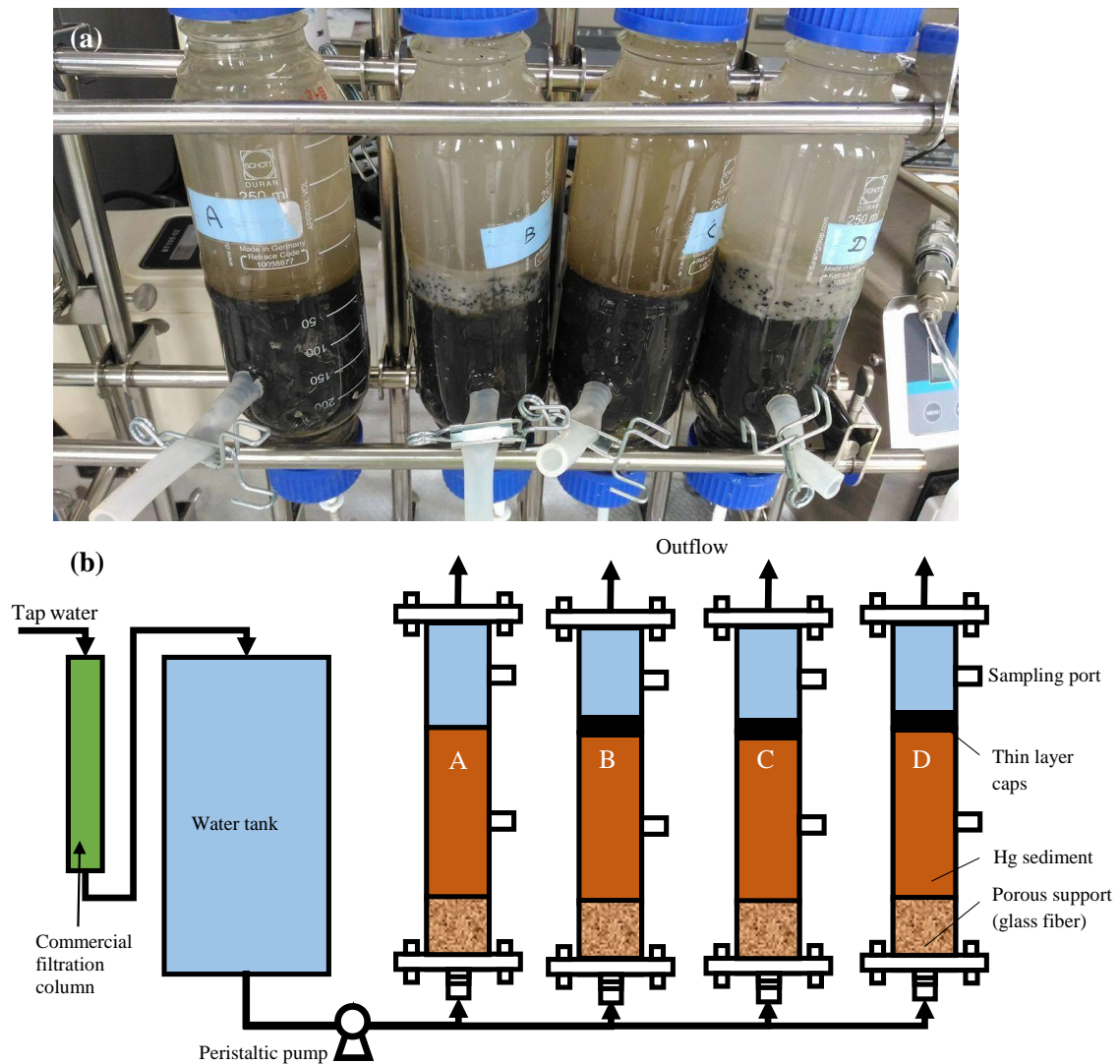
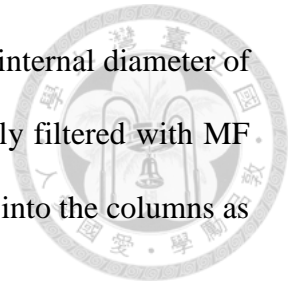
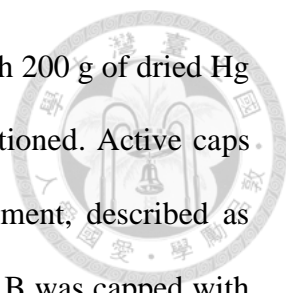


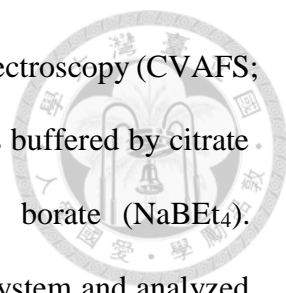
Figure 3-1. (a) photo image; (b) scheme diagram of vertical up-flow microcosms construction. Vertical flows were delivered from the bottom of the columns. The depth of sediment (TY03) is approximately 15 cm. From column A to D: (A) no caps; (B) SAC + bentonite; (C) SAC + additional TY03 sediment; (D) AC + bentonite.



Four columns were set in this study, with each column filled with 200 g of dried Hg sediment containing 250 mg-Hg/kg-sediment prepared as aforementioned. Active caps were deployed by mixing adsorbents with bentonite or clean sediment, described as follows. Column A was set with no caps as the control unit; column B was capped with the SAC (6 g; i.e. 3 wt% SAC added) and bentonite (6 g) mixture; column C was capped with the SAC (6 g) and additional TY03 sediment (6 g) mixture; column D was capped with the AC (6 g; i.e. 3 wt% added) and bentonite (6 g) mixture. To start up microcosms, dried Hg sediment was added into the column and filled with filtered water for 24 h to settle, then the mixtures of active caps were gently added on top of the column and let the mixtures be settled to the surface of the sediment. After 1 h of settling, 1.0 mL/min flow was given and counted as the operation day 1. Outflows of the systems were carried out with tubing and the top of the column was sealed without headspace. Temperature, ORP, and pH value of the overlying water were measured constantly, and water samples for THg and MeHg analyses were collected weekly.

3.2.6 Mercury and Methylmercury Analysis

Water samples for THg and MeHg analyses were filtered through 0.45 μm mixed cellulose ester filter (DISMIC-25AS, Toyo Roshi Kaisha, Ltd), then added 0.1% BrCl_2 solution (THg) or 0.2% HCl (MeHg) and stored in 50 mL glass bottles (THg) or 40 mL brown glass bottles with Teflon caps (MeHg), respectively. THg in sediment and water was measured following USEPA 1631 and NIEA W331.50B, and measurement of MeHg in sediment and water followed NIEA S341.60B and NIEA W540.50B. Before analysis, Hg in THg sample was oxidized to Hg^{2+} by stored with 0.1% BrCl . Halogens in THg sample were destructed by $\text{H}_3\text{NO}_3 \cdot \text{HCl}$, and final reduction of Hg^{2+} to Hg^0 was completed by SnCl_2 . The sample was purged and Hg^0 was collected on a gold trap. After thermal



desorption, the Hg^0 was injected to cold vapor atomic fluorescence spectroscopy (CVAFS; Brooks Rand Automated Total Mercury System). MeHg sample was buffered by citrate buffer, and MeHg was ethylated by adding sodium tetraethyl borate (NaBEt_4). Ethylmercury was volatile and thus carried through purge and trap system and analyzed by GC/CVAFS (Brooks Rand MERX Integrated Automated MeHg Analyzer). Quality assurance (QA) and quality control (QC) were checked by analyzing duplicate samples, quality control samples, and spiked samples from each batch.

3.3 Results and Discussion

3.3.1 Characteristics of Sediment and Adsorbent

The characteristics of sediment (TY03) are listed in Table S3-1. TY03 had a pH value of 5.23 and soil organic content (SOC) of 3.66 wt%. Organic content in sediment is an important parameter for adsorption. As shown in previous research, SOCs of sediments have been observed as low as 1–2%, while can be as high as 15–20% [65, 105, 106]. Therefore, TY03 may be considered acidic sediment with relatively low organic content. THg of TY03 was averaged 0.6232 mg/kg. The texture of sediment can be categorized as sandy loam with sand, silt, and clay content of 73.6, 9.6, and 16.8 wt%, respectively.

The characteristics of adsorbent AC and SAC including BET surface area, total pore volume, median pore width, and element content (C, H, O, N, S) are shown in Table 3-1, indicating that the characteristic of ACs was different after sulfur treatment. Raw AC had a high specific area of 818.3 m^2/g . After sulfurization, the BET specific area decreased to 728 m^2/g for SAC. Similar results have been observed in several studies [12, 14, 41, 74]. Asasian and Kaghazchi [74] reported that sulfurization with elemental sulfur to coal-based AC resulted in a decrease in surface area by 58% (from 828 to 596 m^2/g). Wang et

al. [12] also observed a marked decrease of surface area by 47% (from 1884 to approximately 1000 m²/g) as sulfurizing the coconut AC with elemental sulfur. In this study, only 10.9% of surface area were lost, the reason may be due to the large granular size (i.e., 10–18 mesh) of AC leading to less block and destruction of the internal porous structure of AC. Shifting of the average pore width toward a larger value and a decrease in total pore volumes were also observed after sulfurization of AC. Comparing the results from surface area analysis and SEM images (Figure S3-1), it may suggest that the reduction of surface area was mainly due to the collapse or block of micropores by heating and sulfur attachment. QSDFT micropore structure analysis (Figure 3-2) supported the reduction of micropores within a pore width of 0.5–1.0 nm after sulfurization. Additionally, the morphology of AC and SAC obtained by SEM images showed no significant difference in the surface structure after sulfurization.

Tables 3-1. Physical and chemical properties of precursor AC and resulting SAC.

	BET surface area	Total pore volume	Mean pore width	C	H	O	N	S
	(m ² /g)	(cm ³ /g)	(nm)	(wt%)				
AC	818.4	0.462	0.9454	78.88	1.41	4.52	0.73	0.47
SAC	728.1	0.416	0.9809	75.42	1.22	6.32	0.73	4.10

After sulfurization, the sulfur content increased from 0.47 to 4.09 wt%. This content was smaller compared to some SAC with sulfur content as large as 10–22 wt% reported in preview research [12, 74] because we intentionally kept the sulfur content less than 5 wt%. By doing so, most of the surface area and pore volume can be maintained because the pores were not markedly blocked by the impregnated sulfur. The sulfur content within

4–5 wt% should be sufficient for Hg capture with various sulfur functional groups in the SAC based on XPS results (Figure 3-3). The deconvoluted XPS S_{2p} signals at binding energies of 163.90, 164.75, 165.24, 166.36, 167.88, 168.67, and 169.41 eV corresponded to functional groups such as sulfide (C-S-C) + thiophene (C-S-C) + thioethers (C-S-C) + mercaptans (C-SH), disulfide (C-S-S-C), sulfinyl group ($C_2S=O$), sulfinyl group ($C_2S=O$), sulfone ($C_2S(=O_2)$), sulfone ($C_2S(=O_2)$), and sulfonate (C-SO₃) reported in previous studies[12, 107-109]. Hsi et al. [110] suggested that impregnated elemental sulfur would remain mainly as elemental sulfur groups on the surface of carbon in the heating condition of 250°C; as temperature increased to 650°C, increasing organic sulfur groups was observed.

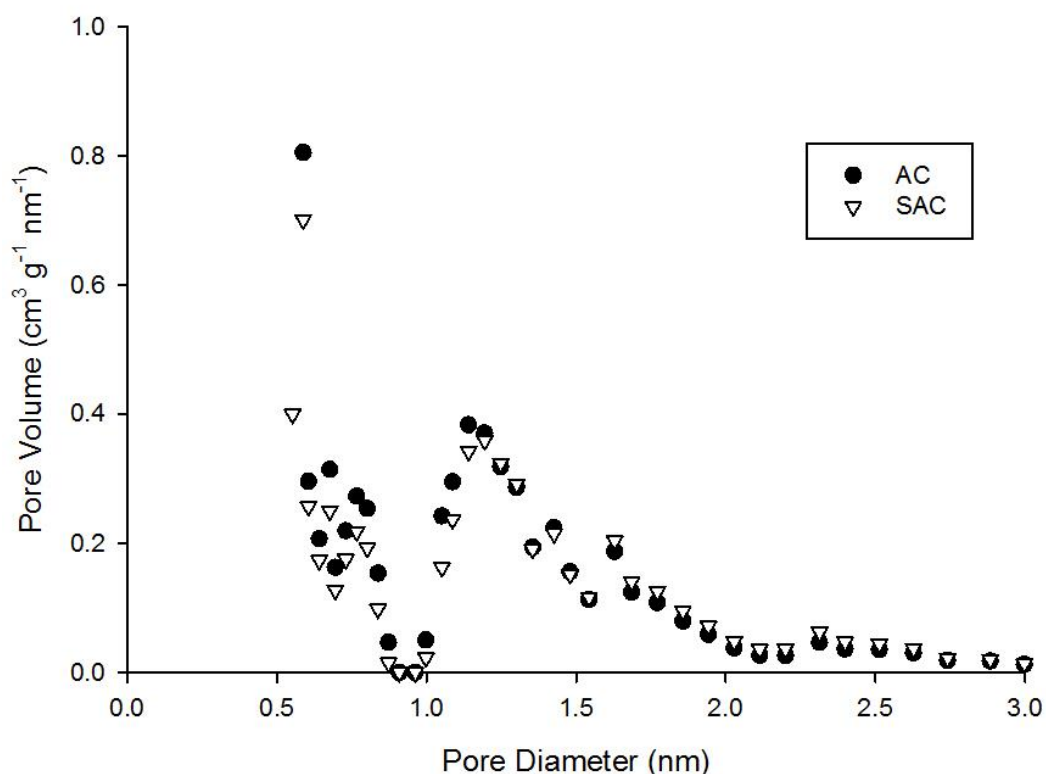


Figure 3-2. Micropores size distribution of raw AC and SAC based on QSDFT model.

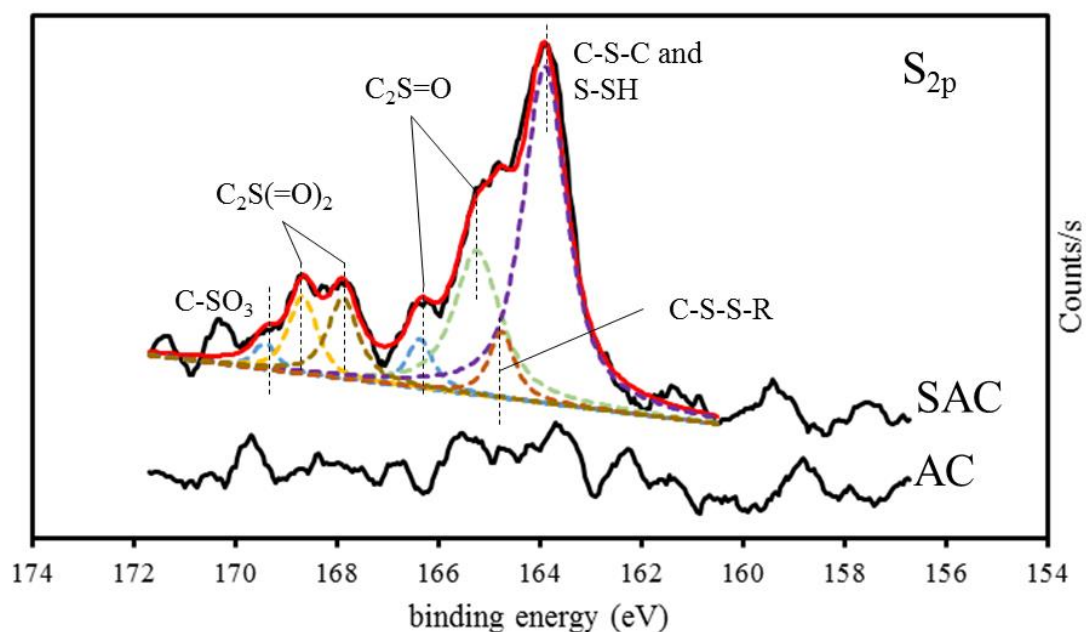


Figure 3-3. Deconvoluted S_{2p} peak for AC and SAC.

3.3.2 Aqueous Adsorption Experiment

Kinetic adsorption tests were carried out with Hg^{2+} adsorbed to AC and SAC (Figure 3-4). The experimental results suggested that about 81% of THg adsorption occurred within the first 6 h, with removal efficiency of Hg^{2+} at approximately 56.3 and 79.1% by AC and SAC adsorption, respectively. The equilibrium was reached at a time between 16 and 24 h. The adsorption rate appeared to be slower due to the larger size of granular AC (i.e., 10–18 mesh), as compared to previous research. For example, Li et al. [13] observed 87% of total Hg adsorption in the first 3 h, achieving equilibrium at around 10 h.

The experimental data were further fitted by pseudo-first and pseudo-second order kinetic models, for which the equations were described as below:

Pseudo-first order rate equations:

$$\frac{dq_t}{dt} = k_{S1}(q_e - q_t) \quad (\text{eq. 1})$$

$$\log(q_e - q_t) = \log(q_e) - \frac{k_{S1}}{2.303} t \quad (\text{eq. 2})$$

Pseudo-second order rate equations:

$$\frac{dq_t}{dt} = k_{S2}(q_e - q_t)^2 \quad (\text{eq. 3})$$

$$\frac{1}{(q_e - q_t)} = \frac{1}{q_e} + k_{S2}t \quad (\text{eq. 4})$$

Whereas q_t = sorption of sorbate concentration on the sorbent at given time t ; q_e = sorption of sorbate concentration on the sorbent at equilibrium state; k_{S1} =rate constant for pseudo-first order model; k_{S2} =rate constant for pseudo-second order model.

Pseudo-first and second order models can, therefore, being employed by eq. 2 and 4 to describe the adsorption data. The kinetic parameters were calculated and shown in Table 2-2. Both the adsorption data of AC and SAC had a better fitting to the pseudo-first order model ($R^2=0.9803$ and 0.9827 , respectively) than to the pseudo-second order model ($R^2= 0.9318$ and 0.8636 , respectively). The pseudo-first order kinetic constant for AC and SAC is 2.994×10^{-3} and $3.224 \times 10^{-3} \text{ min}^{-1}$, respectively, indicating that SAC had a faster rate of reaching adsorption equilibrium than AC. This adsorption rate appears to be lower than previous research [13], but it is in prediction since the AC used in this research is granular ($> 300 \mu\text{m}$ in diameter) rather than in powder ($< 300 \mu\text{m}$ in diameter). Coarser AC has been long regarded slower and less effective in adsorption reaction as compared to finer AC [5, 9, 47]. Zimmerman et al. [47] discovered that GAC (400–1700 μm in diameter) was less effective in reducing hydrophobic organic contaminant bioaccumulation in one-month tests. Cornelissen et al. [9] compared different field tests and found that finer AC ($<45 \mu\text{m}$ in diameter) showed higher adsorption effectiveness than coarser AC (75–300 μm in diameter) but less capping stability. Although slower



adsorption rate of GAC was observed in previous studies and in this work, it is still reasonable to use coarser GAC because it is more stable to serve as the thin layer capping material [9].

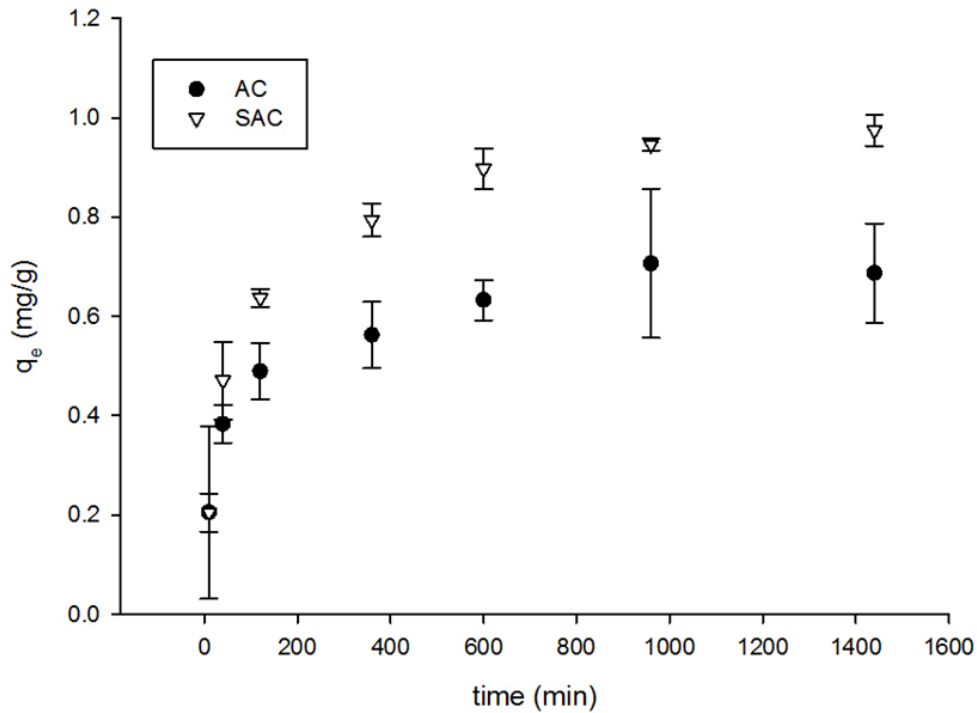
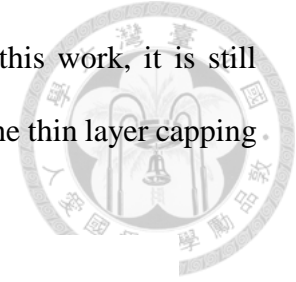
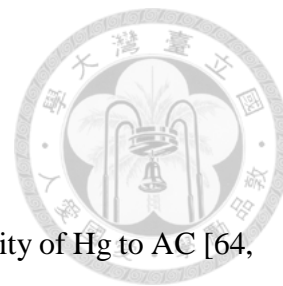


Figure 3-4. Hg^{2+} adsorption by AC and SAC as a function of time. For here $[\text{Hg}^{2+}] = 1$ mg/L, Hg solution = 50 mL, adsorbent dosage = 50 mg, and $\text{pH} = 7.0 \pm 0.1$.

Table 3-2. Fitting parameters of AC and SAC adsorption by pseudo-first and second

Temperature (°C)	Hg concentration (mg Hg/L)	Adsorbent	Pseudo-first order			Pseudo-second order		
			q_e (mg/g)	k_{s1} (min^{-1})	R_1^2	q_e (mg/g)	k_{s2} (g/mg- min)	R_2^2
30	1.0	AC	0.6232	0.002994	0.9803	0.5237	0.0249	0.9318
		SAC	0.8040	0.003224	0.9874	1.1130	0.0327	0.8636

order reaction models.



Distribution coefficient (K_D) is a useful tool to describe the affinity of Hg to AC [64, 65] in a linear relationship, defined as the ratio of the concentration of sorbate sorbed to the sorbent divided by its concentration in solution. This concept includes an assumption that the solute concentration is very low that the sorption of sorbent only controls by concentration of solution rather than remaining sorption sites on the sorbent. It was recently discovered that the distribution of adsorbate on black carbon should be considered with two separated mechanisms (adsorption and partition) [111], and by definition, Hg uptake by black carbon should be mainly governed by adsorption mechanism because Hg uptake capacity does not increase after reaching maximum capacity, which was observed in previous research [13, 73, 74]. However, it may still be plausible to introduce K_D concept since the Hg concentration used in this study was very low and far from reaching the maximum adsorption capacity of AC.

Adsorption isotherms of AC and SAC are shown in Figure 3-5. The results showed that K_D of SAC (9.426×10^4 , $R^2=0.996$) to Hg^{2+} was more than two-fold larger than that for AC (i.e., 3.694×10^4 , $R^2=0.958$). Notably, the affinity of ACs to MeHg was almost 10-times larger than that to Hg^{2+} , as shown in our results, that K_D for AC and SAC to MeHg was 2.254×10^5 ($R^2=0.983$) and 7.661×10^5 ($R^2=0.834$), respectively. The reason for SAC having greater adsorption affinity to Hg^{2+} than AC is expected. As aforementioned, Hg can be immobilized by sulfide to form highly stable HgS (i.e., $\log K \approx 52.7-53.3$) [23]. SAC had larger sulfur content (4.09 wt%) than that of AC (0.47 wt%). Additionally, based on the XPS results, SAC possessed various sulfur functional groups; all of which lead to the higher affinity to Hg^{2+} for SAC than for AC [12, 13, 74].

On the contrary, results of AC and SAC having higher affinity to MeHg than Hg^{2+} in this work is not completely consistent with those from previous studies. Gomez-Eyles et al. [64] compared K_D of various black carbons to MeHg and Hg and found that six materials with Hg K_D to MeHg K_D ratios significantly greater than one, two materials with the ratios close to one, and six materials with the ratios significantly smaller than one. These results may suggest that adsorption of Hg^{2+} and MeHg involves different mechanisms.

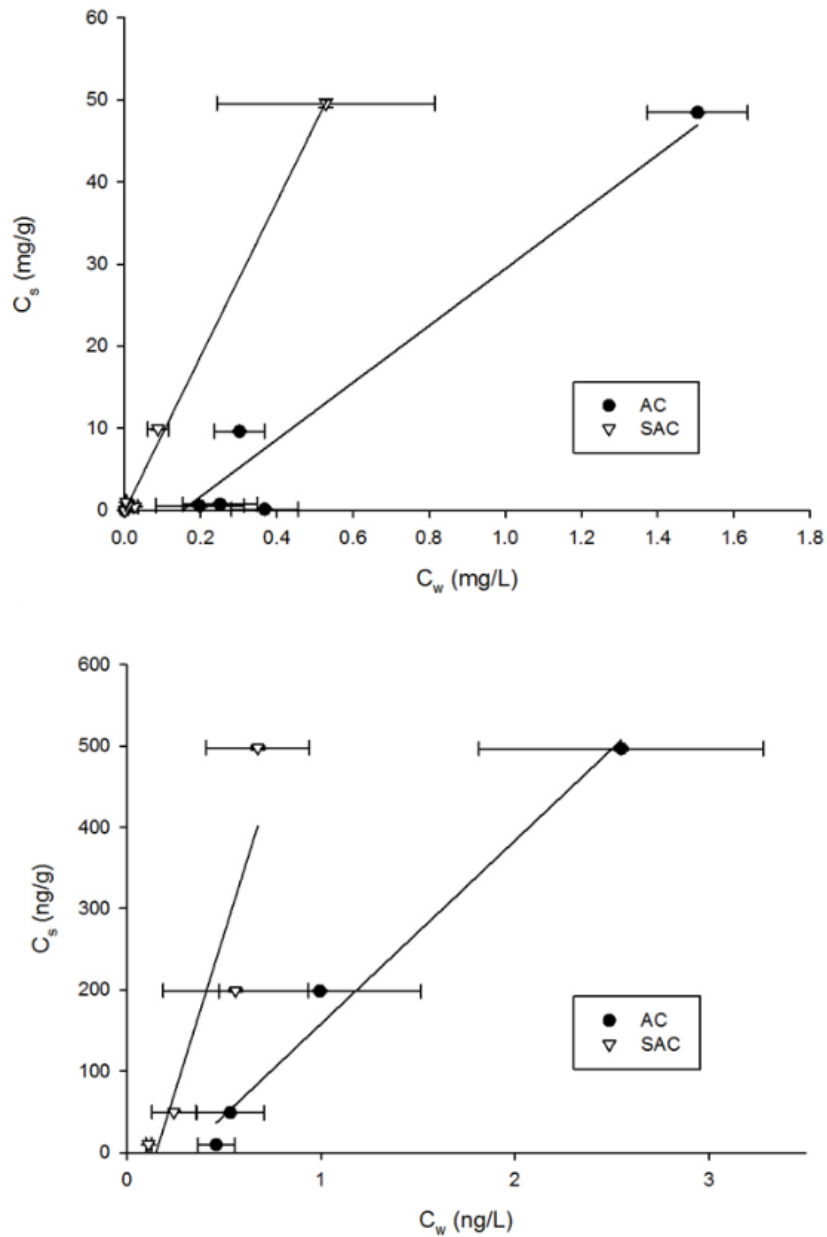
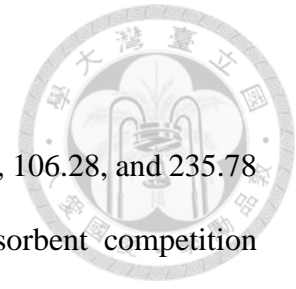


Figure 3-5. Adsorption isotherm of AC and SAC adsorbing (a) Hg^{2+} and (b) MeHg.

Adsorption time = 24 h. Hg solution = 50 mL, adsorbent dosage = 50 mg, pH = 7.0 ± 0.1

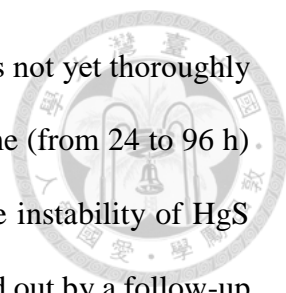
3.3.3 Sediment Competition Adsorption Experiment



Three spiked Hg-containing sediments with Hg content of 14.23, 106.28, and 235.78 mg/kg were prepared by 117-d incubation, and the sediment/adsorbent competition adsorption tests were carried out by measuring Hg concentrations in the sediment and porewater for 1, 3, and 6 wt% activated carbon addition, which is shown in Figure 3-6. Under the condition of 1 wt% adsorbent dosage (Figure 3-6a), porewater THg was reduced by 73.4–96.2% by AC and 83.25–95.21% by SAC in the sediment with Hg range of 14.23–106.28 mg/kg. The decrease of effectiveness at 235.78 mg/kg may be due to reaching the equilibrium adsorption capacity of AC and SAC. At 3 wt% adsorbent amendment (Figure 3-6b), AC reduced 91.9–99.9% porewater THg in the Hg sediment range of 106.28–235.78 mg/kg, while SAC reduced 86.4–90.5% porewater THg. Notably, at the adsorbent dosage 3–6 wt%, the enhancement in porewater THg reduction was less obvious as compared to the dosage from 1–3 wt%.

Surface water Hg concentration of 1.3 $\mu\text{g/L}$ was set by Preliminary Remediation Goal (PRG) for an ecological endpoint [112], and 3 wt% dosage of AC can cause porewater THg concentration beneath this level throughout the tested sediment Hg range in this study. It indicates that 3 wt% of AC or SAC could be an optimum dosage for thin layer capping remediation of Hg sediment with wide Hg concentration range up to 235.78 mg/kg, in terms of amount and cost as compared to amending 6 wt% adsorbent.

Surprisingly, amendment of SAC led to lesser porewater THg reduction as compared to that of AC, especially at the dosages of 3 and 6 wt%, which is inconsistent to the results obtained from our batch-scale aqueous adsorption tests aforementioned. Notably, for the sediment with Hg content of 14.23 mg/kg, 1 wt% of SAC addition significantly reduced porewater Hg to 83.3%; but with the amendment of 3 and 6 wt%, the reduction ratio was



only -31.3 and 6.4%, respectively. The reason of the inconsistency is not yet thoroughly understood, but may be attributed to the elongation of adsorption time (from 24 to 96 h) and the influence of inherent components in sediment leading to the instability of HgS complexes on the SAC surface. However, this possibility can be ruled out by a follow-up test (Figure S3-2) showing that no obvious Hg was re-dissolved in the aqueous phase for up to 72 h, and no aggregation was observed by measuring the aqueous samples filtered by different pore-sized membranes.

Another reason causing the lesser porewater THg reduction by SAC may be due to the re-dissolution of HgS_(s) nanoparticles after adsorption on SAC, triggered by sediment. This mechanism has not yet reported but is reasonable in explaining the inconsistency of aqueous adsorption and sediment competition adsorption experiments in this study. Hg is well-known to have high affinity to sulfur. However, the formed fine particles of HgS_(s), via interaction of Hg with impregnated elemental sulfur present in SAC surface, may dissolve again into Hg²⁺ and SO₄²⁻ in an oxic environment [113, 114]. In addition, as sulfur exists in an aqueous environment, Hg²⁺ and S²⁻ could precipitate and form β-HgS_(s) nanoparticles at sulfur concentration even as low as 1 nM [23]. Without interference, β-HgS_(s) nanoparticles would gradually aggregate forming larger particles with a diameter of 200–500 nm [114]. However, when the aqueous environment exists dissolved organic matter (DOM), the aggregation of β-HgS_(s) nanoparticles may be inhibited and even re-dissolved to the aqueous phase [115].

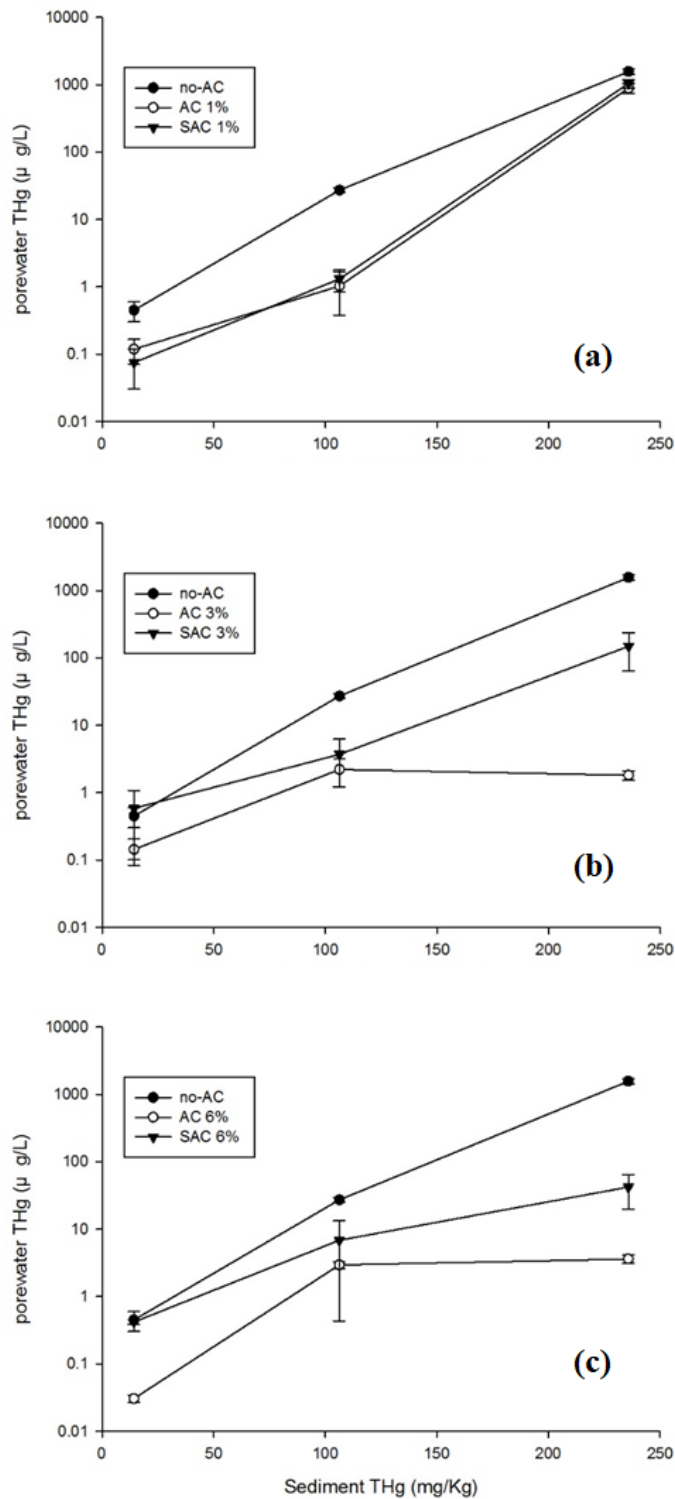


Figure 3-6. Hg concentrations in porewater versus in sediment at (a) 1 wt%; (b) 3 wt%; (c) 6 wt% adsorbent addition based on sediment competition adsorption test. DI water is 50 mL and Hg sediment is 5.0 g.

As aforementioned, SAC had higher Hg^{2+} and MeHg affinity compared to AC based on aqueous adsorption tests and the reason was attributed to the stable bonding of Hg-S. As reported by Liu et al. [116], Hg has high tendency to bind to carbon-sulfur functionality such as C-S-S-C, C-S-C, and C-SH, which are abundant in SAC based on the XPS examination. However, in the sediment adsorption experiments, as the adsorption time increased from 24 to 96 h, with the possible release of DOM from sediment, sulfur functional groups may be destructed and dissolved, thus causing the Hg to form Hg-S-DOM cluster, as proposed in Figure 3-7. Consequently, The porewater THg reduction by SAC amendment was less pronounced as compared to that by AC amendment.

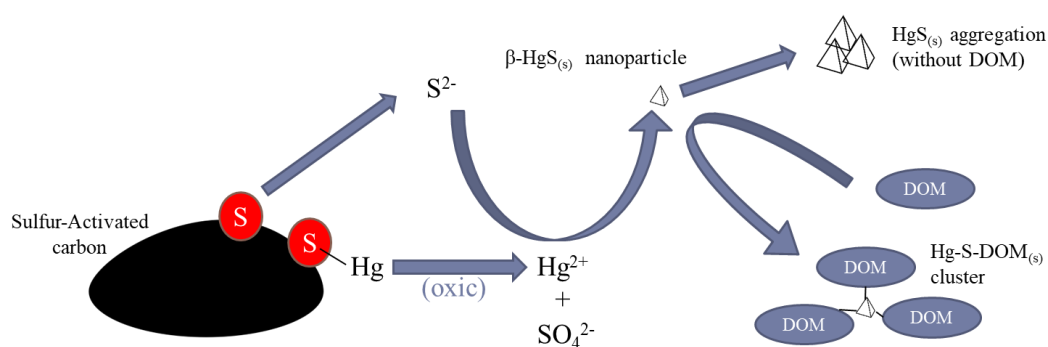
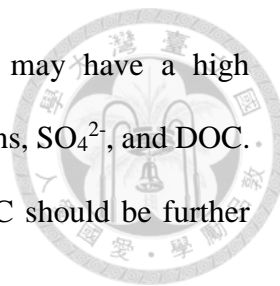


Figure 3-7. Proposed adsorption/desorption mechanisms of Hg adsorption on SAC in the sediment environment.

Although a similar phenomenon was observed previously, this is the first study to report the potential sulfur release from sulfur-impregnated activated carbon during sediment competition adsorption tests causing an increase in porewater Hg concentration. Liu et al. [116] also reported the SO_4^{2-} released from biochar causing Hg adsorption ability to decrease in a 48 h adsorptions tests. Similarly, Liu et al. [117] conducted

microcosms experiments and discovered that the release of Hg may have a high correlation to aqueous parameters such as the concentrations of Fe ions, SO_4^{2-} , and DOC. The influence of these parameters on Hg release from AC and SAC should be further comprehended.



3.3.4 Microcosm Experiment

During the 86-d microcosms operation, pH, ORP, temperature, and flow rate were recorded (Figs. S3-3–S3-6). In brief, the temperature of microcosms was maintained at around 25°C, pH value was typically in the range of 6.6–7.0, with few exceptions at the range of 6.2–7.4. Original ORP was around -200 to -300 mV after the operation started, ORP was dramatically increased and maintained at around 0–100 mV due to the supplied water had greater ORP.

Overlying water THg and MeHg concentrations of microcosms during operation are shown in Figure 3-8. As soon as the active caps deployed, a dramatic decrease of overlying water THg concentration by 91.2–95.9% (not shown in the graph) and MeHg (77.8–99.8%) in capped microcosms was observed at day 2. Throughout the operation period, the influence of caps to overlying water THg concentration was insignificant between days 17 and 47. While after day 47, THg started to leach and caused high amount of Hg in overlying water, with the highest THg concentration at day 63 recorded at 0.791, 0.281, 0.654, and 0.417 $\mu\text{g/L}$ for those from column A (control), column B (SAC+bentonite), column C (SAC+TY03), and column D (AC+bentonite), respectively. These leaching processes were also observed in Liu et al. [117] as leaching of Hg occurred at around day 80, with high correlation with the rising of Fe and SO_4^{2-} concentrations. Notably, previous studies have shown that re-dissolution of Hg-S complexes into Hg^{2+} and SO_4^{2-} may occur in an oxic environment [113, 116]. Therefore, with the increase of

ORP in our microcosms, the adsorbed Hg may be re-dissolved into the aqueous phase, which may partly lead to the increase in THg concentration after 47 d of operation time, especially for Columns A (control) and D (AC + bentonite) (Figure 3-8).

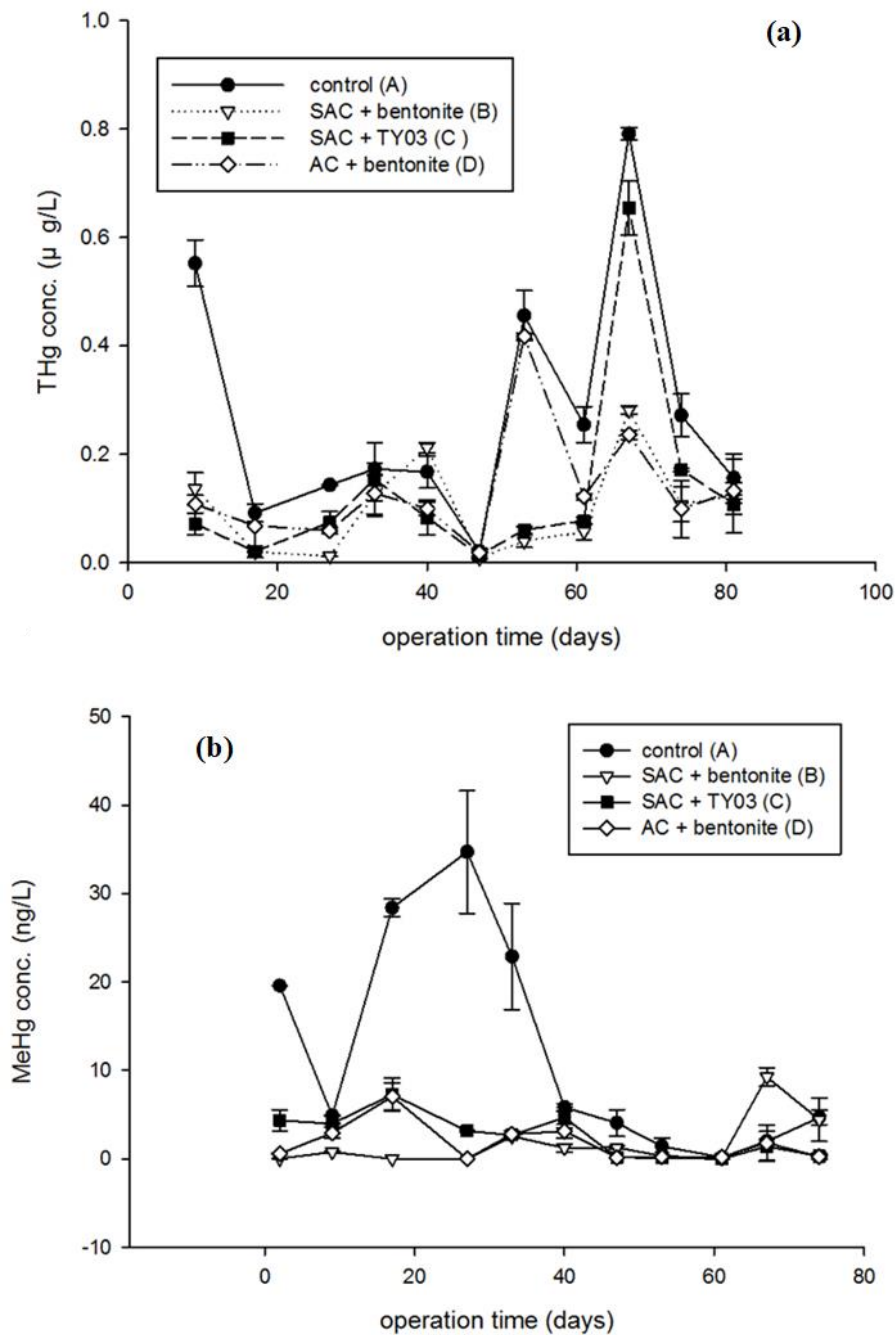
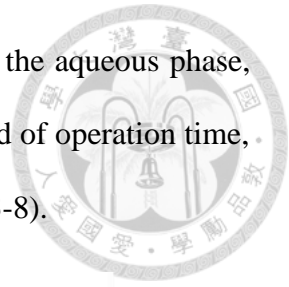
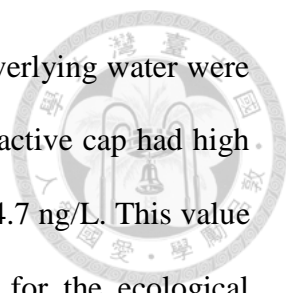


Figure 3-8. Overlying water (a) THg and (b) MeHg concentrations of vertical up-flow microcosms during operation.



Compared to THg, different inhibition patterns of MeHg into overlying water were observed in microcosms. As in the first 40 d, the sediment without active cap had high overlying water MeHg, with the highest concentration recorded as 34.7 ng/L. This value was 13 times higher than the Preliminary Remediation Goal set for the ecological endpoint (i.e., 2.6 ng/L) [112]. Microcosm results also showed that the presence of active caps had great leaching inhibition ability to MeHg, with MeHg reduction efficiency of higher than 79.1%. After day 60, all microcosms had relatively low MeHg, it may be due to increasing ORP in the system, causing microbiome shift, thus reducing biomethylation.

The microcosm results further demonstrated that using SAC or AC as thin layer capping can reduce the overlying water concentration of MeHg to a level far below ecology threat consideration, thus is applicable in reducing the risk from Hg-contaminated sediment since MeHg is the most toxic species of Hg.

3.4 Summaries

Feasibility of using raw and sulfur-impregnated activated carbon (SAC) for remediation of Hg sediment was evaluated. Prepared SAC had high porosity with efficient micropores, and sulfur on SAC was insufficient content and with various forms. Aqueous Hg adsorption results indicated that SAC had higher affinity to both Hg²⁺ and methylmercury (MeHg) compared to the raw AC precursor in 24 h of equilibrium time. However, as compared to the results from sediment competitive adsorption tests, the Hg adsorption performance of SAC was reduced with elongation of adsorption time, and possibly by the presence of certain components in the sediment environment leading the release of Hg. Fe ions, SO₄²⁻, and dissolved organic matter have been reported and could cause marked impacts on Hg sequestration; therefore should be further clarified. Microcosm studies showed that all combinations including SAC+bentonite, SAC+TY03,

and AC+bentonite caps had good efficiency in reducing the MeHg concentration of overlying water. In contrast, active caps did not show corresponding high effectiveness in reducing the overlying water THg. Again, the release of Hg may stem from the re-dissolution of formed Hg-S complexes in SAC and need to be further examined.

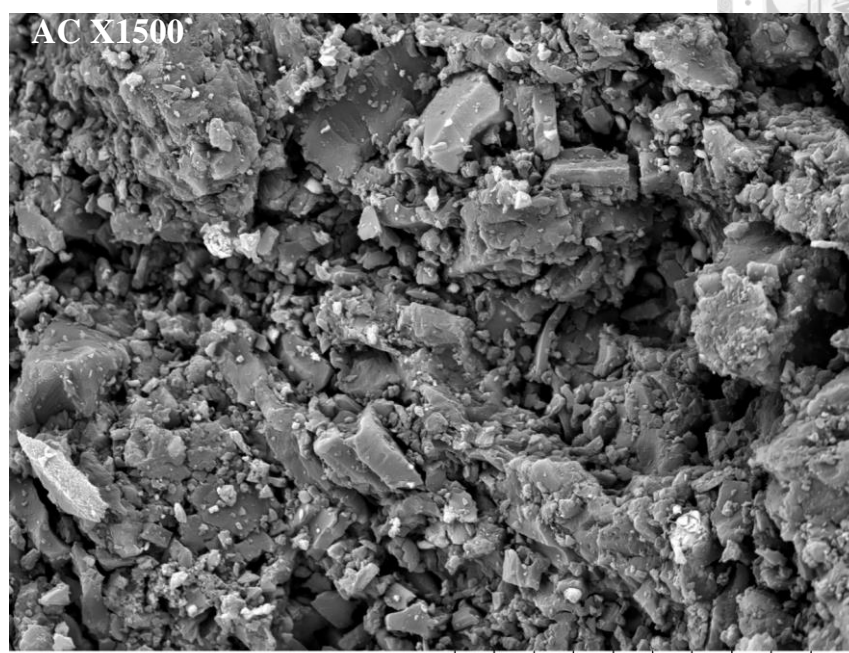
SAC shows higher affinity toward Hg^{2+} and MeHg in short-term aqueous experiments than raw AC; nevertheless, sulfur-containing adsorbents do not necessarily enhance inhibition of Hg release from the sediment environment. In desire of applying SAC or other thiol-functionalized materials to thin layer capping, one should carefully evaluate the long-term effects in the complex conditions. A thorough examination on the stability of various sulfur functional groups on SAC as they interact with Hg species under aqueous sediment environment containing various components should be further conducted.

3.5 Supporting Information

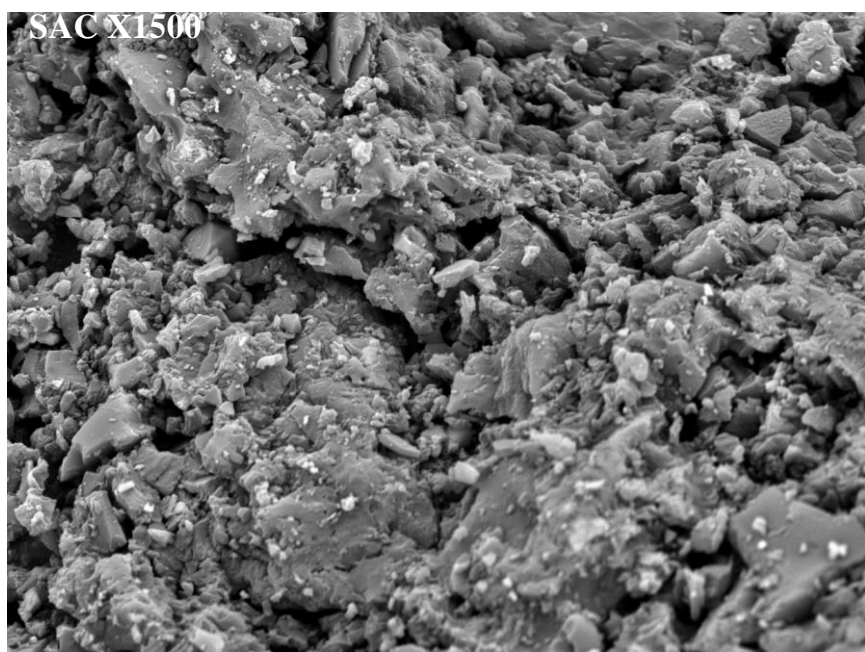


Table S3-1. Characteristics of sediment TY03 sampled from a river in Northern Taiwan.

Sediment Code	TY03
Water content	2.70±0.00 wt%
Sand	73.6±0.6 wt%
Silt	9.6±0.1 wt%
Clay	16.8±1.6 wt%
pH	5.23±0.01
ORP	-93.2 mV
SOC	3.66±0.09 wt%
CEC	34.66±0.47 cmol/kg
Available NH₄⁺-N	0.273±0.001 mg/g
Available NO₃⁻-N	0.0054±0.0003 mg/g
Fe	49.67±2.61 mg/g
Mn	0.39±0.04 mg/g
Al	6.36±0.34 mg/g
K	3.97±0.17 mg/g
Na	3.03±0.60 mg/g
Ca	4.81±0.60 mg/g
Mg	0.20±0.05 mg/g
Hg	0.6232±0.0089 mg/kg



2017/07/10 H x1.5k 50 um



2017/07/10 H x1.5k 50 um

Figure S3-1. SEM images of raw AC and AC after sulfurization (i.e., SAC) under x1500 magnification.

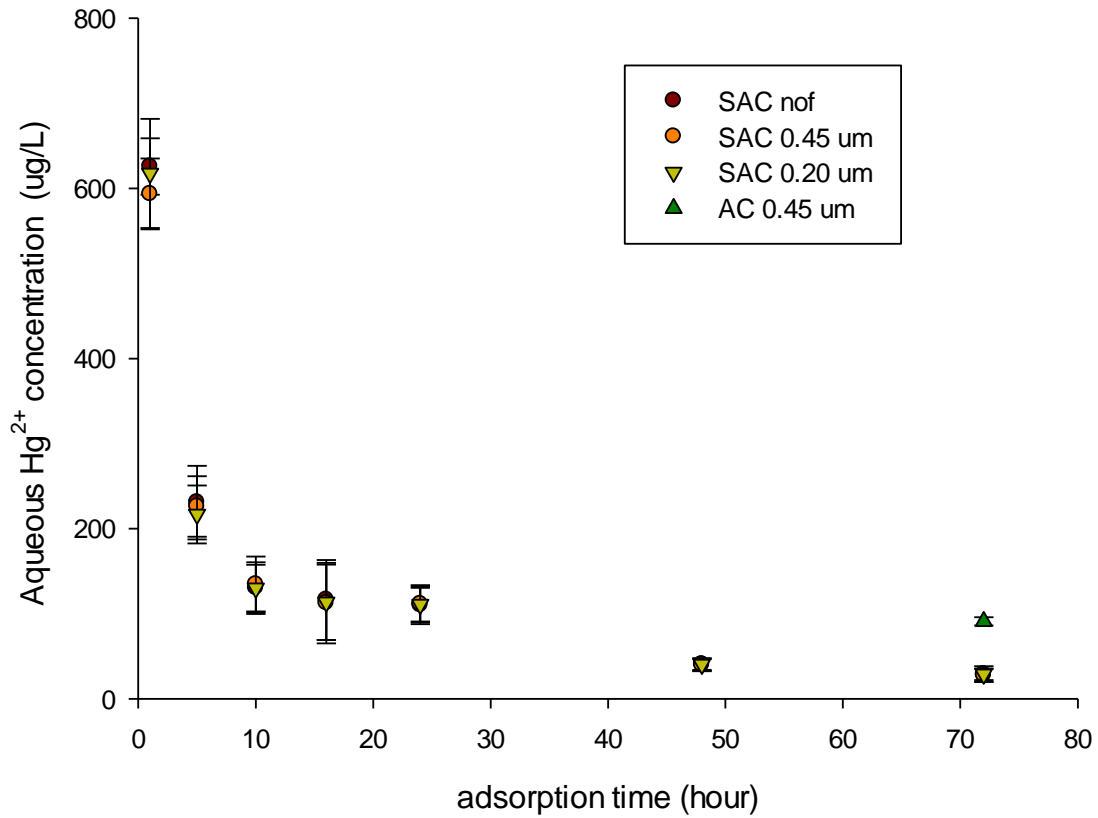


Figure S3-2. Follow-up aqueous adsorption tests of AC and SAC to justify the discussion in Section 3.3. The adsorption condition is as the same as the aqueous adsorption tests described in Section 2.3. $[Hg]_0 = 1 \text{ mg/L}$, Temperature = 30°C , 125 rpm, $n = 3$. Adsorption time was extended to 48 h and 72 h. Aqueous samples obtained with different pore-sized filtration are compared. SAC: sulfurized activated carbon; AC: raw activated carbon; “nof”: no filtered treatment after adsorption test; “0.20”: 0.20 μm filtered treatment; “0.45”: 0.45 μm filtered treatment.

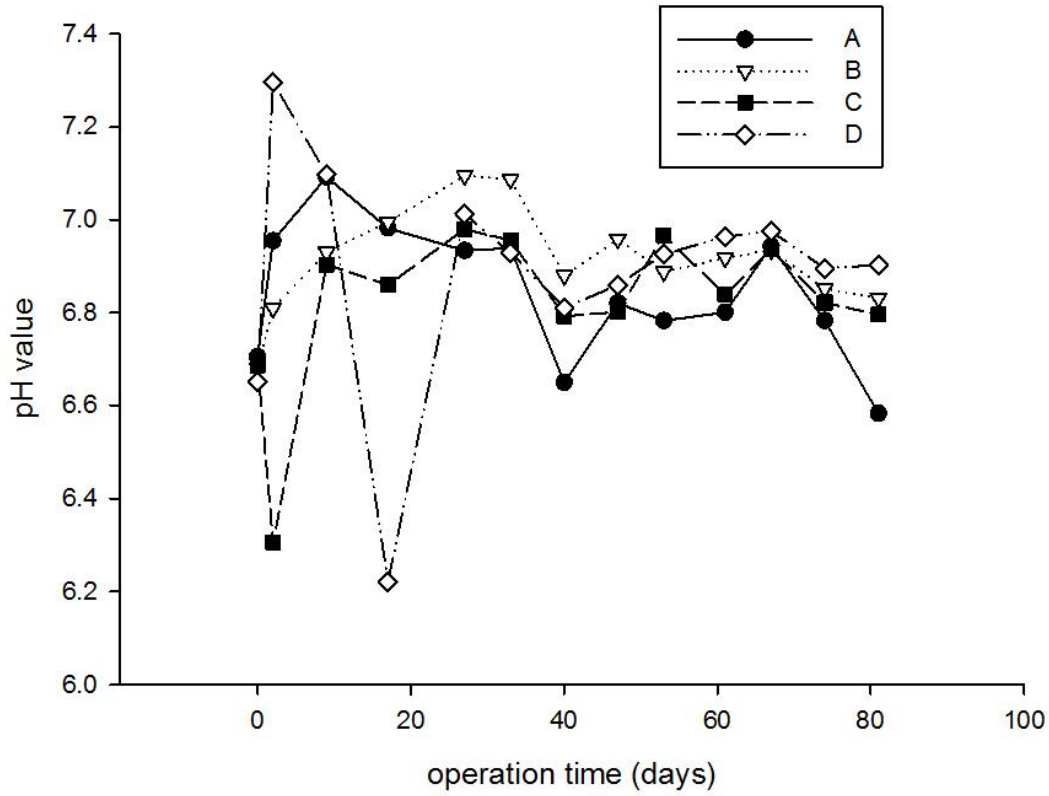


Figure S3-3. pH value variation of four vertical up-flow microcosms (A–D) during the operation of 86 days. From column A to D: (A) no caps; (B) SAC + bentonite; (C) SAC + additional TY03 sediment; (D) AC + bentonite.

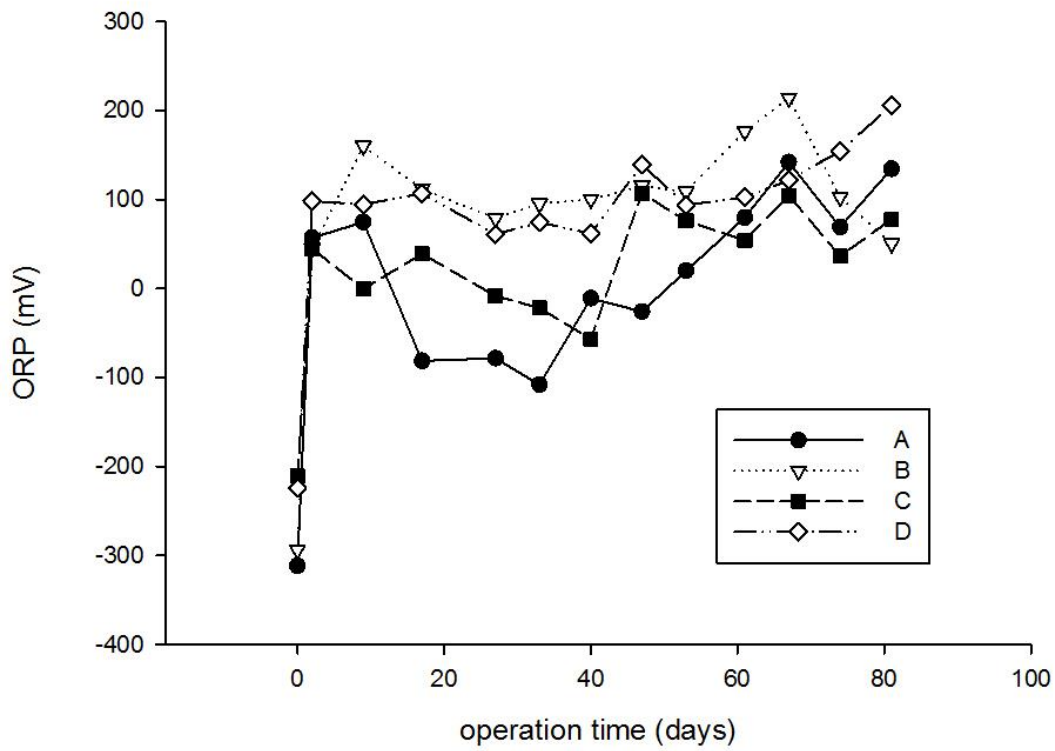


Figure S3-4. ORP variation of four vertical up-flow microcosms (A–D) during the operation of 86 days. From column A to D: (A) no caps; (B) SAC + bentonite; (C) SAC + additional TY03 sediment; (D) AC + bentonite.

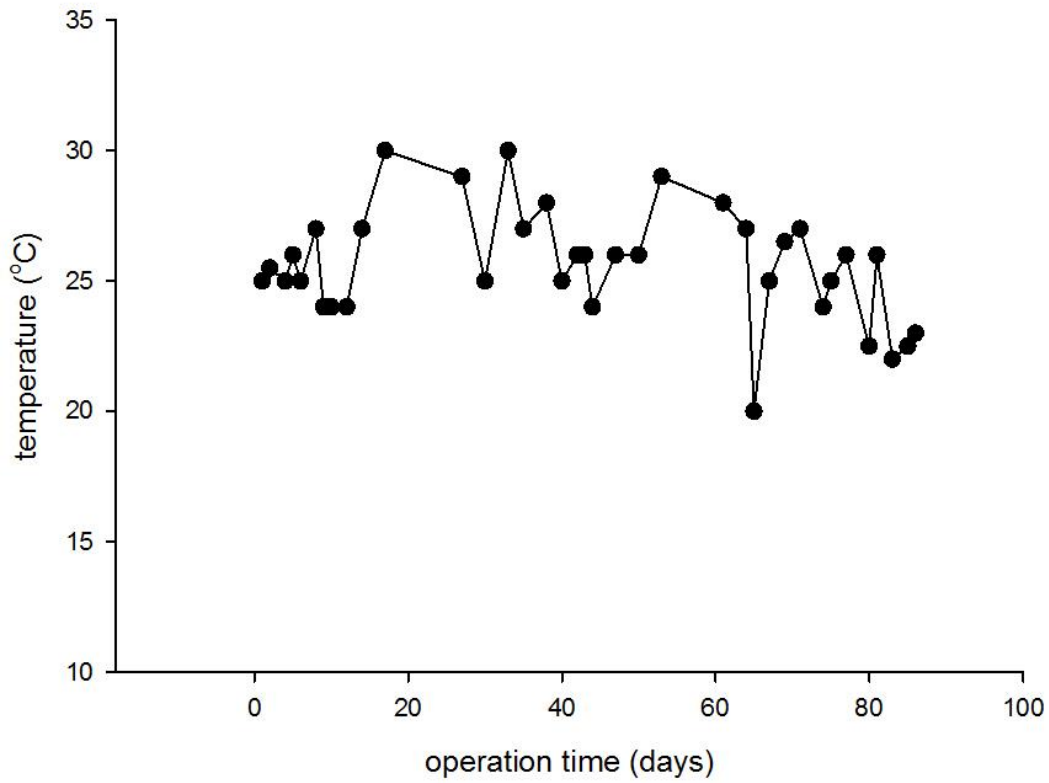


Figure S3-5. Temperature variation of four vertical up-flow microcosms (A–D) during the operation of 86 days. From column A to D: (A) no caps; (B) SAC + bentonite; (C) SAC + additional TY03 sediment; (D) AC + bentonite.

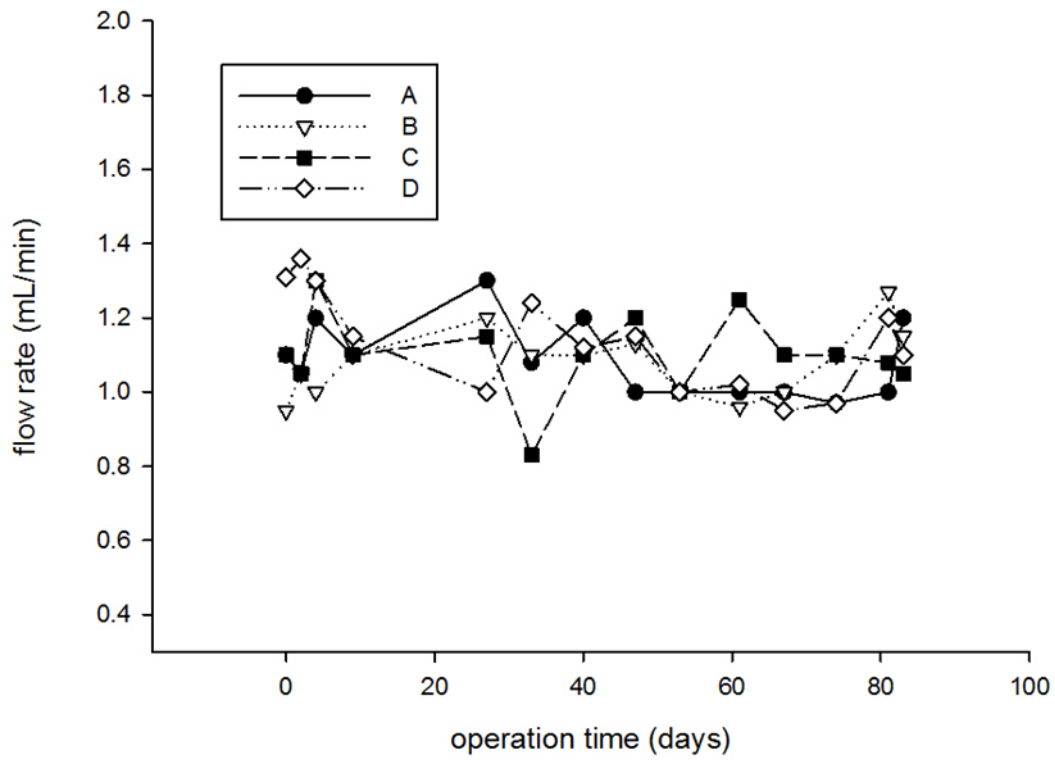
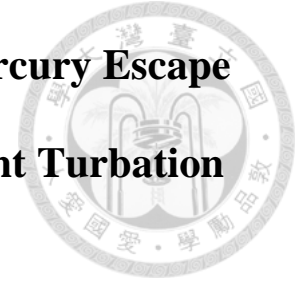


Figure S3-6. Flow rate variation of four vertical up-flow microcosms (A–D) during the operation of 86 days. From column A to D: (A) no caps; (B) SAC + bentonite; (C) SAC + additional TY03 sediment; (D) AC + bentonite.

Chapter 4 AC/clay-based Caps Reduce Mercury Escape under Horizontal Flows and Sediment Turbation

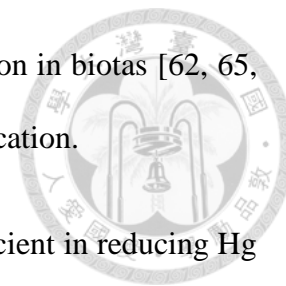


4.1 Introduction

Over decades, anthropogenic mercury (Hg) in the aquatic environment has been posing severe contamination and put the health of the environment biotas and human beings into risks. Wastewater discharge from industries (i.e. chlor-alkali and metallurgy) was particularly hazardous and has resulted in legacy Hg contamination in wetlands or estuaries worldwide [15, 27]. Although the sediment underneath water body acts as an ideal sink to retain Hg [16, 17] sediment-to-water Hg flux may continuously occur [93, 118] by occasional turbation events [15-18]. Sediments also provide an anoxic environment, facilitating the production of methylmercury (MeHg), which is a potent neurotoxin with a high bioaccumulative ability [119]. Consequently, Hg in contaminated sites was found entering the food webs and being biomagnified to each trophic level [119, 120].

In recent years, in-situ thin layer capping has emerged as a promising remediation approach as an alternative for solving the Hg contamination problems [64-66, 68, 69]. The success of applying thin layer capping to persistent organic pollutants (POPs)-contaminated sediment [8-11] has also shed light on the Hg-contaminated sediments. The feasibility of applying thin layer capping with black carbon (BC) to the Hg-contaminated sediment remediation has been evaluated in various bench-scale studies [64-66, 69, 121] and field-scale studies [8, 68]. Several BCs were found to have efficient sorption affinity to either inorganic Hg ($\log K_D = 3.0-7.0$) or MeHg ($\log K_D = 3.0-5.0$) within a certain Hg

concentration range [64, 121]. Also, reduction of Hg bioaccumulation in biotas [62, 65, 66] and porewater Hg [62, 65, 66, 121] was observed with BC application.



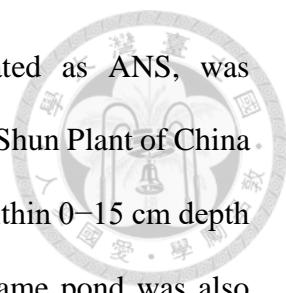
Although thin layer capping with BCs was found generally efficient in reducing Hg mobility and bioavailability, some major concerns including the capping stability and the potential risks of Hg escape from caps have been addressed [66, 68, 121]. The sediment turbations caused by bioturbation or physical erosion (e.g., tidal effect and temporal oxidation effect) have been identified as critical mechanisms in contaminant transport in the natural aquatic environment. Multiple studies have noted that inorganic Hg and MeHg were carried by fine-grained sediment from river erosion [17, 18] and tidal effects [15, 16]. Temporal oxidation event in sediment was also observed to cause Hg remobilization [121, 122].

It is intriguing how sediment turbation may affect the efficiency of the thin layer capping in treating Hg-contaminated sediment, but related studies remain little information. One of the reasons may be due to the difficulty of simultaneously quantifying turbation magnitude [94, 95] and providing a comparable condition to real site capping application. For these purposes, microcosm tests were carried out in this study to establish the crucial connection between capping stability and Hg immobilizing efficiency with sediment turbation.

4.2 Materials and Methods

4.2.1 Sorbents Preparation, Sediment Collection, and Characterization

A commercial granular AC (10–18 mesh) was selected and has been confirmed with efficient Hg sorption and leaching inhibition [121]. Bentonite, kaolin, and montmorillonite were purchased from Sigma-Aldrich® (CAS no. 1302789, 1332587, and



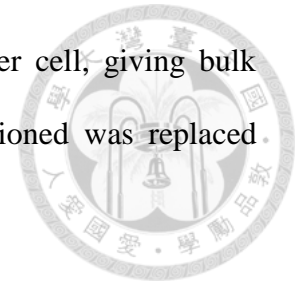
1318930, respectively). The Hg-contaminated sediment, designated as ANS, was collected from an estuary pond in a former chlor-alkali plant, the An-Shun Plant of China Petrochemical Development Corp., Tainan, Taiwan. The sediment within 0–15 cm depth was collected using a stainless crab bucket. Surface water in the same pond was also collected. Both sediment and water were transported to the laboratory (<10 h) and stored in room temperature without sunlight. Sediment was air-dried in a hood, picked out branches and benthic biotas, and ground and sieved (20 mesh). The pH and organic content of ANS sediment were 7.52 ± 0.03 and 0.80 ± 0.65 (wt%), respectively, indicating that ANS was a mildly alkaline organic poor estuary sediment (Table S4-1). The texture of pre-treated ANS belongs to sandy loam, and total Hg (THg) level was measured to be 76.0 ± 2.593 mg/kg (Figure S4-1, Table S4-1). The electrical conductivity (EC), pH, total Fe, sulfide, sulfate, chloride, THg, and MeHg of the ANS surface water were also measured (Table S4-2).

4.2.2 Artificial Vibration System

A lab-made vibration system was designed to remobilize the thin surface layer, few millimeters from the top of the sediment, in which the depth may be comparable to bioturbation [94] or tidal movement [123] in short timescale. The system was composed of commercial brushless DC vibration motors (Figure S4-2; RISUN PVN 1305D 3V) and a lab-made current controller (Figure S4-3). The motors were coated with 2–3 layers of Hg-free epoxy resin and plastic steel for waterproof (Figure S4-2). Motors were tested to create 34.2 mA of current under 3.0 V. The power output was estimated to be 102.6 mW for each motor.

During the operation of the microcosm, five motors were placed in equidistance of 6 cm to each other in each cell (Figure S4-4) and the voltage was set to 3.0 ± 0.2 V by the

controller. The total power was thus estimated to be 513 mW per cell, giving bulk turbation magnitude of 12.8 W/m². Every motor found malfunctioned was replaced within a week and recorded (Table S4-3).



It would be arbitrary to conclude this vibration system a perfect method to produce quantifiable sediment turbation, especially when more sophisticated and precise methods [95] or models [94, 124] exist. However, previously developed methods may find difficulty in applying to a more complex system. The vibration system in this study may provide a viable and straightforward method for sediment turbation quantification in a more complex system.

4.2.3 Microcosms Setup and Operation

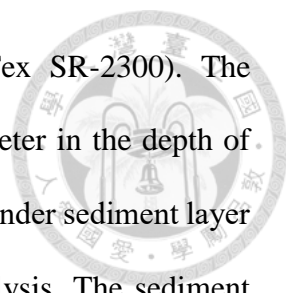
The microcosm was composed of four cells (A, B, C, and D) (Figures S4-4 and S4-5). Cell A was set without a cap as the control unit; cells B, C, and D were set with thin layer caps application (around 1.5 cm thick) composed of AC (3%; 105 g) + bentonite (3%; 105 g), AC (3%) + kaolin (3%), and AC (3%) + montmorillonite (3%), respectively. Each cell was composed with an open canal segment (50×10×10; l×w×h; cm³) on top of a sediment tank segment (40×10×10 cm³). The microcosm was designed to fill the sediment tank with 3.50 kg dry ANS sediment to approximately 9.0 cm in depth. The overlying water in the microcosm was introduced by the stored ANS surface water and set to 8.5 cm height in the open canal segment. Marks were made to locate the water line. The circular flow in each cell was carried by PE tubing, driven by a commercial submerged pump (Eden 105) in a PP water tank (1 L). The flow rate in each cell was corrected initially to 5 L/min (bulk velocity in microcosm = 58 cm/min). Also, the supplement of the overlying water was made daily by adding ANS surface water (due to sampling) or deionized water (due to evaporation or other loss) to the water line mark,

maintaining the unity of the water properties. A rectifier was provided by a plastic net bag with 200 g of ceramsite and was fixed at the inlet of overlying water in each cell. A black box was constructed around the microcosm, and the light was provided by two aquarium LED lights (10 W each) and set to a 14:10 h, light:dark cycle.

The microcosm was established before the trial (i.e., recorded as day -98) allowing the aging of the sediment (Figure S4-6, Table S4-3). The trial started (day 1) as the artificial vibration system was placed in each cell (5 motors per cell; -12.8 W/m^2 in each cell). The microcosm stabilized for days, then thin layer caps were applied (day 12) with materials aforementioned after sediment was sampled. Capping materials were premixed in ANS surface water and applied to sediment surface evenly. The horizontal flow and turbation were stopped overnight allowing caps to settle. An intermittent turbation test was carried out by stopping the vibration system during day 20–31.

4.2.4 Sample Collection and Analysis

During the trial, temperature and dissolved oxygen (DO) were measured weekly. Overlying water of each cell was sampled and filtered ($0.45 \mu\text{m}$) each week. The room temperature of the microcosm was measured by a thermometer. DO of the overlying water was directly measured by a DO meter (EXStik[®], DO600). pH, EC, total Fe, sulfide, sulfate, and chloride of the water samples were analyzed immediately after sampling. pH value was measured by a pH meter (SunTex SR-2300). EC was measured by a conductivity meter (6021, EZDO). Sulfide, sulfate, chloride, and total Fe was measured by an ultraviolet spectrophotometer (Spectroquant[®] Prove 600, Merck) with kits (Catalogue no. 114779, 114548, 114897, and 100796, respectively). The detection limits of total Fe, sulfide, sulfate, and chloride were 0.05, 0.05, 5.0, 2.5, and 5.0 mg/L, respectively. The oxidation-reduction potential (ORP) of sediment with a depth of 1–3



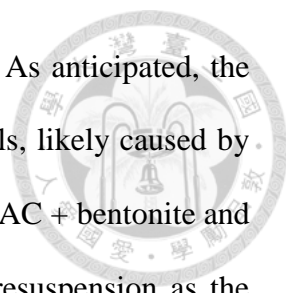
cm of thin layer caps was measured by an ORP meter (SunTex SR-2300). The measurement was prosecuted by inserting the sensor of the ORP meter in the depth of 1–3 cm and stabilized for 2 h. Sediment was sampled 1–3 cm depth under sediment layer (not account for cap layer), stored at -20°C before subsequent analysis. The sediment measurement was controlled at fixed position in each cell (34 cm from the front; Figure S4-4). Although the sediment can be highly heterogeneous can may affect the results, careful measurement and triplicated sampling was prosecuted.

Overlying water for THg analysis was stored with 0.1% BrCl solution (< 1 week). Sediments for THg analysis were freeze-dried and digested (95–120% recovery). THg concentrations were determined following USEPA Method 1631 using BrCl oxidation, SnCl₂ reduction, purge and trap, and cold vapor atomic fluorescence spectroscopy (CVAFS; Brooks Rand Automated Total Mercury System) (85–100% recovery). Water samples for MeHg analysis were stored with 0.1% HCl solution in dark (< 2 d). MeHg was measured by distillation and ethylation, purge and trap and GC/CVAFS (Brooks Rand Automated Total Mercury System) by USEPA Method 1630 (water) and Taiwan-EPA method NIEA S341.60B (sediment) (93–115% and 93–110% recovery, respectively). QA/QC was checked by analyzing duplicate samples, quality control samples, and spiked samples from each batch.

4.3 Results and Discussion

4.3.1 Microcosms Operation

The combination of horizontal flow and artificial turbation has resulted in a visible suspension in the microcosm (Figure S4-7). Without turbation, no suspension was observed during the pre-test (Figure S4-6). A similar observation was reported by Xie et



al. [93] as the flow and bioturbation enhance sediment suspension. As anticipated, the overlying water of the control was highly turbid throughout the trials, likely caused by the fine particles released from the uncovered sediment surface. The AC + bentonite and the AC + kaolin caps were found successful to inhibit sediment resuspension as the overlying water was found less turbid than the control. However, the AC + montmorillonite was observed with high turbidity in overlying water comparable to the control, indicating that montmorillonite was less stable as compared to kaolin and bentonite. The reason may be that montmorillonite is a 2:1 type clay mineral and was considered efficient to absorb large amounts of water in the interlayer space [125]. To further inference, bentonite consists chiefly of one or more members of the smectite-groups (montmorillonite) minerals [126], therefore should also be possible to absorb water and become labile when applied as thin layer caps. However, AC + bentonite shown quite stable under turbation. This may be because that bentonite is a non-pure material consists of complex minerals, thus may help to stabilize the cap. Different from bentonite and montmorillonite, kaolin is a 1:1 type clay minerals, therefore may not be labile due to water sorption. In terms of Hg sorption capacity, bentonite (<1 mg/g [127]), kaolin (< 1 mg/g [128]) and montmorillonite (< 10 mg/g [129]) were known to have much lower sorption capacity as compared to coconut AC (~150 mg/g [12]). Therefore, the mechanism for the clays to inhibit sediment resuspension should be by forming barriers to block fine sediment particles.

The temperature in the microcosm throughout the experiment was stable at 25 ± 1 °C (Figure S4-8a, Table S4-4) with a few exceptions. DO in the overlying water was also stable between 6.0 and 7.0 in all cells throughout the trials (Figure S4-8b). The aeration may be caused by the little waterfall created by the reflux water in the PP tanks. This

value matches the An-Shun real-site conditions, as the overlying water in the estuary ponds was shallow and highly aerated. The pH value of overlying water in all cells was between 8.0 and 8.3 (Figure S4-8c) and is comparable to ANS surface water (Table S4-2).

EC in the overlying water was around $3.0\text{--}4.0 \times 10^4$ $\mu\text{S}/\text{cm}$ (Figure S4-8d), partially lower than that in ocean water (approximately 5.0×10^4 $\mu\text{S}/\text{cm}$). After the thin layer caps application, a decrease of EC in the AC + bentonite and the AC + kaolin was observed to be $2.0\text{--}2.5 \times 10^4$ $\mu\text{S}/\text{cm}$. In contrast, EC of the AC + montmorillonite remained comparable to that in the control, probably because of the lower capping stability (Figure S4-7). This result may indicate that the salt mud (originated from chlor-alkali brine (O'Brien et al. 2007)) was released to the overlying water as the turbation occurred. Thin layer caps may form the barrier thus reducing partial salt released from sediment.

4.3.2 Sulfide, Sulfate, Chloride, and Total Fe in Overlying Water

Sulfate, chloride and total Fe in the overlying water were measured throughout the study (Figure 4-1, Table S4-5). Sulfide concentration in the microcosm was smaller than the detection limit (<0.05 mg/L) throughout the operation. The reason may be the aerated condition in the overlying water causing sulfide re-oxidized to sulfate as released from the sediment, therefore, existed in a small concentration [130]. However, sulfide may still have a profound impact on Hg speciation even as low as 1 nM [23].

Sulfate, chloride, and total Fe in the overlying water in all cells were generally larger than those in the ANS surface water (Figure 4-1, Table S4-2), indicating that the ions measured were concentrated in the sediment and escaped to the overlying water by sediment-to-water flux.

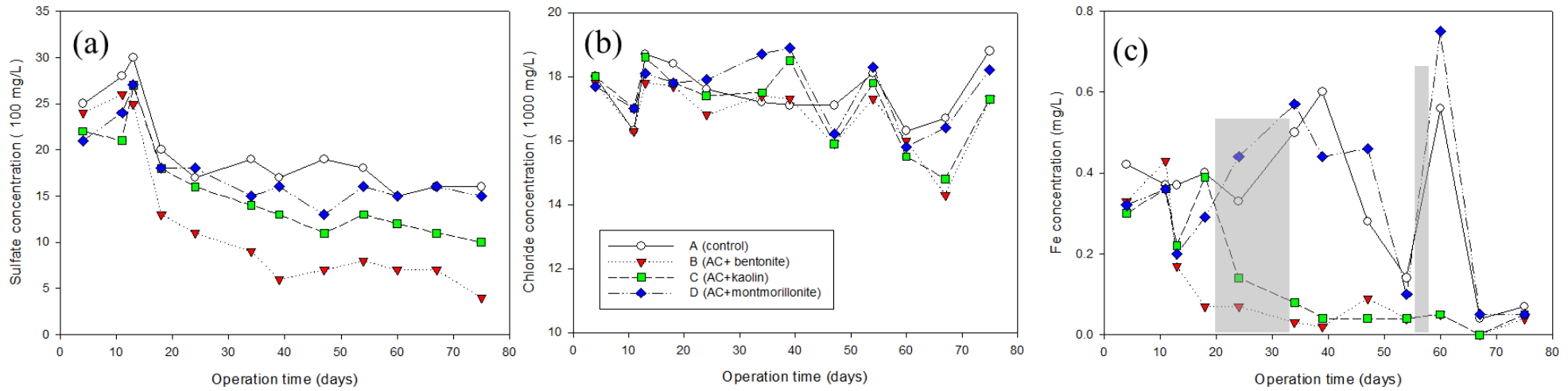
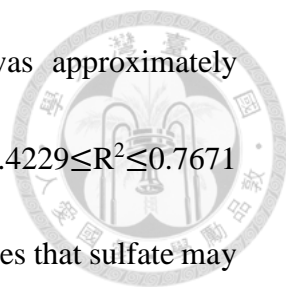


Figure 4-1. (a) Sulfate, (b) chloride, and (c) total Fe concentration in the overlying water of four cells of the microcosm. The gray bar between day 20 and 30 represents intermittent turbation test; the gray bar at day 54 represents the sediment sampling event.



The pattern of sulfate in overlying water (Figure 4-1a) was approximately $2.0\text{--}2.5\times 10^3$ mg/L and found positively correlated ($R^2 = 0.5950$; $0.4229 \leq R^2 \leq 0.7671$ under 95% confidence level) to EC (Figure S4-9). This result indicates that sulfate may contribute to a large portion of EC that was concentrated in the sediment. Both the AC + bentonite and the AC + kaolin caps were found to decrease sulfate concentration in the overlying water significantly as compared to the control. In contrast, the AC + montmorillonite cap was not favorable for the sulfate reduction. Previous studies have found sulfate sorption behavior for bentonite [131] and kaolin [132]. However, it was suggested that montmorillonite has the permanent negative charge in silica structure [125], therefore could be unfavorable for sulfate sorption. Also, sulfate concentration was observed to gradually decrease in all microcosms. The reason behind may be that the overlying water was gradually diluted by the ANS surface water, which had lower sulfate, during every water sampling events (200 mL/cell).

Chloride concentration in overlying water was ranged within $1.6\text{--}1.9\times 10^4$ mg/L (Figure 4-1b). Thin layer caps had an unobvious influence on chloride ions throughout the study.

Total Fe concentration ranged between 0.3 and 0.4 mg/L (Figure 4-1c). Total Fe was found to have a slightly positively correlation ($R^2 = 0.3393$; $0.1207 \leq R^2 \leq 0.5579$

under 95% confidence level) with sulfate concentrations (Figure S4-9).

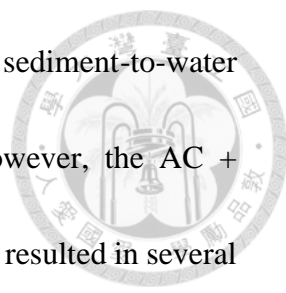


Both the intermittent turbation test (the vibration system was stopped during day 20–31) and the sediment sampling events (non-purposed incident) have caused impact to Fe escape into the overlying water. Two concentration peaks of total Fe were observed in the AC + montmorillonite caps and the control experiment after the intermittent turbation test and the sediment sampling event. Capping with the AC + bentonite and the AC + kaolin showed little response to these two events and resulted in low total Fe concentration throughout the study.

The results of sulfate and total Fe indicate that the thin layer caps could provide a barrier to decrease sediment-to-water flux of these elements. Capping with the AC + bentonite and the AC + kaolin was found to decrease sediment-to-water flux of sulfate (35.0–75.0% and 5.9–37.5% reduction, respectively) and total Fe (71.4–96.7% and 28.6–93.3% reduction, respectively); while capping with the AC + montmorillonite showed profound escape of sulfate and total Fe comparable to the control (0.0–11.1% and -64.3–28.6% reduction, respectively).

4.3.3 Reduction of Aqueous THg and MeHg by Thin Layer Cap

Similar to the aqueous sulfate and total Fe, the application of thin layer caps with



the AC + bentonite and the AC + kaolin successfully inhibited Hg sediment-to-water flux under the turbation condition (Figure 4-2, Table S4-6). However, the AC + montmorillonite cap showed less effectiveness in Hg reduction, also resulted in several Hg escape incidents likely referring to two sediment turbation events. In general, THg reduction by the AC + bentonite and the AC + kaolin reached 40.1–95.8% and 34.9–94.3%, respectively in comparison to that shown in the control (Figure S4-10a); while the AC + montmorillonite showed fluctuated THg reduction (-109.4–79.2%) and was highly dependent on the turbation events.

THg reduction in the overlying water was observed after all three caps were applied. This result may be due to the high Hg sorption of AC or instant barrier blocking of the Hg flux by clays. During the intermittent test, THg reached the smallest concentration in all cells due to the less Hg resuspension without turbation. After the intermittent test, THg in all cells raised dramatically likely due to the artificial turbation. During this phase (day 34–54), the AC + bentonite (27.3–179.4 ng/L) and the AC + kaolin (46.1–130.9 ng/L) showed better resistance for THg resuspension into the overlying water as compared to the AC + montmorillonite (206.3–348.3 ng/L) and the control (198.4–415.7 ng/L). After day 54, an unintentional sediment sampling event partially disturbed the surface sediment (1–3 cm), causing a dramatic THg escape in the control

and the AC + montmorillonite.

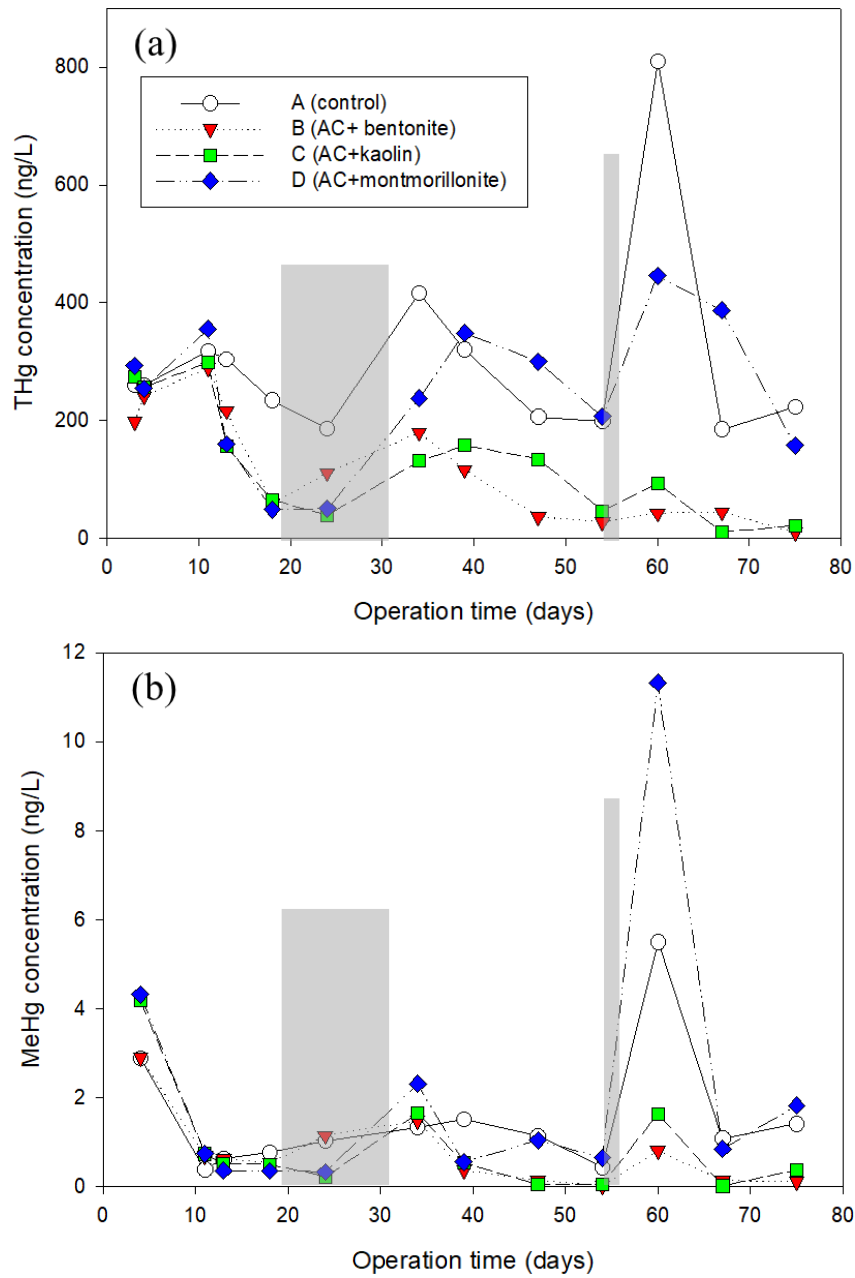


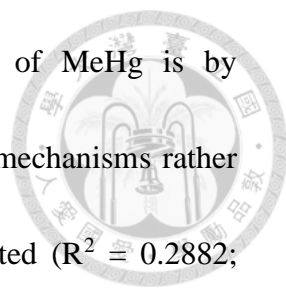
Figure 4-2. (a) THg and (b) MeHg concentration in the overlying water of four cells of the microcosm. The gray bar between day 20 and 30 represents intermittent turbation test; the gray bar at day 54 represents the sediment sampling event.

MeHg in the overlying water showed a similar pattern to THg (Figure 4-2, Table

4-S6). The AC + bentonite and the AC + kaolin showed smaller MeHg concentration (0.01–1.48 ng/L and 0.01–1.65 ng/L, respectively) as compared to the AC + montmorillonite and the control (0.43–5.50 ng/L and 0.32–11.33 ng/L, respectively).

Although the MeHg reduction by capping was not obvious in the earlier phase (< 34 d), probably due to the complex microbial community alteration after the thin layer capping was applied, after day 34, both the AC + bentonite and the AC + kaolin caps were highly efficient in MeHg reduction (by 75.89–98.06% and 64.7–98.9%, respectively) in comparison to the control (Figure S4-10b). In contrast, MeHg reduction by the AC + montmorillonite showed contradicted results (-106.1–63.4%). A breakthrough of MeHg (11.33 ng/L) was observed after the unintentional sediment sampling events (day 60).

Based on these experimental observations, the levels of sulfate, total Fe, THg, and MeHg in overlying water were concluded to be highly dependent on the sediment-to-water flux altered by the quality of the caps. The relationships of THg/MeHg to sulfate and total Fe were carried out in Figures S4-11 and S4-12. THg was found to be mildly strong positive correlated to sulfate ($R^2 = 0.3415$; $0.1229 \leq R^2 \leq 0.5601$ under 95% confidence level) and to total Fe ($R^2 = 0.3653$; $0.1474 \leq R^2 \leq 0.5832$ under 95% confidence level). In comparison, the correlation for MeHg to sulfate and to total Fe



was less correlated. This may be because of that the origin of MeHg is by biosynthesized and thus can be altered may much more complex mechanisms rather than direct Hg release. THg also showed mildly positive correlated ($R^2 = 0.2882$; $0.0712 \leq R^2 \leq 0.5052$ under 95% confidence level) with MeHg (approximately 0.21% of THg) (Figure S4-13). The connection between biogeochemical factors (e.g. sulfate and Fe) toward Hg fate was exceedingly complex and has drawn much attention to scientists. Under sulfate-limiting conditions (<20–30 mg/L) [133, 134], sulfate was considered favorable to Hg methylation process by facilitating microbial processes. However, greater sulfate concentration may result in inhibiting methylation by sulfide toxicity toward methylators or reducing more bioavailable HgS_0 form [135]. The high sulfate concentration ($2.0\text{--}2.5 \times 10^3$ mg/L) obtained in this study may partly explain the MeHg/THg ratio (0.21%) at the low end as compared to other salt marsh or sediments [136].

4.3.4 ORP, THg, and MeHg in Sediment

All thin layer caps showed the reduction of ORP in sediment in the 75-days trial (Figure 4-3). Without caps, the ORP of sediment ranged -148– -176 mV. As anticipated, all capping showed a decrease in ORP [137, 138]. Capping with the AC + bentonite and the AC + kaolin showed the greatest reduction to -250.5 – -257.5 mV and -257.2–

-265.4 mV, respectively. Capping with the AC + montmorillonite was observed to have a smaller reduction in ORP (-177.4– -226.1 mV) as compared to the other two caps scenarios, probably due to lacking stability.

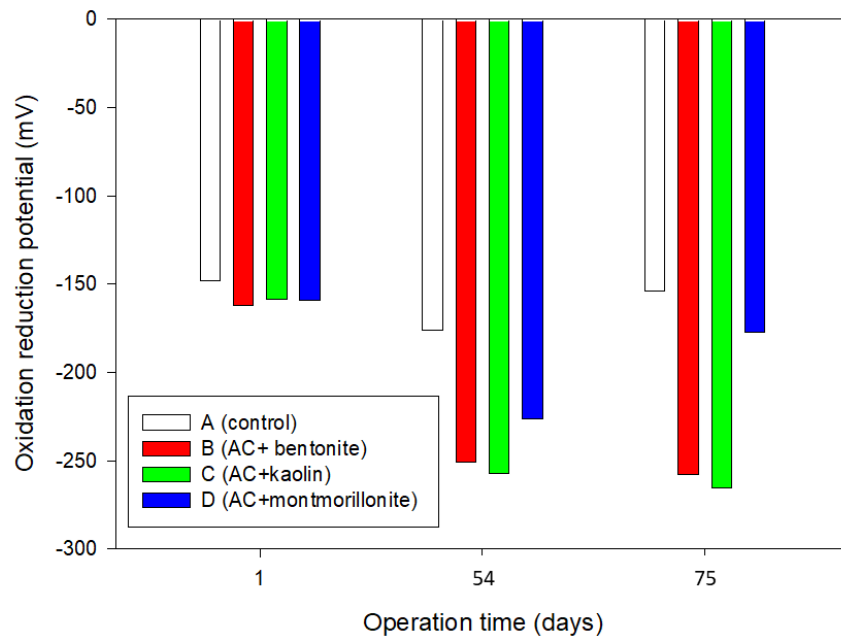
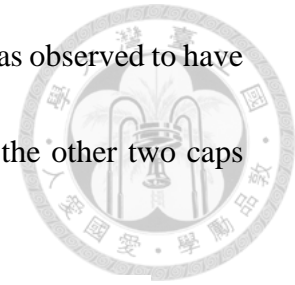


Figure 4-3. The ORP in sediment of the four cells of the microcosm. The ORP was measured within 1–3 cm depth.

The sediment THg (1–3 cm) in all cells was found to decrease from original concentration (76.0 mg/kg) to 58.6–64.52 mg/kg (with caps) and 66.46±2.38 mg/kg (control) (Figure 4-4). Since the microcosm is an open-channel system, it was reasonable that Hg escape may stem from the THg gradient from sediment to open air by diffusion or Hg reduction into the gaseous phase (as Hg⁰). After capping, all capping groups had slightly smaller sediment THg (46.6–66.4 mg/kg) as compared to control (66.5–67.0 mg/kg), likely due to the sorption of Hg by caps, or the caps served as

barriers preventing from Hg-containing particulates to re-supply to the sediment (1–3 cm).



Sediment MeHg remained steady in the control (2.70–3.34 $\mu\text{g}/\text{kg}$) but showed fluctuation in different caps (Figure 4-4). In the AC + bentonite, MeHg in sediment gradually decreased from 3.10 ± 0.11 to 1.94 ± 0.74 $\mu\text{g}/\text{kg}$. However, the AC + kaolin and the AC + montmorillonite showed a decrease in sediment MeHg in day 54, but increase to up to 5.391 ± 0.09 and 4.60 ± 0.32 $\mu\text{g}/\text{kg}$ in day 75, respectively. The decrease in MeHg can be explained by microbial communities shift after the capping events. The other reason may be because the AC application to the sediment reduced MeHg production potential, which was obtained by other microcosms studies [65, 66]. The lateral increase (day 75) of sediment MeHg may be because of the ORP decrease due to capping [137, 138], facilitating the occupation of anaerobic methylators in sediments. The fluctuation of sediment MeHg under thin layer caps may be governed by complex mechanisms and can thus be variable or not altogether predictable.

A significant breakthrough of Hg in the overlying water occurred for a labile cap, such as the AC + montmorillonite, after sediment sample events (which disturbed the sediment in depth of 1–3 cm). However, for the more stable caps (i.e., AC + bentonite and AC + kaolin), the stability of caps enhanced the resistance for Hg breakthrough to

the overlying water. The reason for greater Hg escape in the control and the AC + montmorillonite may be due to the destruction of the anoxic zone beneath sediment by turbation, resulting in releasing MeHg, which was stably stored under the caps [138] to the overlying water. On the other hand, the AC + bentonite and the AC + kaolin were more capable of recovering the destruction zone by the immediate settling clay.

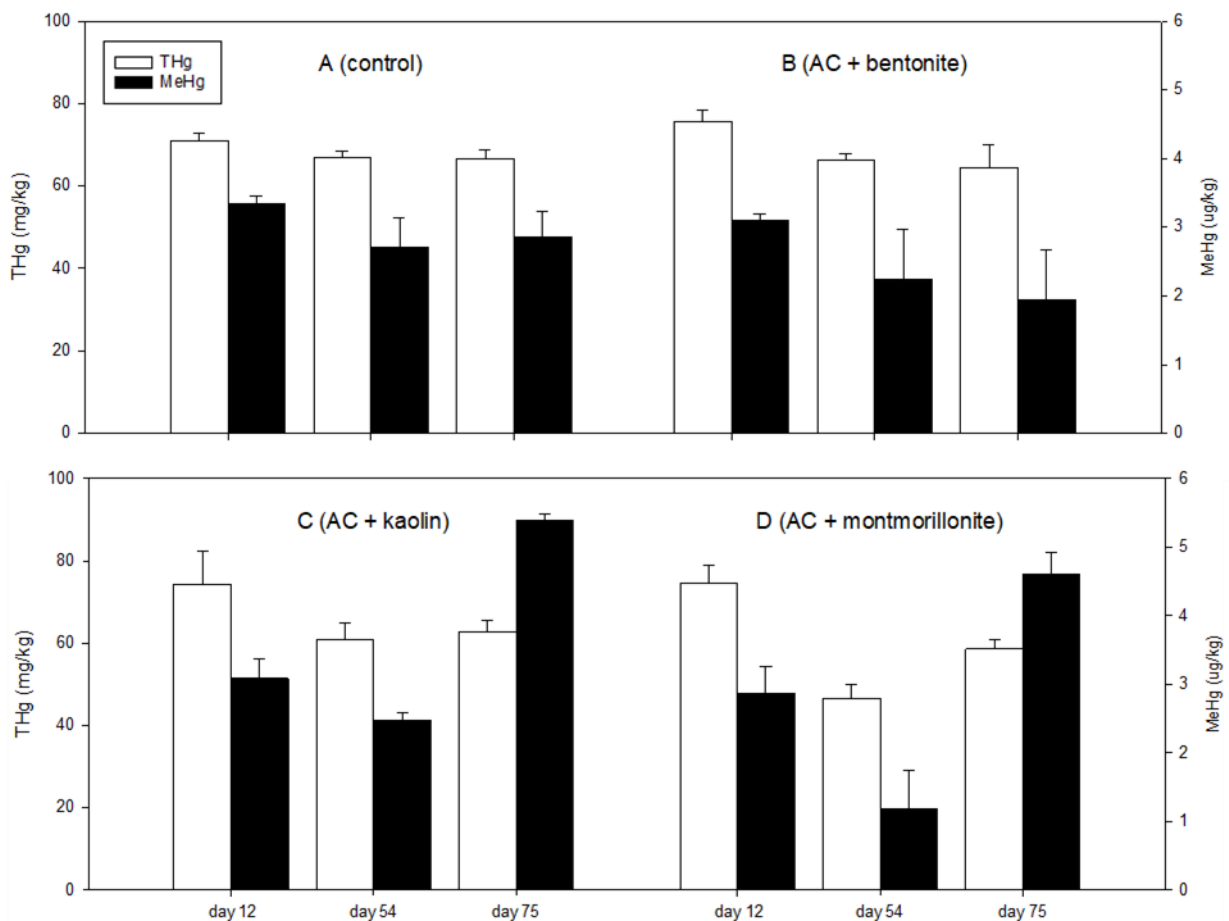


Figure 4-4. THg and MeHg in the sediment (1–3 cm depth) of the four cells of the microcosm (n = 3).

4.3.5 The Stability of Thin Layer Caps during Turbation

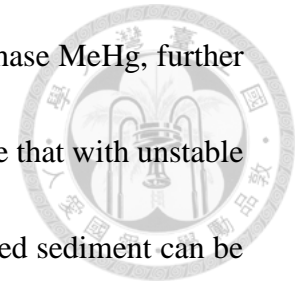


A more explicit scope has been revealed that the stability of thin layer caps significantly alters multiple elements (sulfate, total Fe, THg, and MeHg) from escaping to the overlying water under turbation environment. Both the AC + bentonite and the AC + kaolin thin layer caps successfully immobilized THg and MeHg as well as sulfate and total Fe from escaping even within horizontal flow and turbation. A labile cap, which is the AC + montmorillonite, was unable to stabilize in the surface of sediment and resulted in dramatic Hg escape when encountered turbation.

4.4 Summaries

The results of this study may provide an explanation for previous studies or new perspectives for direction to future capping technologies. Previous studies have shown contradicting results, as some studies suggested that turbation promotes contaminant sequestration in sediment by promoting mixing process of the surface sediment [124], but some also suggested the turbation may increase sediment-to-water contaminant flux [34, 118]. Some studies focused on the porewater Hg reduction while BC materials were applied to the Hg-contaminated sediment [65, 66, 68]. However, the transport of Hg did not always rely on porewater diffusion but instead on fine particle resuspension [15, 16, 93]. As the transport of Hg on the fine particles was discovered in Penobscot

[15, 16], the risk exists if the biochar amendment increases solid-phase MeHg, further escapes to surface water with tidal movements. It is essential to note that with unstable caps, a high concentration of MeHg breakthrough from contaminated sediment can be expected in the occurrence of turbation in a given depth. Concerning using thin layer caps as the solution for Hg-contaminated sites, the stability of thin layer caps is crucial and great attention should be paid to.





4.5 Supporting Information

Table S4-1. Properties for ANS sediment.

	Water content (wt%)	pH (-)	CEC (cmol+/kg)	Organic content (wt%)	Sand (wt%)	Silt (wt%)	Clay (wt%)	THg (mg/kg)
ANS sediment	2.33±0.01	7.52±0.03	3.3±0.2	0.80±0.65	71.4±2.9	14.3±0.0	14.3±2.9	76.0±2.593

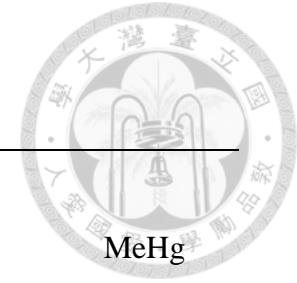


Table S4-2. Properties for ANS surface water.

	Electrical conductivity ($\mu\text{S}/\text{cm}$)	pH (-)	Total Fe (mg/L)	Sulfide (mg/L)	Sulfate (100 mg/L)	Chloride (10^3 mg/L)	THg (ng/L)	MeHg (ng/L)
ANS surface water	$2.15 \pm 0.14 \times 10^4$	8.342	ND(<0.05)	ND(<0.05)	7.5 ± 0.3	14.9 ± 0.7	143.7 ± 3.4	ND(<0.02)



Table S4-3. Operation record for the microcosm.

Date	Op. day	Operator	Op. record	Motors malfunction
2018 May 2nd	-98	Yu Ting	3.5 kg ANS sediment added, pumps stopped for a night.	-
2018 May 3rd	-97	Yu Ting	Pumps started, added 200 g rectifier medium to each cell.	-
2018 July 7th	-31	Yu Ting	First attempt adding vibration system to each cell (5 motors/cell).	-
2018 July 10th	-28	Yu Ting	Vibration stopped, all motors retrieved.	-
2018 August 8th	1	Yu Ting	Second attempt adding vibration system to each cell (5 motors/cell). ORP measured.	A3, C1
2018 August 10th	3	Yu Ting	Overlying water sampled in all cells for measurement.	B1, C4, D3
2018 August 11th	4	Yu Ting	Overlying water sampled in all cells for measurement.	D2
2018 August 15th	8	Yu Ting	Motors replacement (A3, B1, C1,C4, D2, D3).	-
2018 August 18th	11	Yu Ting	Overlying water sampled in all cells for measurement.	B2
2018 August 19th	12	Yu Ting	Sediment sampled for each cell. Thin layers caps were added in cell B, C, and D. Pumps and motors stopped overnight.	A1, C3, D1, D2
2018 August 20th	13	Yu Ting	Pumps and motors started for 5 h. Overlying water sampled in all cells for measurement.	A3, B3, C1, C2
2018 August 21st	14	Yu Ting	Accumulate motors replacement in this week (A1,A3, B2, B3, C1,C2, C3, D1, D2).	-
2018 August 25th	18	Yu Ting	Overlying water sampled in all cells for measurement.	B2, C1
2018 August 27th	20	Yu Ting	All motors stopped for testing the effect of variation of turbation.	-
2018 August 31st	24	Yu Ting	Overlying water sampled in all cells for measurement.	-
2018 September 7th	31	Yu Ting	All motors started.	-
2018 September 10th	34	Yu Ting	Overlying water sampled in all cells for measurement.	A1, A3, B1, C5, D2



Table S4-3 continued.

2018 September 12th	36	Yu Ting	Motors replacement (A1, A3, B1, B2, C1, C5, D2).	-
2018 September 15th	39	Yu Ting	Overlying water sampled in all cells for measurement.	-
2018 September 20th	44	Yu Ting	Pump of D cell malfunctioned and replaced.	A3, B2, C2
2018 September 23rd	47	Yu Ting	Overlying water sampled in all cells for measurement.	A4, B3, D1, D3
2018 September 26th	50	Yu Ting	Motors replacement (A3, A4, B2, B3, B5, C2, D1, D3).	-
2018 September 30th	54	Yu Ting	Overlying water sampled in all cells for measurement. Sediment sampled for each cell. ORP measured.	A1, A4, B4
2018 October 2nd	56	Yu Ting	Motors replacement (A1, A4, B4).	
2018 October 6th	60	Yu Ting	Overlying water sampled in all cells for measurement.	A3, B3, C3, D1
2018 October 9th	63	Yu Ting	Motors replacement (A3, B3, C3, D1).	-
2018 October 13 th	67	Yu Ting	Overlying water sampled in all cells for measurement.	-
2018 October 18 th	73	Yu Ting	wire reformed. Motors replacement (B5)	B5
2018 October 20 th	75	Yu Ting	Overlying water sampled in all cells for measurement. Sediment sampled for each cell. ORP measured.	-



Table S4-4. Temperature, DO, pH, and EC of the overlying water in the microcosm.

Day	Temperature	DO				pH				EC			
	(°C)	A	B	C	D	A	B	C	D	(100 μ S/cm)			
4	26	6.01	6.09	6.26	6.37	7.77	7.78	7.73	7.77	362.0	353.0	379.0	364.0
11	22	6.56	6.96	6.96	6.58	7.73	8.02	8.03	8.06	391.0	278.0	306.0	306.0
13	24	6.17	6.10	6.13	6.32	8.14	8.11	8.16	8.22	339.0	286.0	332.0	308.0
18	25	5.86	6.19	6.17	6.22	8.18	8.21	8.25	8.22	308.0	270.0	318.0	343.0
34	25	6.65	6.05	5.87	6.46	8.25	8.10	8.07	8.05	332.0	222.0	291.0	312.0
39	26	6.50	6.16	5.67	6.04	8.03	8.16	8.27	8.24	336.0	205.0	290.0	308.0
47	26	6.50	6.08	6.07	6.04	8.04	8.15	8.06	8.23	335.0	204.0	258.0	303.0
54	24	6.43	6.65	6.28	6.84	8.07	8.23	8.15	8.14	323.0	208.0	274.0	309.0
60	22	6.56	6.61	5.89	6.61	8.17	8.29	8.24	8.24	312.0	219.0	253.0	330.0
67	22	6.69	6.86	6.69	6.60	8.29	8.35	8.20	8.22	319.0	200.0	253.0	323.0
75	24	6.95	5.85	6.43	6.97	8.26	8.39	8.15	8.11	310.0	222.0	259.0	328.0



Table S4-5. chloride, sulfide, sulfate and total Fe contents of the overlying water in the microcosm.

Day	Cl ⁻				S ²⁻				SO ₄ ²⁻				Fe ion			
	(1000 mg/L)				(mg/L)				(100 mg/L)				(mg/L)			
	A	B	C	D	A	B	C	D	A	B	C	D	A	B	C	D
4	18.0	17.8	18.0	17.7	ND	ND	ND	ND	25.0	24.0	22.0	21.0	0.42	0.33	0.30	0.32
11	16.3	16.3	17.0	17.0	ND	ND	ND	ND	28.0	26.0	21.0	24.0	0.37	0.43	0.36	0.36
13	18.7	17.8	18.6	18.1	ND	ND	ND	ND	30.0	25.0	27.0	27.0	0.37	0.17	0.22	0.20
18	18.4	17.7	17.8	17.8	ND	ND	ND	ND	20.0	13.0	18.0	18.0	0.4	0.07	0.39	0.29
24	17.6	16.8	17.4	17.9	ND	ND	ND	ND	17.0	11.0	16.0	18.0	0.33	0.07	0.14	0.44
34	17.2	17.4	17.5	18.7	ND	ND	ND	ND	19.0	9.0	14.0	15.0	0.50	0.03	0.08	0.57
39	17.1	17.3	18.5	18.9	ND	ND	ND	ND	17.0	6.0	13.0	16.0	0.60	0.02	0.04	0.44
47	17.1	15.9	15.9	16.2	ND	ND	ND	ND	19.0	7.0	11.0	13.0	0.28	0.09	0.04	0.46
54	18.1	17.3	17.8	18.3	ND	ND	ND	ND	18.0	8.0	13.0	16.0	0.14	0.04	0.04	0.10
60	16.3	16.0	15.5	15.8	ND	ND	ND	ND	15.0	7.0	12.0	15.0	0.56	0.05	0.05	0.75
67	16.7	14.3	14.8	16.4	ND	ND	ND	ND	16.0	7.0	11.0	16.0	0.04	0.00	0.00	0.05
75	18.8	17.3	17.3	18.2	ND	ND	ND	ND	16.0	4.0	10.0	15.0	0.07	0.04	0.05	0.05



Table S4-6. THg and MeHg of the overlying water in the microcosm.

Day	Total Hg (ng/L)				MeHg (ng/L)			
	A	B	C	D	A	B	C	D
3	260.18	197.40	274.70	292.78	-	-	-	-
4	260.27	240.68	256.61	254.13	2.88	2.89	4.19	4.32
11	317.94	289.08	298.13	355.17	0.38	0.69	0.73	0.74
13	303.84	216.38	156.28	159.63	0.62	0.63	0.52	0.35
18	234.41	58.22	64.95	48.62	0.76	0.53	0.49	0.35
24	185.77	110.69	38.59	50.02	1.03	1.14	0.21	0.32
34	415.65	179.36	130.88	237.75	1.33	1.48	1.65	2.31
39	320.25	116.10	157.50	348.30	1.50	0.36	0.53	0.55
47	205.86	36.22	134.11	300.00	1.14	0.14	0.04	1.03
54	198.43	27.32	46.11	206.32	0.43	0.01	0.04	0.64
60	809.77	42.33	92.90	445.55	5.50	0.80	1.63	11.33
67	184.83	44.06	10.62	387.01	1.08	0.13	0.01	0.84
75	223.46	9.35	20.11	157.56	1.41	0.11	0.37	1.82

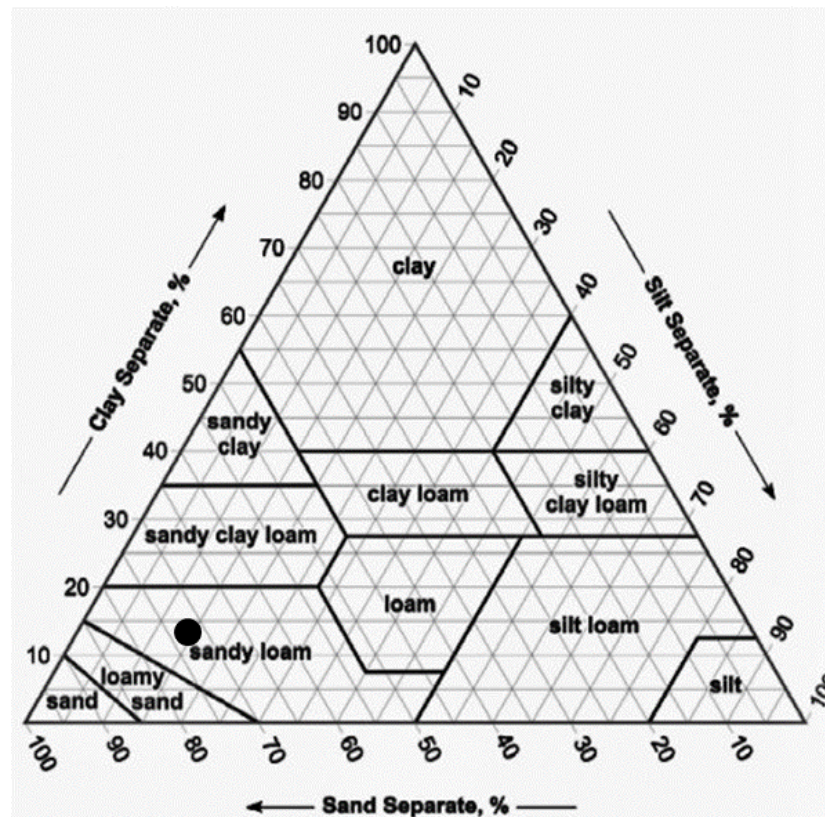


Figure S4-1. The texture of ANS sediment.



Figure S4-2. Photo diagrams for commercial motors (RISUN PVN 1305D 3V) before (left) and after (right) coated with layers of Hg-free epoxy resin and plastic steels.

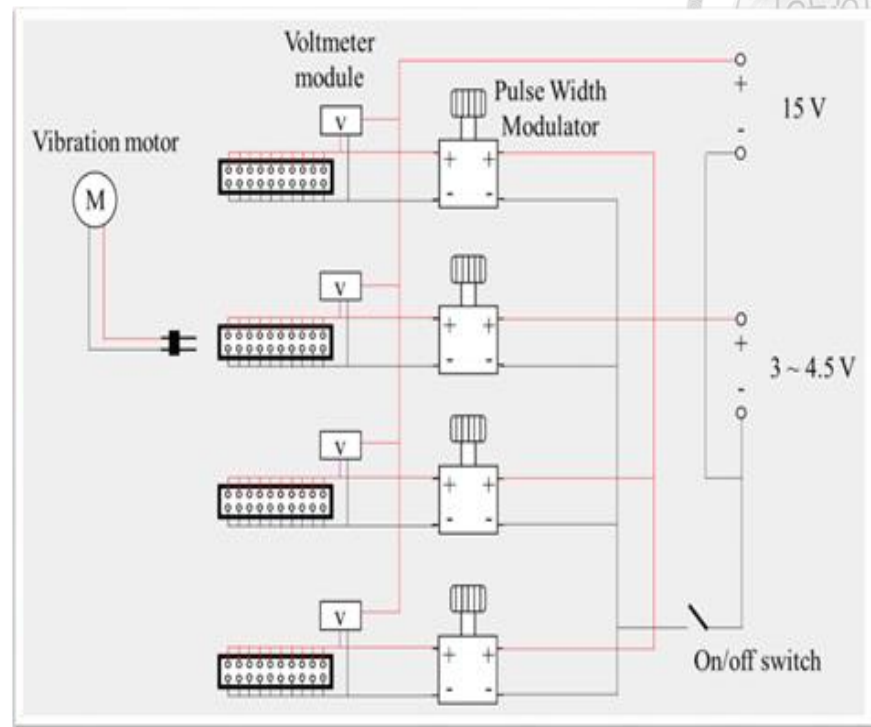
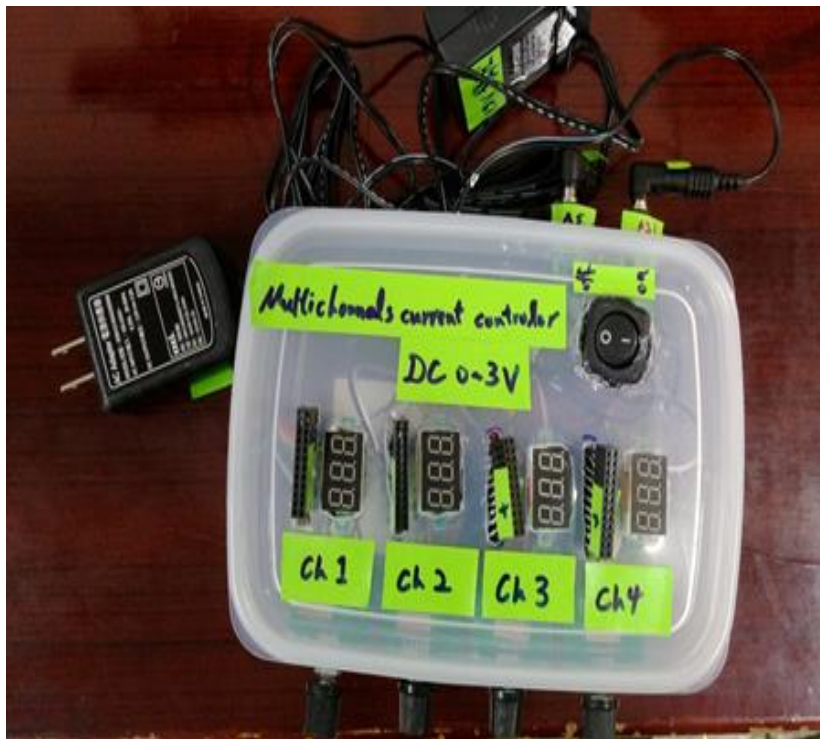


Figure S4-3. Photo diagram (left) and circuit diagram (right) of the lab-made current controller.

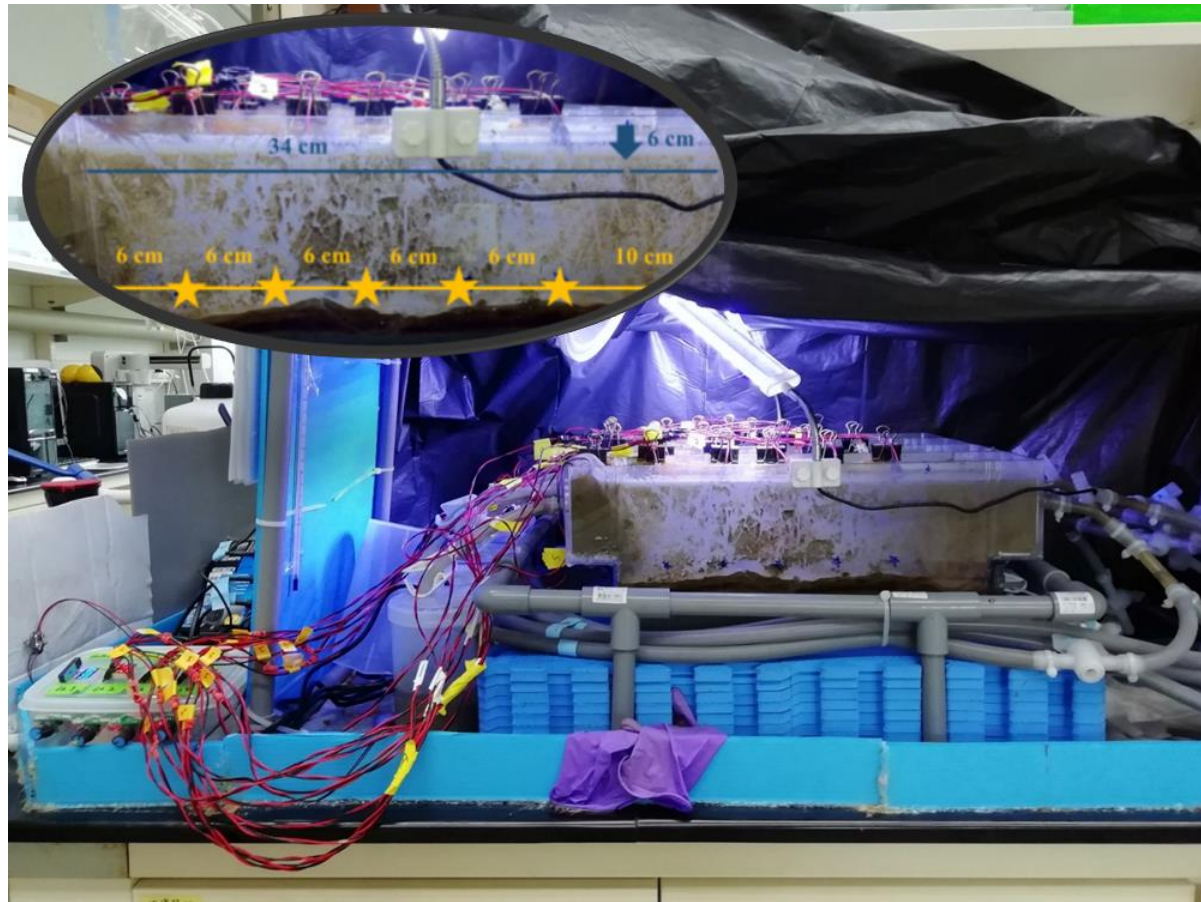


Figure S4-4. Photo diagram of the whole microcosm. The yellow stars represent the location of the motors; the blue arrow represents the sampling point for overlying water and the beneath sediment.

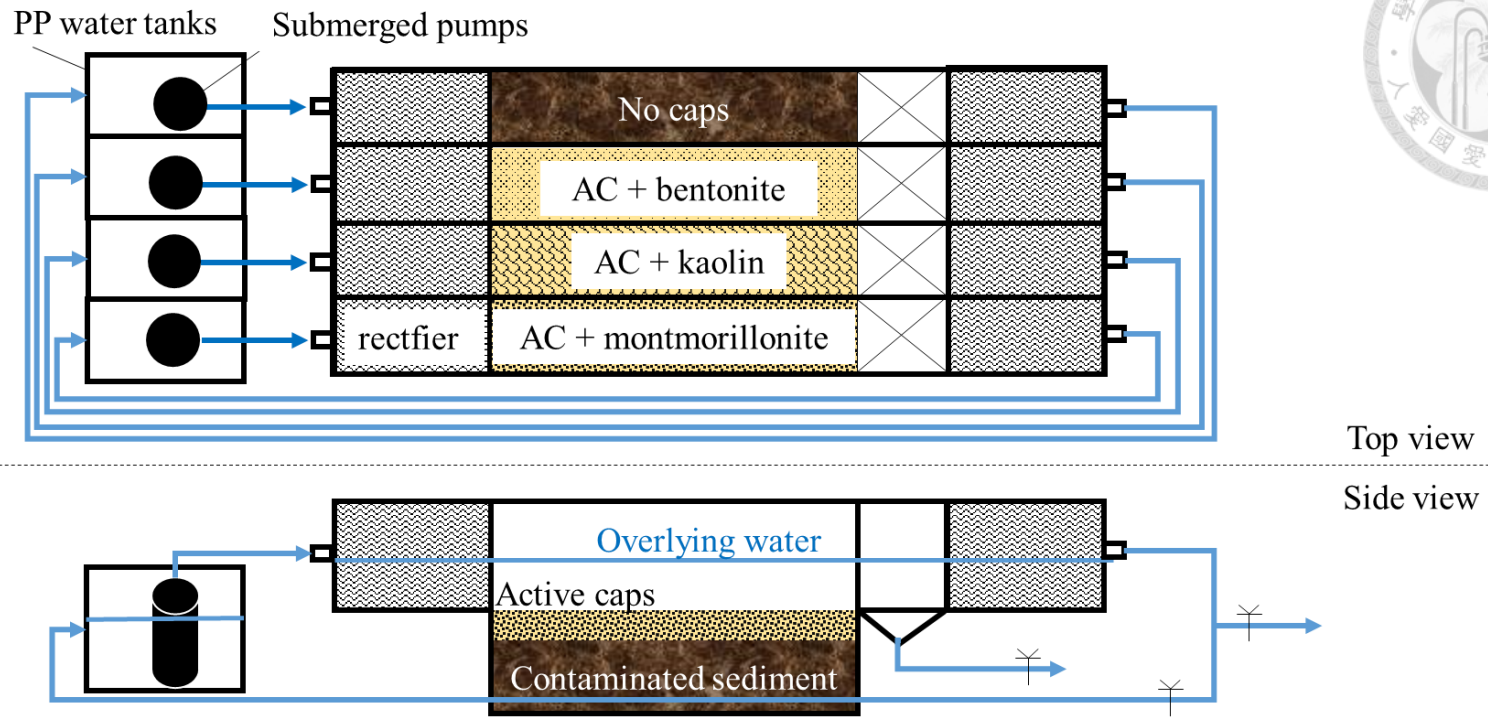


Figure S4-5. Scheme diagram of the microcosm construction.

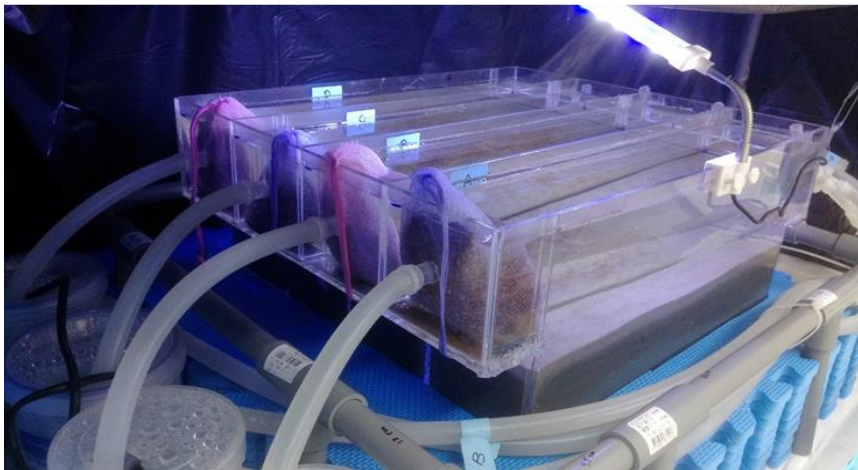
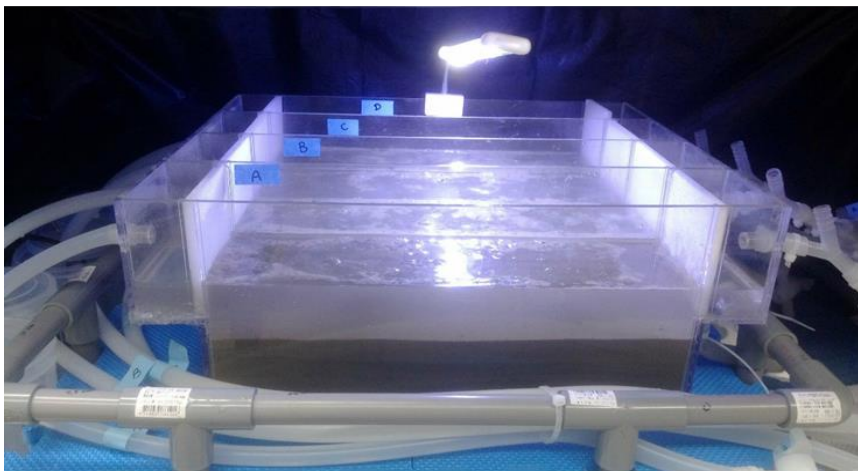
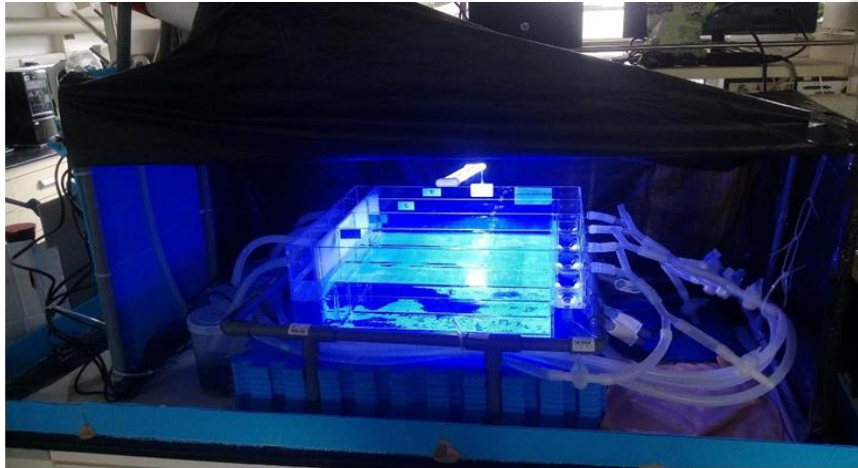


Figure S4-6. Photo diagrams for the start-up of the microcosm, including the pressure test (up), sediment incubation (middle; day -98) and rectifier added (down; day -97).

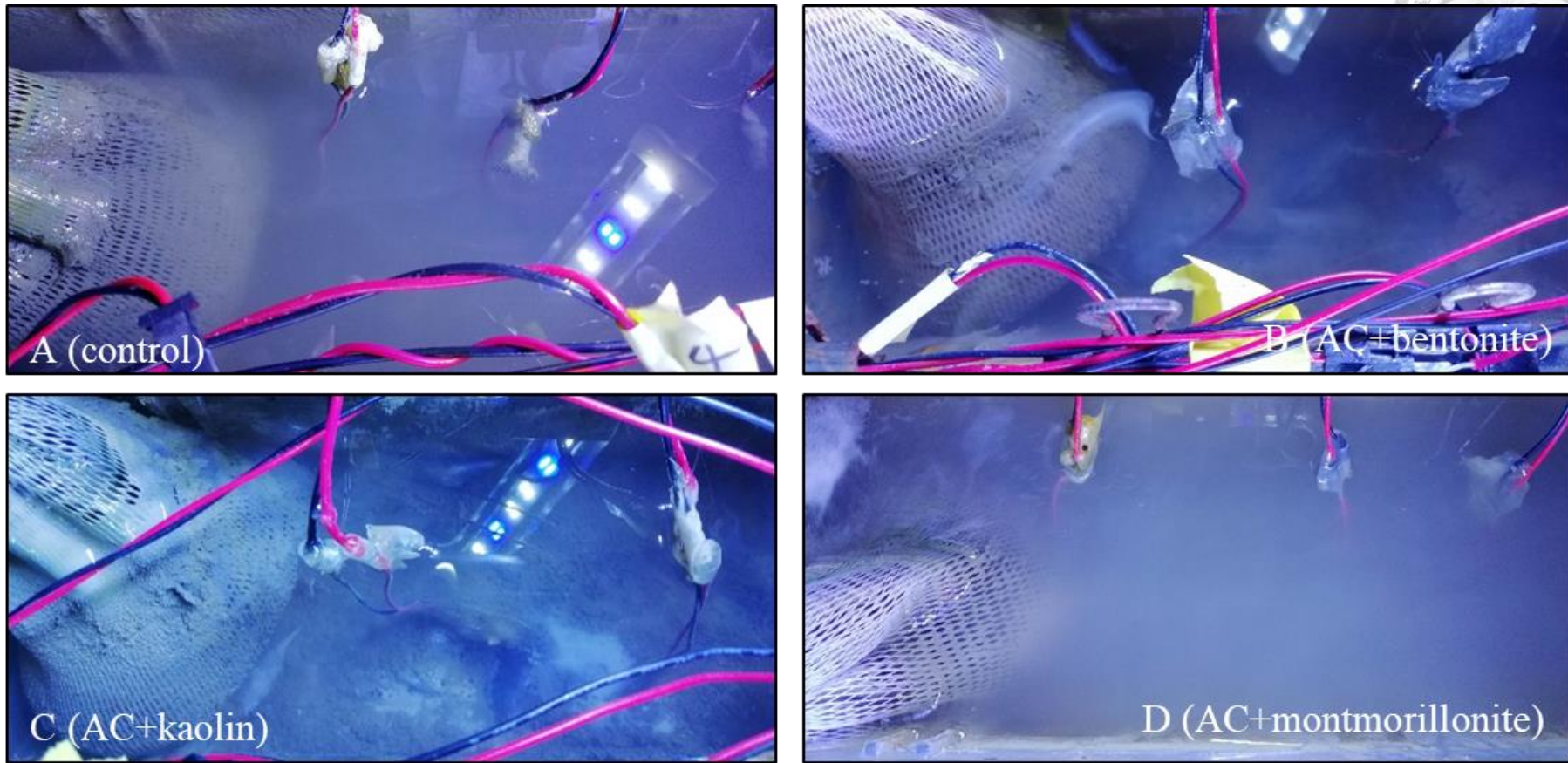


Figure S4-7. Top view of cell A (control), cell B (AC + bentonite), cell C (AC + kaolin) and cell D (AC + montmorillonite); the photographs were taken at day 70.

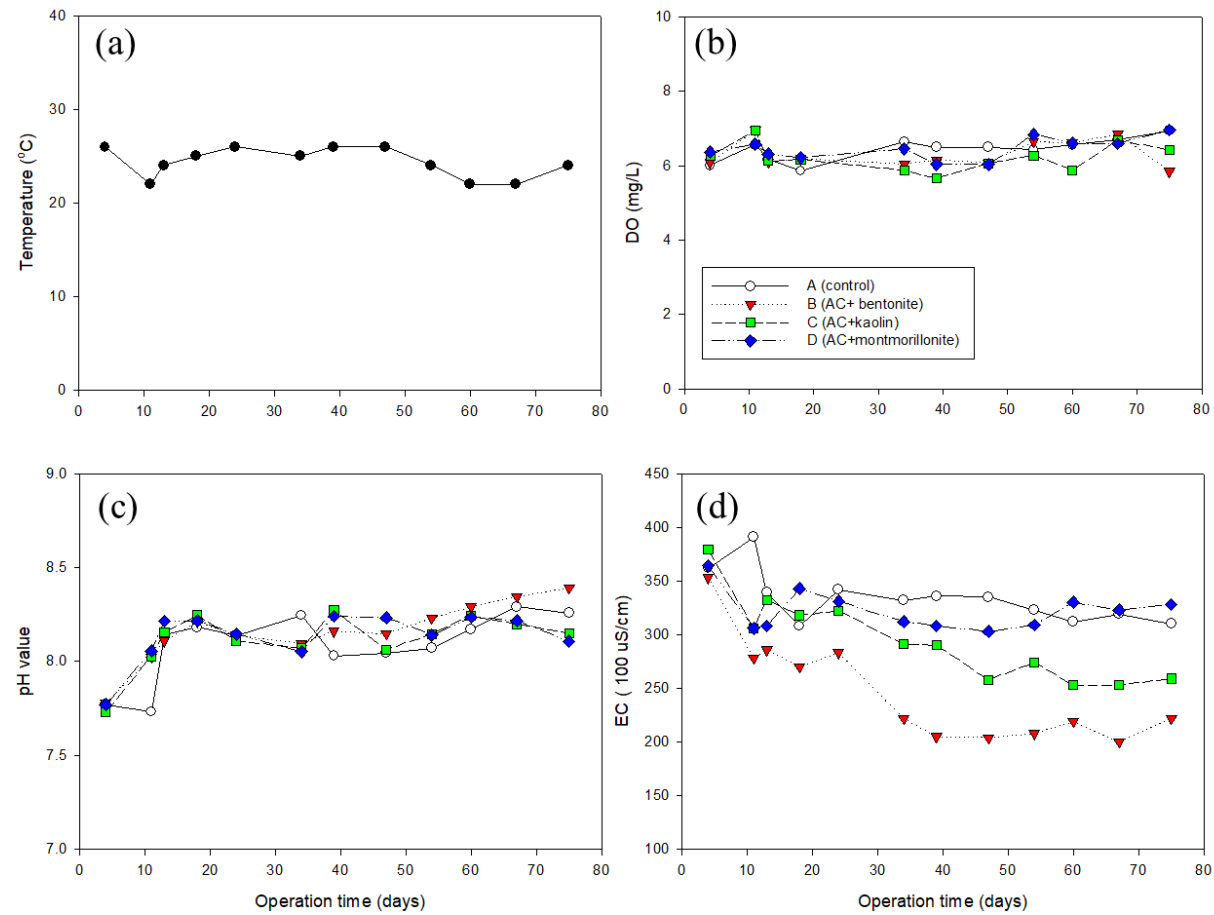


Figure S4-8. (a) Temperature, (b) DO, (c) pH, and (d) EC of the overlying water in the microcosm.

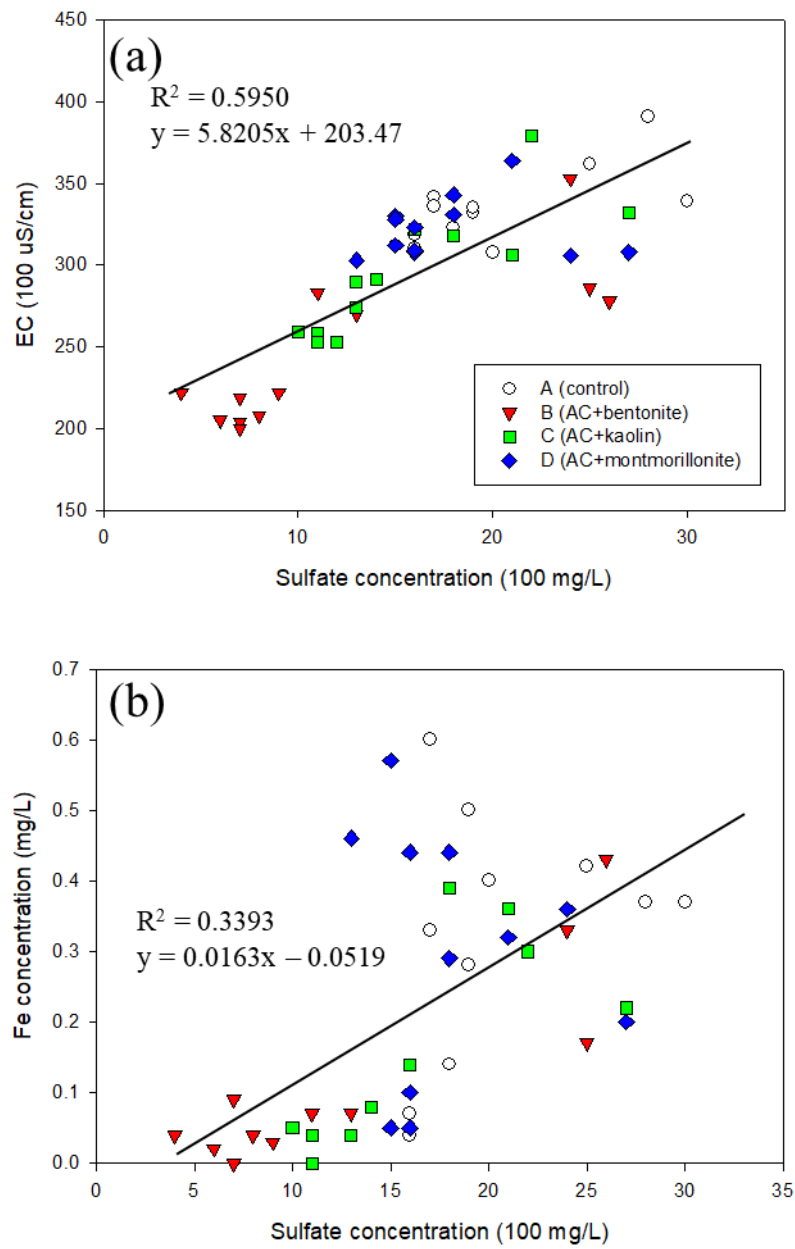


Figure S4-9. Correlation of sulfate to (a) EC (n = 46) and (b) total Fe (n = 43). An extreme data point of day 60 was removed from the plot.

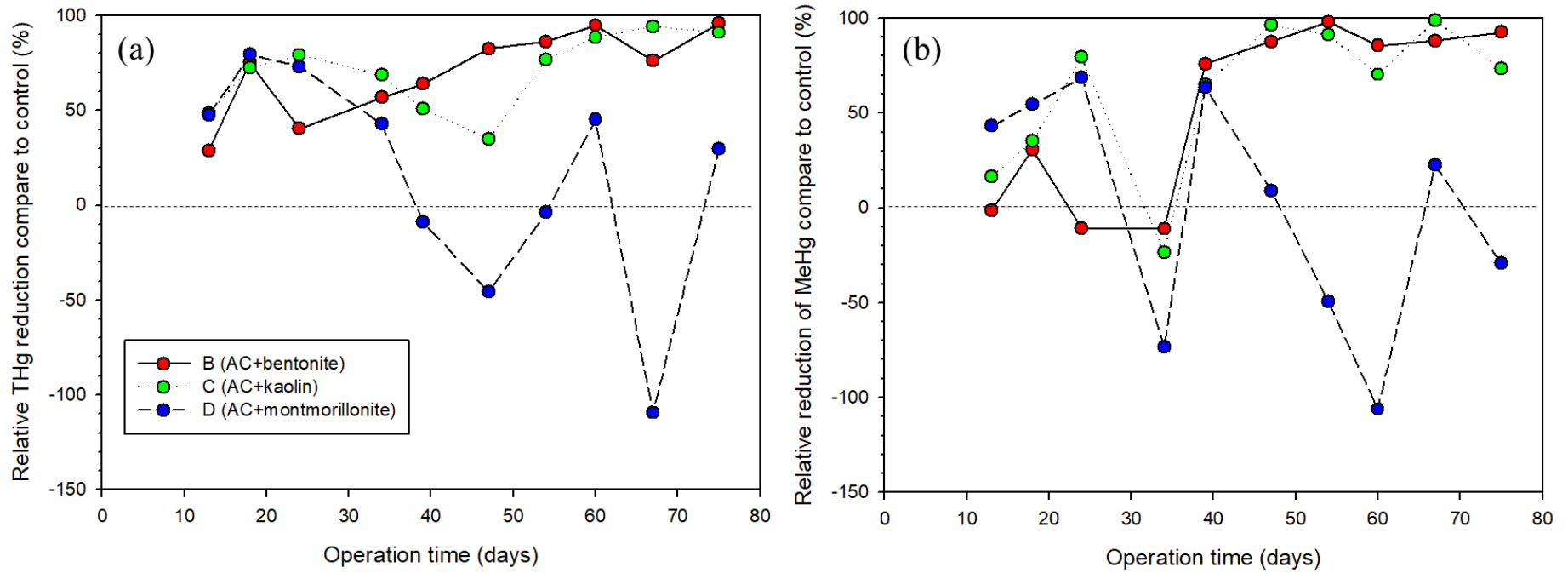
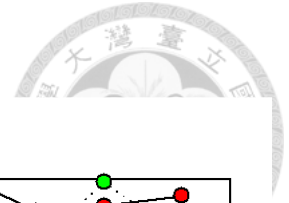


Figure S4-10. (a) THg reduction and (b) MeHg reduction efficiency of thin layer caps in comparison to control.

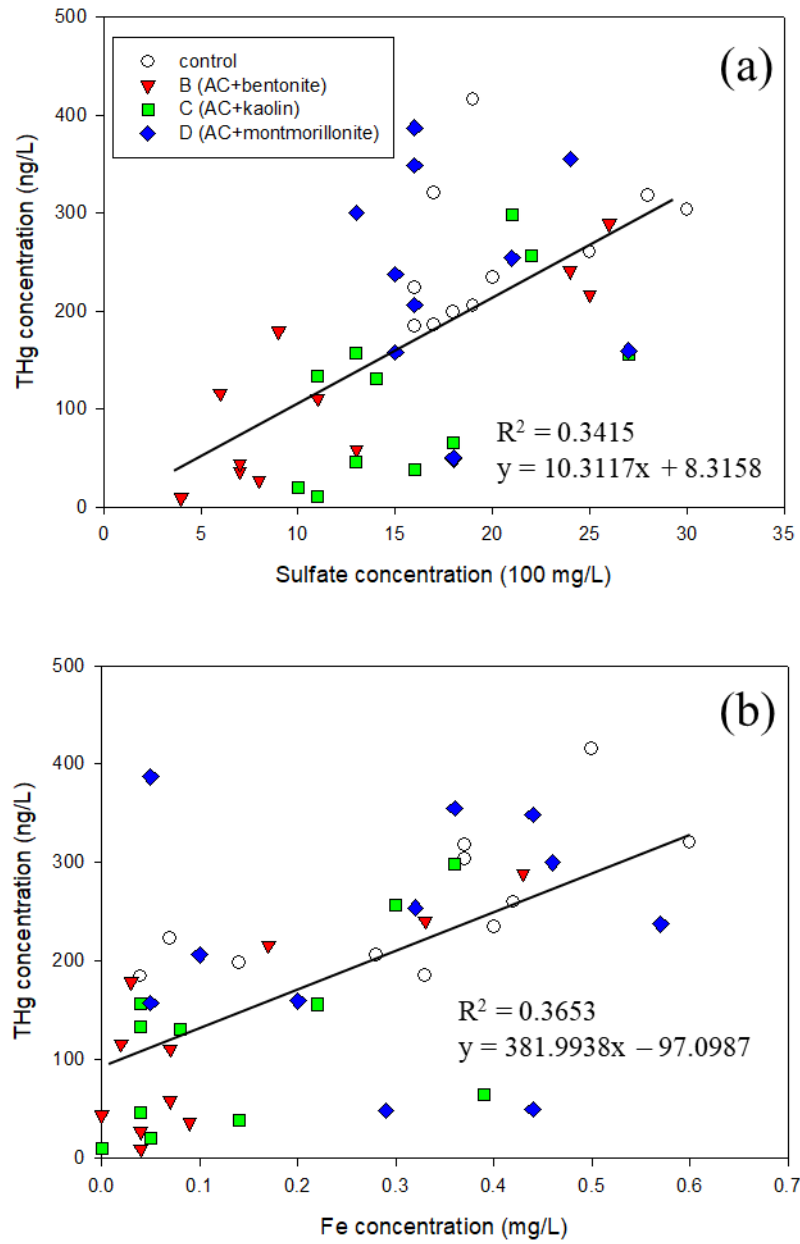


Figure S4-11. Correlation of THg to (a) sulfate and (b) total Fe. Extreme data points of day 60 were removed. (n = 43)

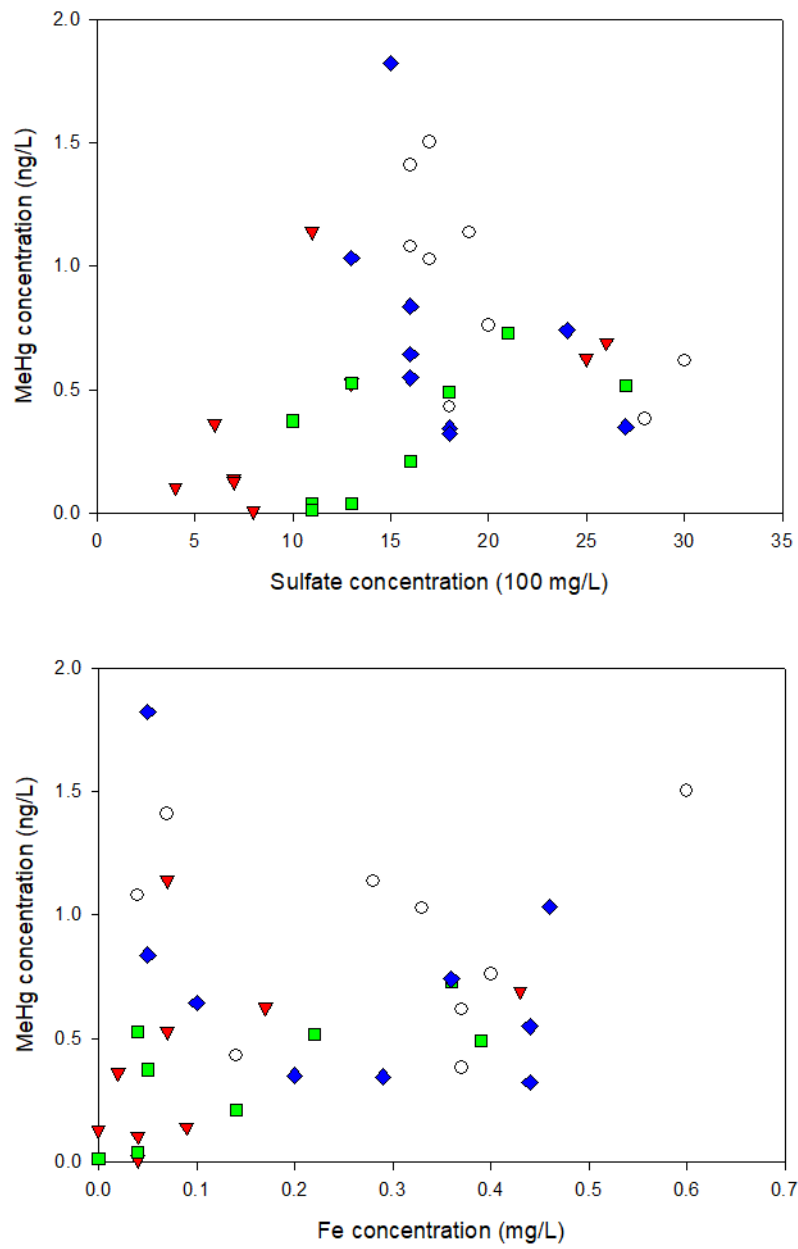


Figure S4-12. Correlation of MeHg to (a) sulfate and (b) total Fe. Extreme data points of day 34 and day 60 were removed.

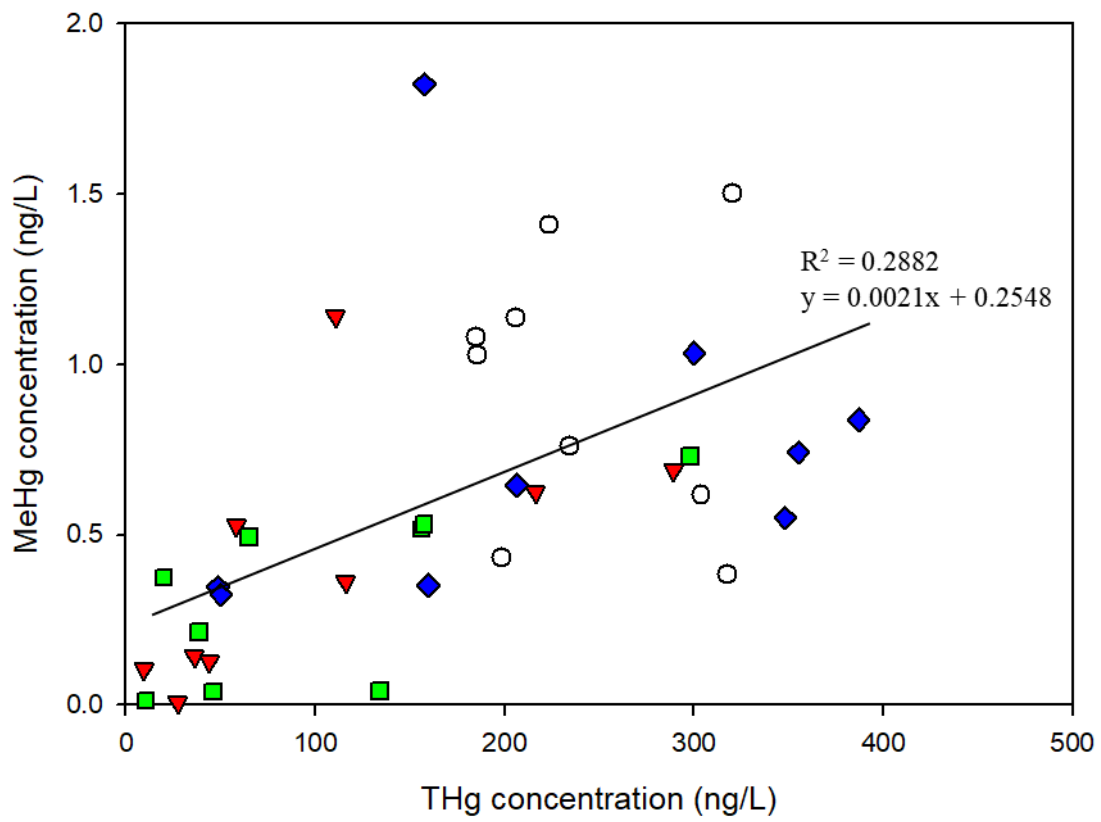
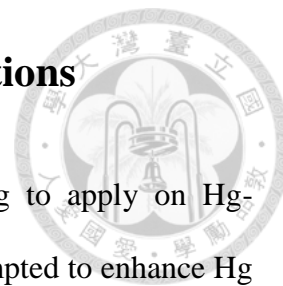


Figure S4-13. Correlation of THg to MeHg. An extreme data point of day 60 was removed. (n = 43)

Chapter 5 Conclusions and Suggestions



This thesis tackled two major aspects for thin layer capping to apply on Hg-contaminated sediment by two separate studies. The first study attempted to enhance Hg sorption ability by modifying sulfur functional groups on AC; the second study evaluated the stability of caps during turbation events.

During the first study, we observed a successful enhancement of Hg sorption affinity by sulfurized raw AC material in aqueous adsorption tests, which is consistent with some past studies proceeded in similar conditions. However, these studies did not account for the effect of sediment environment which may contain complex biogeochemical factors (e.g. DOM) that alter the fate of Hg. We observed a reversal results as SAC had lower Hg sorption compare to AC in the sediment competition tests. We thus suspect that the sulfur functional groups on the surface of AC can be released and mobilized Hg in the aqueous phase in DOM-rich environments, as described in section 3.3.3. In further inference, it suggests that the sulfurized AC may not enhance Hg sorption during thin layer capping remedy but rather the opposite. However, we also do not suggest that all sorbents with sulfur functional groups may be useless in terms of in-situ sediment remediation, as sulfur functional groups present in various forms and can be varied in results. The results of the microcosm study also differ from sediment adsorption tests as all caps performed with similar Hg reduction efficiency. Further studies to find out the relation between sulfurized sorbents and DOM can be crucial in this technology.

The second study provided some pioneer findings of the relations between the stability of thin layer caps and sediment turbation, which were often questioned by the scientific community. Our results suggested caps with AC + kaolin and AC + bentonite

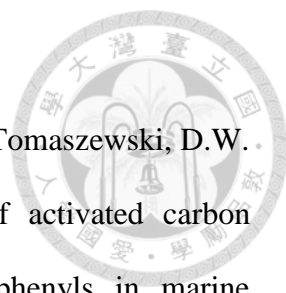
can be stable and were efficient in reducing both THg and MeHg in overlying water and observed with better resistance during occasional turbation events. On the other hands, AC + montmorillonite showed poor Hg reduction efficiency in general and Hg breakthrough in occasional turbation events. Our results suggested that the successfulness of this remedy can be altered not only by the main sorbents but also anchoring materials (e.g. clay minerals). The previous studies related in this field have focused on the porewater Hg as the parameter for the effectiveness of the sorption tests. However, transportation of Hg through sediment particles was proposed and observed in recent studies, which is also consistent with our observation. Also, the different levels of Hg breakthrough may not necessary alters by the different Hg methylation activities, as observed in our results. Thus, it requires further studies to explore the relations between sediment turbation and the Hg reduction efficiency of thin layer caps.

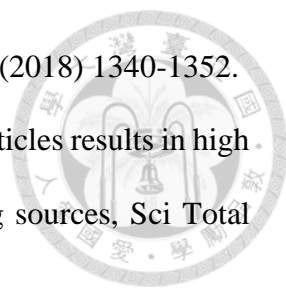
References

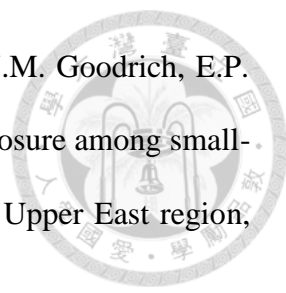


- [1] H.W. Hsiao, S.M. Ullrich, T.W. Tanton, Burdens of mercury in residents of Temirtau, Kazakhstan I: hair mercury concentrations and factors of elevated hair mercury levels, *Sci Total Environ*, 409 (2011) 2272-2280.
- [2] L. Windham-Myers, M. Marvin-Dipasquale, D.P. Krabbenhoft, J.L. Agee, M.H. Cox, P. Heredia-Middleton, C. Coates, E. Kakouros, Experimental removal of wetland emergent vegetation leads to decreased methylmercury production in surface sediment, *J Geophysic Res Biogeosci*, 114 (2009).
- [3] J. Wang, X. Feng, C.W. Anderson, Y. Xing, L. Shang, Remediation of mercury contaminated sites—a review, *J Hazard Mater*, 221 (2012) 1-18.
- [4] M. Morris, R. Sams, G. Gillis, R. Helsel, E. Alperin, T. Geisler, A. Groen, D. Root, Bench-and pilot-scale demonstration of thermal desorption for removal of mercury from the Lower East Fork Poplar Creek floodplain soils, in, *Oak Ridge National Lab.*, 1995.
- [5] D. Kupryianchyk, M.I. Rakowska, D. Reible, J. Harmsen, G. Cornelissen, M. van Veggel, S.E. Hale, T. Grotenhuis, A.A. Koelmans, Positioning activated carbon amendment technologies in a novel framework for sediment management, *Integr Environ Assess Manag*, 11 (2015) 221-234.
- [6] T.S. Bridges, K.E. Gustavson, P. Schroeder, S.J. Ells, D. Hayes, S.C. Nadeau, M.R. Palermo, C. Patmont, Dredging processes and remedy effectiveness: Relationship to the 4 Rs of environmental dredging, *Integr Environ Assess Manag*, 6 (2010) 619-630.
- [7] U. Ghosh, R.G. Luthy, G. Cornelissen, D. Werner, C.A. Menzie, In-situ sorbent amendments: a new direction in contaminated sediment management, *Environ Sci*

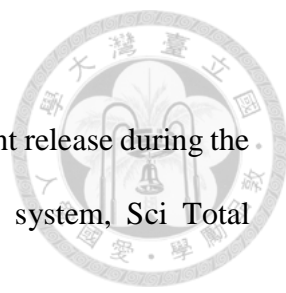
Technol, 45 (2011) 1163-1168.

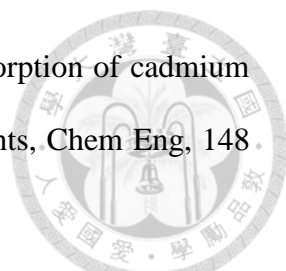
- 
- [8] Y.M. Cho, U. Ghosh, A.J. Kennedy, A. Grossman, G. Ray, J.E. Tomaszewski, D.W. Smithenry, T.S. Bridges, R.G. Luthy, Field application of activated carbon amendment for in-situ stabilization of polychlorinated biphenyls in marine sediment, *Environ Sci Technol*, 43 (2009) 3815-3823.
- [9] G. Cornelissen, M. Elmquist Kruså, G.D. Breedveld, E. Eek, A.M. Oen, H.P.H. Arp, C. Raymond, G.r. Samuelsson, J.E. Hedman, Ø .J.E.S. Stokland, Remediation of contaminated marine sediment using thin-layer capping with activated carbon: a field experiment in Trondheim Harbor, Norway, *Environ Sci Technol*, 45 (2011) 6110-6116.
- [10] B. Beckingham, U. Ghosh, Field-scale reduction of PCB bioavailability with activated carbon amendment to river sediments, *Environ Sci Technol*, 45 (2011) 10567-10574.
- [11] S. Abel, J. Akkanen, A Combined Field and Laboratory Study on Activated Carbon-Based Thin Layer Capping in a PCB-Contaminated Boreal Lake, *Environ Sci Technol*, 52 (2018) 4702-4710.
- [12] J. Wang, B.L. Deng, X.R. Wang, J.Z. Zheng, Adsorption of Aqueous Hg(II) by Sulfur-Impregnated Activated Carbon, *Environ Eng Sci*, 26 (2009) 1693-1699.
- [13] Z.C. Li, L.Y. Wu, H.J. Liu, H.C. Lan, J.H. Qu, Improvement of aqueous mercury adsorption on activated coke by thiol-functionalization, *Chem Eng*, 228 (2013) 925-934.
- [14] P. Hadi, M.H. To, C.W. Hui, C.S. Lin, G. McKay, Aqueous mercury adsorption by activated carbons, *Water Res*, 73 (2015) 37-55.
- [15] J.W.M. Rudd, R.A. Bodaly, N.S. Fisher, C.A. Kelly, D. Kopec, C. Whipple, Fifty years after its discharge, methylation of legacy mercury trapped in the Penobscot

- 
- Estuary sustains high mercury in biota, *Sci Total Environ*, 642 (2018) 1340-1352.
- [16] C.A. Kelly, J.W.M. Rudd, Transport of mercury on the finest particles results in high sediment concentrations in the absence of significant ongoing sources, *Sci Total Environ*, 637-638 (2018) 1471-1479.
- [17] J.R. Flanders, R.R. Turner, T. Morrison, R. Jensen, J. Pizzuto, K. Skalak, R. Stahl, Distribution, behavior, and transport of inorganic and methylmercury in a high gradient stream, *Appl Geochem*, 25 (2010) 1756-1769.
- [18] R.Q. Yu, J.R. Flanders, E.E. Mack, R. Turner, M.B. Mirza, T. Barkay, Contribution of coexisting sulfate and iron reducing bacteria to methylmercury production in freshwater river sediments, *Environ Sci Technol*, 46 (2012) 2684-2691.
- [19] J. Mutter, J. Naumann, C. Sadaghiani, H. Walach, G. Drasch, Amalgam studies: disregarding basic principles of mercury toxicity, *Int J Hyg Environ Health*, 207 (2004) 391-397.
- [20] P. Holmes, K. James, L. Levy, Is low-level environmental mercury exposure of concern to human health?, *Sci Total environ*, 408 (2009) 171-182.
- [21] A.H. Stern, A review of the studies of the cardiovascular health effects of methylmercury with consideration of their suitability for risk assessment, *Environ Res*, 98 (2005) 133-142.
- [22] H.T. Hogberg, A. Kinsner-Ovaskainen, S. Coecke, T. Hartung, A.K. Bal-Price, mRNA expression is a relevant tool to identify developmental neurotoxicants using an in vitro approach, *J Toxicol Sci*, 113 (2009) 95-115.
- [23] F.M.M. Morel, A.M.L. Kraepiel, M. Amyot, The chemical cycle and bioaccumulation of mercury, *Annu Rev Ecol Syst*, 29 (1998) 543-566.
- [24] J.G. Yu, B.Y. Yue, X.W. Wu, Q. Liu, F.P. Jiao, X.Y. Jiang, X.Q. Chen, Removal of mercury by adsorption: a review, *Environ Sci Pollut Res Int*, 23 (2016) 5056-5076.

- 
- [25] Y. Paruchuri, A. Siuniak, N. Johnson, E. Levin, K. Mitchell, J.M. Goodrich, E.P. Renne, N. Basu, Occupational and environmental mercury exposure among small-scale gold miners in the Talensi–Nabdam District of Ghana's Upper East region, *Sci Total Environ*, 408 (2010) 6079-6085.
- [26] H.M. Amos, D.J. Jacob, D. Kocman, H.M. Horowitz, Y. Zhang, S. Dutkiewicz, M. Horvat, E.S. Corbitt, D.P. Krabbenhoft, E.M. Sunderland, Global biogeochemical implications of mercury discharges from rivers and sediment burial, *Environ Sci Technol*, 48 (2014) 9514-9522.
- [27] D. Kocman, S.J. Wilson, H.M. Amos, K.H. Telmer, F. Steenhuisen, E.M. Sunderland, R.P. Mason, P. Outridge, M. Horvat, Toward an assessment of the global inventory of present-day mercury releases to freshwater environments, *Int J Environ Res Public Health*, 14 (2017) 138.
- [28] G. Batley, R. Stahl, M. Babut, T. Bott, J. Clark, L. Field, K. Ho, D. Mount, R. Swartz, A. Tessier, Scientific underpinnings of sediment quality guidelines, (2005).
- [29] E.M. Sunderland, F.A.P.C. Gobas, A. Heyes, B.A. Branfireun, A.K. Bayer, R.E. Cranston, M.B. Parsons, Speciation and bioavailability of mercury in well-mixed estuarine sediments, *Mar Chem*, 90 (2004) 91-105.
- [30] R.P. Mason, E.H. Kim, J. Cornwell, D. Heyes, An examination of the factors influencing the flux of mercury, methylmercury and other constituents from estuarine sediment, *Mar Chem*, 102 (2006) 96-110.
- [31] T.L. Clarke, B. Lesht, R.A. Young, D.J.P. Swift, G.L. Freeland, Sediment resuspension by surface-wave action - an examination of possible mechanisms, *Mar Geol*, 49 (1982) 43-59.
- [32] L.C. Lund-Hansen, M. Petersson, W. Nurjaya, Vertical sediment fluxes and wave-induced sediment resuspension in a shallow-water coastal lagoon, *Estuaries*, 22

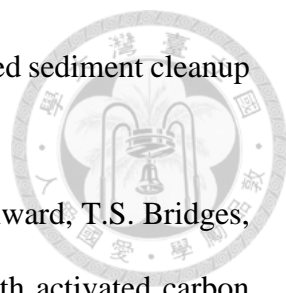
(1999) 39-46.

- 
- [33] B. Morgan, A.W. Rate, E.D. Burton, Water chemistry and nutrient release during the resuspension of FeS-rich sediments in a eutrophic estuarine system, *Sci Total Environ*, 432 (2012) 47-56.
- [34] S. Josefsson, K. Leonardsson, J.S. Gunnarsson, K. Wiberg, Bioturbation-driven release of buried PCBs and PBDEs from different depths in contaminated sediments, *Environ Sci Technol*, 44 (2010) 7456-7464.
- [35] M. Ravichandran, Interactions between mercury and dissolved organic matter—a review, *Chemosphere*, 55 (2004) 319-331.
- [36] C.T. Driscoll, Y.J. Han, C.Y. Chen, D.C. Evers, K.F. Lambert, T.M. Holsen, N.C. Kamman, R.K. Munson, Mercury contamination in forest and freshwater ecosystems in the Northeastern United States, *Biosci*, 57 (2007) 17-28.
- [37] A.M. Kraepiel, K. Keller, H.B. Chin, E.G. Malcolm, F.M. Morel, Sources and variations of mercury in tuna, *Environ Sci Technol*, 37 (2003) 5551-5558.
- [38] R. Liu, Q. Wang, X. Lu, F. Fang, Y. Wang, Distribution and speciation of mercury in the peat bog of Xiaoxing'an Mountain, northeastern China, *Environ Pollut*, 124 (2003) 39-46.
- [39] L.L. Loseto, S.D. Siciliano, D.R. Lean, Methylmercury production in High Arctic wetlands, *Environ Toxicol Chem*, 23 (2004) 17-23.
- [40] S.M. Ullrich, T.W. Tanton, S.A. Abdrashitova, Mercury in the aquatic environment: A review of factors affecting methylation, *Crit Rev Env Sci Tec*, 31 (2001) 241-293.
- [41] H. Shamsijazeyi, T. Kaghazchi, Simultaneous activation/sulfurization method for production of sulfurized activated carbons: characterization and Hg(II) adsorption capacity, *Water Sci Technol*, 69 (2014) 546-552.

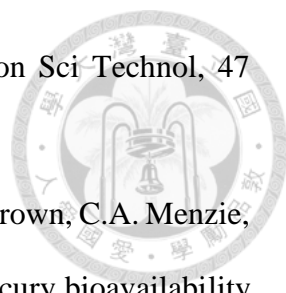
- 
- [42] M. Nadeem, M. Shabbir, M. Abdullah, S. Shah, G. McKay, Sorption of cadmium from aqueous solution by surfactant-modified carbon adsorbents, *Chem Eng*, 148 (2009) 365-370.
- [43] T. Wajima, K. Murakami, T. Kato, K. Sugawara, Heavy metal removal from aqueous solution using carbonaceous K₂S-impregnated adsorbent, *J Environ Sci*, 21 (2009) 1730-1734.
- [44] M. Martins, P.M. Costa, J. Raimundo, C. Vale, A.M. Ferreira, M.H. Costa, Impact of remobilized contaminants in *Mytilus edulis* during dredging operations in a harbour area: bioaccumulation and biomarker responses, *Ecotoxicol Environ Saf*, 85 (2012) 96-103.
- [45] G. Petruzzelli, F. Pedron, M. Grifoni, M. Barbafieri, I. Rosellini, B. Pezzarossa, Soil remediation technologies towards green remediation strategies, *Int J Environ Chem Ecol Geol Geophys Eng*, 10 (2016) 654-658.
- [46] D.D. Reible, *Processes, assessment and remediation of contaminated sediments*, Springer, 2014.
- [47] J.R. Zimmerman, D. Werner, U. Ghosh, R.N. Millward, T.S. Bridges, R.G. Luthy, Effects of dose and particle size on activated carbon treatment to sequester polychlorinated biphenyls and polycyclic aromatic hydrocarbons in marine sediments, *Environ Toxicol Chem*, 24 (2005) 1594-1601.
- [48] Y. Choi, Y.M. Cho, R.G. Luthy, In situ sequestration of hydrophobic organic contaminants in sediments under stagnant contact with activated carbon. 1. Column studies, *Environ Sci Technol*, 48 (2014) 1835-1842.
- [49] P.B. McLeod, M.J. van den Heuvel-Greve, S.N. Luoma, R.G. Luthy, Biological uptake of polychlorinated biphenyls by *Macoma balthica* from sediment amended with activated carbon, *Environ Toxicol Chem*, 26 (2007) 980-987.

- 
- [50] J.E. Tomaszewski, D. Werner, R.G. Luthy, Activated carbon amendment as a treatment for residual DDT in sediment from a superfund site in San Francisco Bay, Richmond, California, USA, *Environ Toxicol Chem*, 26 (2007) 2143-2150.
- [51] X.L. Sun, U. Ghosh, PCB bioavailability control in *Lumbriculus variegatus* through different modes of activated carbon addition to sediments, *Environ Sci Technol*, 41 (2007) 4774-4780.
- [52] S.E. Hale, J.E. Tomaszewski, R.G. Luthy, D. Werner, Sorption of dichlorodiphenyltrichloroethane (DDT) and its metabolites by activated carbon in clean water and sediment slurries, *Water Res*, 43 (2009) 4336-4346.
- [53] S.E. Hale, D. Werner, Modeling the mass transfer of hydrophobic organic pollutants in briefly and continuously mixed sediment after amendment with activated carbon, *Environ Sci Technol*, 44 (2010) 3381-3387.
- [54] E.M.-L. Janssen, M.-N.I. Croteau, S.N. Luoma, R.G. Luthy, Measurement and modeling of polychlorinated biphenyl bioaccumulation from sediment for the marine polychaete *Neanthes arenaceodentata* and response to sorbent amendment, *Environ Sci Technol*, 44 (2009) 2857-2863.
- [55] R.N. Millward, T.S. Bridges, U. Ghosh, J.R. Zimmerman, R.G. Luthy, Addition of activated carbon to sediments to reduce PCB bioaccumulation by a polychaete (*Neanthes arenaceodentata*) and an amphipod (*Leptocheirus plumulosus*), *Environ Sci Technol*, 39 (2005) 2880-2887.
- [56] R.C. Brandli, T. Hartnik, T. Henriksen, G. Cornelissen, Sorption of native polyaromatic hydrocarbons (PAH) to black carbon and amended activated carbon in soil, *Chemosphere*, 73 (2008) 1805-1810.
- [57] C.R. Patmont, U. Ghosh, P. LaRosa, C.A. Menzie, R.G. Luthy, M.S. Greenberg, G. Cornelissen, E. Eek, J. Collins, J. Hull, T. Hjartland, E. Glaza, J. Bleiler, J. Quadrini,

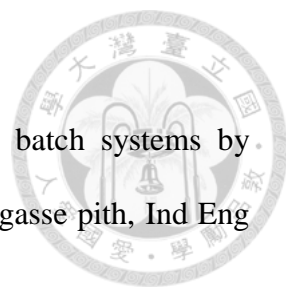
In situ sediment treatment using activated carbon: a demonstrated sediment cleanup technology, *Integr Environ Assess Manag*, 11 (2015) 195-207.

- 
- [58] Y.M. Cho, D.W. Smithenry, U. Ghosh, A.J. Kennedy, R.N. Millward, T.S. Bridges, R.G. Luthy, Field methods for amending marine sediment with activated carbon and assessing treatment effectiveness, *Mar Environ Res*, 64 (2007) 541-555.
- [59] Y.M. Cho, D. Werner, Y. Choi, R.G. Luthy, Long-term monitoring and modeling of the mass transfer of polychlorinated biphenyls in sediment following pilot-scale in-situ amendment with activated carbon, *J Contam Hydrol*, 129-130 (2012) 25-37.
- [60] G. Cornelissen, K. Amstaetter, A. Hauge, M. Schaanning, B. Beylich, J.S. Gunnarsson, G.D. Breedveld, A.M. Oen, E. Eek, Large-scale field study on thin-layer capping of marine PCDD/F-contaminated sediments in Grenlandfjords, Norway: physicochemical effects, *Environ Sci Technol*, 46 (2012) 12030-12037.
- [61] G. Cornelissen, M. Schaanning, J.S. Gunnarsson, E. Eek, A large-scale field trial of thin-layer capping of PCDD/F-contaminated sediments: sediment-to-water fluxes up to 5 years post-amendment, *Integr Environ Assess Manag*, 12 (2016) 216-221.
- [62] C. Menzie, B. Amos, S.K. Driscoll, U. Ghosh, C. Gilmour, Evaluating the efficacy of a low-impact delivery system for in situ treatment of sediments contaminated with methylmercury and other hydrophobic chemicals, in, *Exponent Alexandria United States*, 2016.
- [63] G.S. Samuelsson, C. Raymond, S. Agrenius, M. Schaanning, G. Cornelissen, J.S. Gunnarsson, Response of marine benthic fauna to thin-layer capping with activated carbon in a large-scale field experiment in the Grenland fjords, Norway, *Environ Sci Pollut Res Int*, 24 (2017) 14218-14233.
- [64] J.L. Gomez-Eyles, C. Yupanqui, B. Beckingham, G. Riedel, C. Gilmour, U. Ghosh, Evaluation of biochars and activated carbons for in situ remediation of sediments

impacted with organics, mercury, and methylmercury, *Environ Sci Technol*, 47 (2013) 13721-13729.

- 
- [65] C.C. Gilmour, G.S. Riedel, G. Riedel, S. Kwon, R. Landis, S.S. Brown, C.A. Menzie, U. Ghosh, Activated carbon mitigates mercury and methylmercury bioavailability in contaminated sediments, *Environ Sci Technol*, 47 (2013) 13001-13010.
- [66] A.S. Lewis, T.G. Huntington, M.C. Marvin-DiPasquale, A. Amirbahman, Mercury remediation in wetland sediment using zero-valent iron and granular activated carbon, *Environmental Pollution*, 212 (2016) 366-373.
- [67] H. Kong, J. He, Y. Gao, H. Wu, X. Zhu, Cosorption of phenanthrene and mercury(II) from aqueous solution by soybean stalk-based biochar, *J Agric Food Chem*, 59 (2011) 12116-12123.
- [68] C. Gilmour, T. Bell, A. Soren, G. Riedel, G. Riedel, D. Kopec, D. Bodaly, U. Ghosh, Activated carbon thin-layer placement as an in situ mercury remediation tool in a Penobscot River salt marsh, *Sci Total Environ*, 621 (2018) 839-848.
- [69] P. Liu, C.J. Ptacek, D.W. Blowes, W.D. Gould, Control of mercury and methylmercury in contaminated sediments using biochars: A long-term microcosm study, *Appl Geochem*, 92 (2018) 30-44.
- [70] E.M. Janssen, B.A. Beckingham, Biological responses to activated carbon amendments in sediment remediation, *Environ Sci Technol*, 47 (2013) 7595-7607.
- [71] E.M. Janssen, Y. Choi, R.G. Luthy, Assessment of nontoxic, secondary effects of sorbent amendment to sediments on the deposit-feeding organism *Neanthes arenaceodentata*, *Environ Sci Technol*, 46 (2012) 4134-4141.
- [72] I. Nybom, G. Waissi-Leinonen, K. Maenpaa, M.T. Leppanen, J.V. Kukkonen, D. Werner, J. Akkanen, Effects of activated carbon ageing in three PCB contaminated sediments: Sorption efficiency and secondary effects on *Lumbriculus variegatus*,

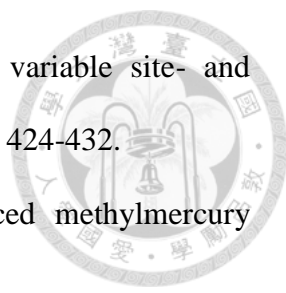
Water Res, 85 (2015) 413-421.

- 
- [73] K.A. Krishnan, T.S. Anirudhan, Uptake of heavy metals in batch systems by sulfurized steam activated carbon prepared from sugarcane bagasse pith, *Ind Eng Chem Res*, 41 (2002) 5085-5093.
- [74] N. Asasian, T. Kaghazchi, Sulfurized activated carbons and their mercury adsorption/desorption behavior in aqueous phase, *Int J Environ Sci Te*, 12 (2015) 2511-2522.
- [75] J.H. Park, G.K. Choppala, N.S. Bolan, J.W. Chung, T. Chuasavathi, Biochar reduces the bioavailability and phytotoxicity of heavy metals, *Plant Soil*, 348 (2011) 439-451.
- [76] A.S.K. Kumar, S. Kalidhasan, V. Rajesh, N. Rajesh, A Meticulous study on the adsorption of mercury as tetrachloromercurate(II) anion with trioctylamine modified sodium montmorillonite and its application to a coal fly ash sample, *Ind Eng Chem Res*, 51 (2012) 11312-11327.
- [77] B. Sarkar, Y. Xi, M. Megharaj, G.S. Krishnamurti, D. Rajarathnam, R. Naidu, Remediation of hexavalent chromium through adsorption by bentonite based Arquad® 2HT-75 organoclays, *J Hazard Mater*, 183 (2010) 87-97.
- [78] B. Sarkar, R. Naidu, M.M. Rahman, M. Megharaj, Y.F. Xi, Organoclays reduce arsenic bioavailability and bioaccessibility in contaminated soils, *J Soil Sediment*, 12 (2012) 704-712.
- [79] V.A. Oyanedel-Craver, J.A. Smith, Effect of quaternary ammonium cation loading and pH on heavy metal sorption to Ca bentonite and two organobentonites, *J Hazard Mater*, 137 (2006) 1102-1114.
- [80] M.J. Wharton, B. Atkins, J.M. Charnock, F.R. Livens, R.A.D. Patrick, D. Collison, An X-ray absorption spectroscopy study of the coprecipitation of Tc and Re with

- mackinawite (FeS), *App Geochem*, 15 (2000) 347-354.
- [81] M. Wolthers, S.J. Van der Gaast, D. Rickard, The structure of disordered mackinawite, *Am Mineral*, 88 (2003) 2007-2015.
- [82] J.W. Morse, T. Arakaki, Adsorption and coprecipitation of divalent metals with mackinawite (FeS), *Geochim Cosmochim Acta*, 57 (1993) 3635-3640.
- [83] D. Ito, K. Miura, T. Ichimura, I. Ihara, T. Watanabe, Removal of As, Cd, Hg and Pb ions from solution by adsorption with bacterially-produced magnetic iron sulfide particles using high gradient magnetic separation, *Ieee T Appl Supercon*, 14 (2004) 1551-1553.
- [84] A. Ö zverdi, M. Erdem, Cu²⁺, Cd²⁺ and Pb²⁺ adsorption from aqueous solutions by pyrite and synthetic iron sulphide, *J Hazard Mater*, 137 (2006) 626-632.
- [85] J.H.P. Watson, D.C. Ellwood, Q.X. Deng, S. Mikhalovsky, C.E. Hayter, J. Evans, Heavy-metal adsorption on bacterially produced FeS, *Miner Eng*, 8 (1995) 1097-1108.
- [86] J. Liu, K.T. Valsaraj, I. Devai, R.D. DeLaune, Immobilization of aqueous Hg(II) by mackinawite (FeS), *J Hazard Mater*, 157 (2008) 432-440.
- [87] G.E. Jean, G.M. Bancroft, Heavy metal adsorption by sulphide mineral surfaces, *Geochim Cosmochim Acta*, 50 (1986) 1455-1463.
- [88] P. Behra, P. Bonnissel-Gissinger, M. Alnot, R. Revel, J.J. Ehrhardt, XPS and XAS study of the sorption of Hg(II) onto pyrite, *Langmuir*, 17 (2001) 3970-3979.
- [89] Y. Sun, D. Lv, J. Zhou, X. Zhou, Z. Lou, S.A. Baig, X. Xu, Adsorption of mercury (II) from aqueous solutions using FeS and pyrite: A comparative study, *Chemosphere*, 185 (2017) 452-461.
- [90] U. Skyllberg, A. Drott, Competition between disordered iron sulfide and natural organic matter associated thiols for mercury (II): An EXAFS study, *Environ Sci*

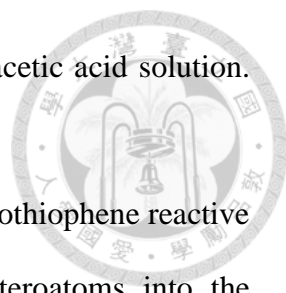


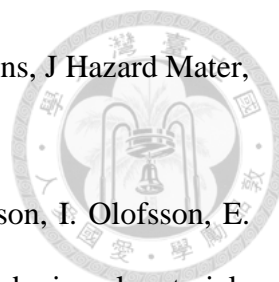
- 
- Technol, 44 (2010) 1254-1259.
- [91] N.R. Council, Sediment dredging at Superfund megasites: Assessing the effectiveness, National Academies Press, 2007.
- [92] C. Liu, J.A. Jay, T.E. Ford, Evaluation of environmental effects on metal transport from capped contaminated sediment under conditions of submarine groundwater discharge, *Environ Sci Technol*, 35 (2001) 4549-4555.
- [93] M. Xie, N. Wang, J.F. Gaillard, A.I. Packman, Interplay between flow and bioturbation enhances metal efflux from low-permeability sediments, *J Hazard Mater*, 341 (2018) 304-312.
- [94] K.R. Roche, A.F. Aubeneau, M. Xie, T. Aquino, D. Bolster, A.I. Packman, An Integrated Experimental and Modeling Approach to Predict Sediment Mixing from Benthic Burrowing Behavior, *Environ Sci Technol*, 50 (2016) 10047-10054.
- [95] E.A. Seelen, G.M. Massey, R.P. Mason, Role of sediment resuspension on estuarine suspended particulate mercury dynamics, *Environ Sci Technol*, 52 (2018) 7736-7744.
- [96] D. Meric, S.M. Barbuto, A.N. Alshawabkeh, J.P. Shine, T.C. Sheahan, Effect of reactive core mat application on bioavailability of hydrophobic organic compounds, *Sci Total Environ*, 423 (2012) 168-175.
- [97] M.T. Jonker, M.P. Suijkerbuijk, H. Schmitt, T.L. Sinnige, Ecotoxicological effects of activated carbon addition to sediments, *Environ Sci Technol*, 43 (2009) 5959-5966.
- [98] B. Beckingham, D. Buys, H. Vandewalker, U. Ghosh, Observations of limited secondary effects to benthic invertebrates and macrophytes with activated carbon amendment in river sediments, *Environ Toxicol Chem*, 32 (2013) 1504-1515.
- [99] Y. Choi, Y.M. Cho, R.G. Luthy, D. Werner, Predicted effectiveness of in-situ

- 
- activated carbon amendment for field sediment sites with variable site- and compound-specific characteristics, *J Hazard Mater*, 301 (2016) 424-432.
- [100] R. Shu, Y. Wang, H. Zhong, Biochar amendment reduced methylmercury accumulation in rice plants, *J Hazard Mater*, 313 (2016) 1-8.
- [101] G. Gee, J. Bauder, A.J.I. Klute, Madison, WIS, USA, Particle-Size Analysis, *Methods of Soil Analysis, Part 1. Physical and Mineralogical Methods*, Soil Science Society of America, (1986).
- [102] O. Mehra, M. Jackson, Iron oxide removal from soils and clays by a dithionite–citrate system buffered with sodium bicarbonate, in: *Clay Miner*, Elsevier, 2013, pp. 317-327.
- [103] A. Walkley, I.A. Black, An examination of the Degtjareff method for determining soil organic matter, and a proposed modification of the chromic acid titration method, *Soil Science*, 37 (1934) 29-38.
- [104] D.R. Keeney, D.W.J.M.o.s.a.P.C. Nelson, m. properties, *Nitrogen—Inorganic Forms 1*, (1982) 643-698.
- [105] N.M. Mazrui, S. Jonsson, S. Thota, J. Zhao, R.P. Mason, Enhanced availability of mercury bound to dissolved organic matter for methylation in marine sediments, *Geochim Cosmochim Acta*, 194 (2016) 153-162.
- [106] M.R. Chaves, K.T. Valsaraj, R.D. DeLaune, R.P. Gambrell, P.M. Buchler, Mercury uptake by biogenic silica modified with L-cysteine, *Environ Technol*, 32 (2011) 1615-1625.
- [107] Y.X. Huang, S.L. Candelaria, Y.W. Li, Z.M. Li, J.J. Tian, L.L. Zhang, G.Z. Cao, Sulfurized activated carbon for high energy density supercapacitors, *Journal Power Sources*, 252 (2014) 90-97.
- [108] T. Grzybek, R. Pietrzak, H. Wachowska, The comparison of oxygen and sulfur

species formed by coal oxidation with O₂/Na₂CO₃ or peroxyacetic acid solution.

XPS studies, *Energy Fuels*, 18 (2004) 804-809.

- 
- [109] M. Seredych, M. Khine, T.J. Bandosz, Enhancement in dibenzothiophene reactive adsorption from liquid fuel via incorporation of sulfur heteroatoms into the nanoporous carbon matrix, *Chemosuschem*, 4 (2011) 139-147.
- [110] H.C. Hsi, M.J. Rood, M. Rostam-Abadi, S. Chen, R. Chang, Effects of sulfur impregnation temperature on the properties and mercury adsorption capacities of activated carbon fibers (ACFs), *Environ Sci Technol*, 35 (2001) 2785-2791.
- [111] C.T. Chiou, J. Cheng, W.N. Hung, B. Chen, T.F. Lin, Resolution of adsorption and partition components of organic compounds on black Carbons, *Environ Sci Technol*, 49 (2015) 9116-9123.
- [112] R. Efroymson, G. Suter, B. Sample, D. Jones, Preliminary remediation goals for ecological endpoints, in, Oak Ridge National Lab., 1996.
- [113] H. Cheng, Y. Hu, Mercury in municipal solid waste in China and its control: a review, *Environ Sci Technol*, 46 (2012) 593-605.
- [114] T. Zhang, B. Kim, C. Levard, B.C. Reinsch, G.V. Lowry, M.A. Deshusses, H. Hsu-Kim, Methylation of mercury by bacteria exposed to dissolved, nanoparticulate, and microparticulate mercuric sulfides, *Environ Sci Technol*, 46 (2012) 6950-6958.
- [115] A.M. Graham, G.R. Aiken, C.C. Gilmour, Dissolved organic matter enhances microbial mercury methylation under sulfidic conditions, *Environ Sci Technol*, 46 (2012) 2715-2723.
- [116] P. Liu, C.J. Ptacek, D.W. Blowes, R.C. Landis, Mechanisms of mercury removal by biochars produced from different feedstocks determined using X-ray absorption spectroscopy, *J Hazard Mater*, 308 (2016) 233-242.
- [117] P. Liu, C.J. Ptacek, D.W. Blowes, Y.Z. Finrock, R.A. Gordon, Stabilization of



mercury in sediment by using biochars under reducing conditions, *J Hazard Mater*, 325 (2017) 120-128.

[118] S. Josefsson, M. Schaanning, G.S. Samuelsson, J.S. Gunnarsson, I. Olofsson, E. Eek, K. Wiberg, Capping efficiency of various carbonaceous and mineral materials for in situ remediation of polychlorinated dibenzo-p-dioxin and dibenzofuran contaminated marine sediments: sediment-to-water fluxes and bioaccumulation in boxcosm tests, *Environ Sci Technol*, 46 (2012) 3343-3351.

[119] G.N. Bigham, K.J. Murray, Y. Masue-Slowey, E.A. Henry, Biogeochemical controls on methylmercury in soils and sediments: Implications for site management, *Integr Environ Assess Manag*, 13 (2017) 249-263.

[120] J.M. Benoit, C.C. Gilmour, R.P. Mason, G.S. Riedel, G.F. Riedel, Behavior of mercury in the Patuxent River estuary, *Biogeochem*, 40 (1998) 249-265.

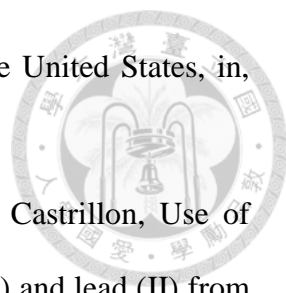
[121] Y. Ting, C. Chen, B.L. Ch'ng, Y.L. Wang, H.C. Hsi, Using raw and sulfur-impregnated activated carbon as active cap for leaching inhibition of mercury and methylmercury from contaminated sediment, *J Hazard Mater*, 354 (2018) 116-124.

[122] B.D. Gibson, C.J. Ptacek, D.W. Blowes, S.D. Daugherty, Sediment resuspension under variable geochemical conditions and implications for contaminant release, *J Soil Sediment*, 15 (2015) 1644-1656.

[123] J.P.Y. Maa, L. Sanford, J.P. Halka, Sediment resuspension characteristics in Baltimore Harbor, Maryland, *Mar Geol*, 146 (1998) 137-145.

[124] D. Lin, Y.M. Cho, D. Werner, R.G. Luthy, Bioturbation delays attenuation of DDT by clean sediment cap but promotes sequestration by thin-layered activated carbon, *Environ Sci Technol*, 48 (2014) 1175-1183.

[125] K. Norrish, The Swelling of Montmorillonite, *Discuss Faraday Soc*, 18 (1954) 120-134.

- 
- [126] J.W. Hosterman, Bentonite and Fuller's earth resources of the United States, in, 1985.
- [127] Y. Fernandez-Nava, M. Ulmanu, I. Anger, E. Maranon, L. Castrillon, Use of granular bentonite in the removal of mercury (II), cadmium (II) and lead (II) from aqueous solutions, *Water Air Soil Poll*, 215 (2011) 239-249.
- [128] Y. Zhu, L.Q. Ma, B. Gao, J.C. Bonzongo, W. Harris, B. Gu, Transport and interactions of kaolinite and mercury in saturated sand media, *J Hazard Mater*, 213-214 (2012) 93-99.
- [129] C. Green-Ruiz, Adsorption of mercury(II) from aqueous solutions by the clay mineral montmorillonite, *Bull Environ Contam Toxicol*, 75 (2005) 1137-1142.
- [130] W. Zhu, Y. Song, G.A. Adediran, T. Jiang, A.T. Reis, E. Pereira, U. Skyllberg, E. Bjorn, Mercury transformations in resuspended contaminated sediment controlled by redox conditions, chemical speciation and sources of organic matter, *Geochim Cosmochim Acta*, 220 (2018) 158-179.
- [131] S. Bachmaf, B. Planer-Friedrich, B.J. Merkel, Effect of sulfate, carbonate, and phosphate on the uranium(VI) sorption behavior onto bentonite, *Radiochim Acta*, 96 (2008) 359-366.
- [132] S.M. Rao, A. Sridharan, Mechanism of sulfate adsorption by kaolinite, *Clay Clay Miner*, 32 (1984) 414-418.
- [133] C. Gilmour, E. Henry, Mercury methylation by sulfate-reducing bacteria-biogeochemical and pure culture studies, in: ABSTRACTS OF PAPERS OF THE AMERICAN CHEMICAL SOCIETY, AMER CHEMICAL SOC 1155 16TH ST, NW, WASHINGTON, DC 20036, 1992, pp. 140-GEOC.
- [134] C. Gilmour, D. Krabbenhoft, W. Orem, G. Aiken, E. Roden, Appendix 3B-2: status report on ACME studies on the control of mercury methylation and

bioaccumulation in the Everglades, *J South Florida Environmental Report*, 1 (2007) 3B-2.

[135] S.E. Rothenberg, X.B. Feng, Mercury cycling in a flooded rice paddy, *J Geophys Res-Bioge*, 117 (2012).

[136] C. Gilmour, J.T. Bell, A.B. Soren, G. Riedel, G. Riedel, A.D. Kopec, R.A. Bodaly, Distribution and biogeochemical controls on net methylmercury production in Penobscot River marshes and sediment, *Sci Total Environ*, 640-641 (2018) 555-569.

[137] N.W. Johnson, D.D. Reible, L.E. Katz, Biogeochemical changes and mercury methylation beneath an in-situ sediment cap, *Environ Sci Technol*, 44 (2010) 7280-7286.

[138] A. Mucci, G. Bernier, C. Guignard, Mercury remobilization in Saguenay Fjord (Quebec, Canada) sediments: Insights following a mass-flow event and its capping efficiency, *Appl Geochem*, 54 (2015) 13-26.

